UNIVERSITEIT VAN PRETORIA
UNIVERSITY OF PRETORIA
YUNIBESITHI YA PRETORIA

PROMOTING CIRCULAR ECONOMY AND SUSTAINABLE CONSTRUCTION PRACTICES: INVESTIGATING THE INTEGRATION OF WASTE UPCYCLING FOR A GREENER FUTURE, WITH A FOCUS ON EGGSHELL AND EGGSHELL MEMBRANE UTILIZATION

By

Samuel Tomi Aina

Submitted in partial fulfilment of the requirements for the degree:

Doctor of Philosophy

in

Chemical Engineering

Faculty of Engineering Built Environment and Information Technology

University of Pretoria

2023

ABSTRACT

PROMOTING CIRCULAR ECONOMY AND SUSTAINABLE CONSTRUCTION PRACTICES: INVESTIGATING THE INTEGRATION OF WASTE UPCYCLING FOR A GREENER FUTURE, WITH A FOCUS ON EGGSHELL AND EGGSHELL MEMBRANE UTILIZATION

by

Samuel Tomi Aina

Supervisor: Professor Hendrik Gideon Brink

Co-supervisor: Dr Vuyo Mjimba

University: University of Pretoria

Faculty: Faculty of Engineering Built Environment and IT

Department: Department of Chemical Engineering

Degree: Doctor of Philosophy (Engineering)

Keywords: Waste Valorisation; Circular Economy, Eggshell; Green Construction; Cytotoxicity; Nanocomposites

As climate change continues to take the centre stage among issues of global discuss, carbon heavy industries including construction and agriculture continue to discover possible ways to foster the implementation of cleaner production technology as well as non-hazardous and sustainable waste disposal solutions. While previous studies have made commendable progress in proposing solutions, much more is still desired. A hybrid approach involving the principles of circular economy and material fusion by adsorption was employed on eggshells. Waste eggshells were valorised and up cycled with its major constituents finding effective use along the chain. This study examined the efficient separation of eggshells from its membrane, the recovery of valuable biochemical compounds and the optimized calcination of the bare shell to

produce calcium oxide which is a viable cement replacement material. In addition, the adsorption kinetics of the shell membrane with silver nanoparticles and the effectiveness of the nanocomposite as a cytotoxic additive in cement mortar was investigated.

The results demonstrated that in seventeen minutes, acetic acid efficiently weakened the bond between the shell and its semipermeable membrane while minimizing the dissolution of calcium and maximizing the leaching of valuable compounds and proteins like collagen. The calcined, leached, and separated shell produced calcium oxide of comparable quality to that derived from limestone during cement production. Further up the value chain, the separated membrane was employed as an adsorbent for silver nanoparticles and the antimicrobial property of the nanocomposite was exemplified on *Pseudomonas aeruginosa* and *Bacillus subtilis*.

Pseudo-first order, Pseudo-second order, Two-phase adsorption, Crank internal mass transfer model, and Weber and Morris (W&M) kinetic models were employed to further understand the adsorption process. All the models were adequately fitted with R^2 values ranging from 0.922 to 0.990 for both AgNPs and $AgNO_3$. Both Langmuir and Freundlich Isotherm models were also fitted.

The adsorption process was optimum at a pH of 6, 25 ◦C, and after 48 h of agitation. Compared to previous studies, a remarkable antimicrobial activity against *Pseudomonas aeruginosa* and *Bacillus subtilis* was exhibited resulting in 27.77% and 15.34% cell death, respectively. Analysis of variance and Tukey multiple comparison statistical tests were carried out to highlight the significance of the cell inhibition results at $P<0.05$ and 95% confidence level. *B. subtilis* exhibited significant tolerance to metabolic inhibition while *P. aeruginosa* was significantly inhibited.

Following this impressive outcome, the cytotoxic property of the nanocomposite was tested in concrete mortar. This is to combat the ever-increasing infrastructure budget relating to the maintenance of concrete structures damaged by microbial attacks in moist environments. Waste activated sludge obtained from a local domestic wastewater treatment plant, *Pseudomonas aeruginosa,* and *Bacillus subtilis* were studied in both aerobic and anaerobic conditions. Waste activated sludge was most

susceptible to the nanocomposite with up to 50% cell death recorded for a 2% cement replacement. In contrast, *Pseudomonas aeruginosa* and *Bacillus subtilis* experienced a maximum of 9% and 5% cell death, respectively. For the same cement replacement approximately 5% reduction in compressive strength and no significant change in Tensile strength were measured. This minimal loss in compressive strength is negligible compared to be antimicrobial benefits.

Furthermore, considering that about 8.7 million metric tons of eggshell was produced globally in 2021, this alternative use of the shell and its membrane is of great importance to the environment. This include reduction in needed landfill, cost saving and reduction in the generation of GHGs. This study presents a multifaceted approach to the valorisation of waste eggshells, demonstrating their potential as a valuable resource in addressing environmental and industrial challenges. This research underscores the importance of exploring innovative solutions that not only reduce waste but also contribute to the development of cleaner and more sustainable practices in various industries. As we continue to grapple with the pressing issues of climate change and resource conservation, such initiatives pave the way for a more environmentally responsible and economically viable future.

This specific upcycling of eggshell and its membrane is of particular economic importance. To start with, the cost associated with managing over 8 million tons of eggshell waste could be invested in more profiting ventures. Through the valorisation process, the shell membrane and other biochemical compounds recovered are valuable sources of income due to the high demand of some of these substances, e.g., collagen. Also, against the backdrop of escalating infrastructure budgets worldwide, employing eggshell membrane as an antimicrobial additive in concrete could result in up to 40% savings in maintenance cost.

To achieve these benefits however, it is paramount for the construction and waste industry to start looking into the possible challenges. These include collection, logistics, large scale implementation and more. Likewise, new policies surrounding waste disposal and reusage need to be implemented. Finally, new standards and safety

regulations need to be developed while critically exploring and understanding the limitations of waste composites in concrete.

In conclusion, this research demonstrates novelty by proposing an optimised eggshell calcination process by ensuring the recovery of the shell membrane and valuable biochemical compounds such as collagen prior to calcination. This will not only ensure the production of high-grade calcium oxide but will also in turn upcycle the net worth of eggshells. Secondly, the study proposes a novel ESM/Nanosilver antimicrobial composite through adsorption. This research also aims to enhance the adsorption efficiency of chemically produced AgNPs and $AgNO_3$ by utilizing the eggshell membrane optimally separated from the shells. Thirdly, this research incorporated the antimicrobial ESM/Ag nanocomposite into cement mortar with the aim of producing an antimicrobial mortar. Lastly, this study demonstrated innovative contribution to academia through 5 publications and 6 conference presentations.

DECLARATION

I, **Samuel Tomi Aina** declare that this thesis, which I hereby submit for the degree of Doctor of Philosophy in Chemical Engineering at the University of Pretoria, is my own work and has not previously been submitted by me for a degree at this or any other tertiary institution.

.. ..

Samuel Tomi Aina

This 22nd day of September 2023

RESEARCH OUTPUTS

Publications

1. Aina, S. T., Kyomuhimbo, H. D., Du Plessis, B., Mjimba, V., Haneklaus, N., & Brink, H. G. (2023). Cytotoxic-Ag-Modified Eggshell Membrane Nanocomposites as Bactericides in Concrete Mortar. International Journal of Molecular Sciences, 24(20). https://doi.org/10.3390/ijms242015463.
2. Aina, S. T., Kyomuhimbo, H. D., Ramjee, S., Du Plessis, B., Mjimba, V., Maged, A., Haneklaus, N., & Brink, H. G. (2023). Synthesis and Assessment of Antimicrobial Composites of Ag Nanoparticles or $AgNO_3$ and Egg Shell Membranes. Molecules, 28(12), 4654. https://doi.org/10.3390/molecules28124654.
3. Aina, S. T., Du Plessis, B. J., Mjimba, V., & Brink, H. G. (2022). From Waste to Best Valorisation and Upcycling of Chicken Eggshells. In Waste Management (1st ed., pp. 140–155). CRC Press. https://doi.org/10.1201/9780429341106-8.
4. Aina, S., du Plessis, B., Mjimba, V., & Brink, H. (2021). Eggshell Valorisation: Membrane Removal, Calcium Oxide Synthesis, and Biochemical Compound Recovery towards Cleaner Productions. Biointerface Research in Applied Chemistry, 12(5), 5870–5883. https://doi.org/10.33263/BRIAC125.58705883.
5. Aina, S. T., Du-Plessis, B. J., Mjimba, V., & Brink, H. G. (2020). Effect of Membrane Removal on The Production of Calcium Oxide from Eggshells Via Calcination. Chemical Engineering Transactions, 81, 1069–1074. https://doi.org/10.3303/CET2081179.

Conference presentations

1. Challenges in Environmental Science and Engineering (CESE) Virtual Conference, Dubai, UAE. 26th to 27th November 2022.
2. The 36th International Conference on Solid Waste Technology and Management, (ICSW), USA. 14th -16th March 2021.

3. International Congress of Chemical and Process Engineering, CHISA Virtually, Czech Republic. 15th -18th March 2021.
4. 23rd Conference on Process Integration, Modelling, and Optimisation for Energy Saving and Pollution Reduction (PRES'20), China. 17th to 21st August 2020.
5. Challenges in Environmental Science and Engineering (CESE) Virtual Conference. 7th to 8th November 2020.
6. Next-Generation Resources conference, NXGEN, South Africa. 23rd – 24th November 2020.

ACKNOWLEDGEMENTS

“Now unto the King eternal, immortal, invisible, the only wise God, be honour and glory for ever and ever.” I am thankful for the gift of life, good health, wisdom, abundant blessings, guidance, and all sorts of providence.

My love and heart goes to my darling and dearest wife Oyebola Aina. Thank you for standing by me through this journey. Your love, presence and support are unquantifiable. My dear daughter, Adira Aina, daddy loves you.

I would like to express my sincere gratitude and extreme appreciation to my academic mentor and supervisor Professor Hendrik Gideon Brink who allowed me to do this research under his custodianship, guidance, mentorship, and sponsorship. Without his motivation, always positive attitude to research, sincerity, leadership, contriving imagination and vision, this research would never have seen the light of day. Special thanks to Dr Vuyo Mjimba for his pivotal role of kick starting this project.

I am also grateful to Professor Evans M.N. Chirwa, Professor Shepherd M. Tichapondwa, and Dr Samuel Iwarere for their advice, support, and guidance. I also express my appreciation to Miss Alettee Devaga and Miss Elmarie Otto for their administrative support; Once again, your assistance and effectiveness were central to the success of this research.

My appreciation also goes to Mrs Wiebke Grote and Mrs Jeanette Dykstra of the Department of Geology, Dr Madelien Wooding of the Department of Chemistry at the University of Pretoria and the Laboratory for Microscopy and Microanalysis at the University of Pretoria; You were a huge part of this research.

I am exceptionally grateful to my family Mr Peter Aina, Mrs Mary Aina, Ifedotun Aina, Fisayo Aina, Mayokun Aina and Joy Aina, for their sacrifices, love, encouragement, and prayers. You are always available when I need you. I will indeed forever be indebted to you all.

To the Sanyas, Dr Damilola Oyejobi, Jeremiah Chimhundi, Samuel Babalola, all my research colleagues at South campus and general friends, I thank you for the hospitality, friendship, support, and motivation. I have never taken it for granted.

LIST OF ABBREVIATIONS

AA	Atomic absorption spectrometry
CRM	Cement Replacement Material
DSC	Differential Scanning Calorimetry
DTG	Derivative thermogravimetry
EDX	Energy dispersive x-ray
ESM	Eggshell membrane
FTIR	Fourier transform infrared spectroscopy.
GHG	Greenhouse gas
HPLC	High Performance Liquid Chromatograph
MTT	3-(4,5-dimethylthiazolyl-2)-2,5-diphenyltetrazolium bromide
PSA	Pseudo-first order
SEM	Scanning Electron Microscope
SPR	Surface plasmon resonance
TEM	Transmission electron microscopy
TGA	Thermogravimetric analysis
TPO	Two-phase adsorption
UPLC-MS	Ultra-performance liquid chromatography-mass spectrometry
UPLC-Q-TOF-MS	Ultra-performance liquid chromatography quadrupole-time-of-flight mass spectrometry
USD	United States Dollar
US EPA	United States Environmental Protection Agency
WAS	Waste activated sludge.
XRD	X-ray diffraction
XRF	X-ray fluorescence analysis
XPS	X-ray Photoelectron spectroscopy

LIST OF FIGURES

Figure 2-1: Longitudinal section of a chicken egg [31]. 24
Figure 2-2: Schematic diagram of the structure and different layers within the eggshell [39]. 26
Figure 2-3: Apparatus for separation of eggshell and membrane [51]..... 30
Figure 3-1: Leaching kinetics..... 49
Figure 3-2: Thermogravimetric analysis of the US, S60, and membrane only in the presence of nitrogen 51
Figure 3-3: RGB colour analysis of calcined eggshells. (a) at 700 ℃; (b) at 900 ℃. 52
Figure 3-4: XRD pattern of eggshell after calcination at 900°C 52
Figure 3-5: XRD quantitative analysis of calcined eggshells at 900°C 53
Figure 4-1: Calcium concentration in acid leachate.. 61
Figure 4-2: Change in pH and measured mass loss of eggshell in acetic acid..... 62
Figure 4-3: Thermogravimetric analysis. 62
Figure 4-4: Calcination analysis..... 64
Figure 4-5: RGB colour analysis..... 65
Figure 4-6: SEM image of eggshell, CaO, and membrane..... 67
Figure 4-7: XRD quantitative analysis 69
Figure 4-8: XRD pattern of eggshell before and after calcination 69
Figure 5-1. UV–vis absorbance spectrometry of AgNPs and $AgNO_3$. 81
Figure 5-2. Log-normal distribution for the AgNPs in suspension. 82
Figure 5-3. AgNPs/ESM absorption parameters at 394 nm. 84
Figure 5-4. $AgNO_3$/ESM absorption parameter at 294 nm. 86
Figure 5-5. Kinetics of adsorption. 89
Figure 5-6: The isotherm model fits for (a,b) AgNPs and (c,d) $AgNO_3$.. 91
Figure 5-7: SEM images (a,c,e) EDS maps (b,d,f) of ESM composite. (a,b) ESM. (c,d) AgNO3/ESM. (e,f) AgNPs/ESM. 93
Figure 5-8: FTIR spectra of ESM, $AgNO_3$/ESM, and AgNPs/ESM. 95
Figure 5-9: XPS spectrum for (A) $AgNO_3$/ESM and (B) AgNPs/ESM. 96
Figure 5-10: Agar well diffusion images. (A) AgNPs with P. aeruginosa, (B) AgNPs with B. subtilis, (C) $AgNO_3$ with P. aeruginosa, (D) $AgNO_3$ with B. subtilis. 98
Figure 5-11: Antimicrobial characterisation of ESM composite..... 99
Figure 6-1: Mixed Mortar in Prism Mould..... 108

Figure 6-2: XRD mineralogy pattern of the mortar mixes. 112
Figure 6-3: XRF oxide compositions of the different concrete mixes. 113
Figure 6-4: Thermogravimetric analysis of a) mixes 1 to 10 and b) eggshell membrane. 114
Figure 6-5: SEM EDS Ag distribution map of (a) $AgNO_3$/ESM Mortar (MIX 4), (b) AgNPs/ESM Mortar (MIX 7), (c) The elemental compositions of the different mortar mixes (as measured by EDS) 114
Figure 6-6: Antimicrobial characterisation and statistical analysis of mortar composite. 117
Figure 6-7: Mechanical results and statistical analysis of mortal composite.. 119

LIST OF TABLES

Table 2-1: Percentage elemental composition of eggshells 27
Table 2-2: Percentage elemental composition of eggshells membrane 27
Table 2-3: Percentage oxide composition of eggshells 28
Table 2-4: Amino acid composition of decalcified eggshell and eggshell membranes (Mol%) 28
Table 4-1: Characteristics of Eggshell and membrane 60
Table 4-2: Oxide composition of the calcinated shell 68
Table 4-3: Identified compounds 71
Table 5-1. Distribution properties of synthesised AgNPs. 82
Table 5-2. Kinetic models for the adsorption of AgNPs and $AgNO_3$ by ESM. 88
Table 5-3. Fitted kinetic and goodness-of-fit parameters for kinetic models presented in Table 5-1. Distribution properties of synthesised AgNPs. 90
Table 5-4: Isotherm models for the adsorption of AgNPs and $AgNO_3$ by ESM 91
Table 5-5: EDS elemental analysis of ESM composites. 92
Table 5-6: FTIR spectra of ESM composites. 95
Table 5-7: XPS analysis of ESM composites. 97
Table 6-1: Mix Design 108

TABLE OF CONTENTS

ABSTRACT …… I

DECLARATION V

RESEARCH OUTPUTS VI

ACKNOWLEDGEMENTS VIII

LIST OF ABBREVIATIONS IX

LIST OF FIGURES X

LIST OF TABLES XII

CHAPTER 1 GENERAL INTRODUCTION 16

1.1 PREAMBLE 16
1.2 PROBLEM DEFINITION 18
1.3 OBJECTIVES 19
1.4 LIMITATIONS 20
1.5 FRAMEWORK OF THE THESIS 20

CHAPTER 2 REVIEW OF LITERATURES 22

2.1 INTRODUCTION 22
2.2 FORMATION AND STRUCTURE OF THE EGGSHELL 25
2.3 CONSTITUENTS OF EGGSHELL AND EGGSHELL MEMBRANE 26
2.4 SEPARATION OF EGGSHELL MEMBRANE AND EGGSHELL 29
2.5 VALORISATION OF EGGSHELL AND EGGSHELL MEMBRANE 32
2.5.1 Industrial Processes 32
2.5.2 Agriculture 33
2.5.3 Health and Food Production 33
2.5.4 Construction 35
2.5.5 Renewable Energy 37
2.5.6 Bioremediation, and Removal of Metals and Non-Metals. 38
2.6 CALCIUM SILICATE HYDRATE GEL 41
2.7 CONCLUSION 41

CHAPTER 3 EFFECT OF MEMBRANE REMOVAL ON THE PRODUCTION OF CALCIUM OXIDE FROM EGGSHELLS VIA CALCINATION 43

3.1 INTRODUCTION 43
3.2 MATERIALS AND METHODS 47
3.2.1 Experimental Methods 47
3.2.2 Analytical Methods 47
3.2.3 Chemical Model used to Estimate $CaCO_3$ Mass Leached 48
3.3 RESULTS AND DISCUSSION 49
3.4 CONCLUSIONS AND RECOMMENDATION 53

CHAPTER 4 EGGSHELL VALORISATION: MEMBRANE REMOVAL, CALCIUM OXIDE SYNTHESIS, AND BIOCHEMICAL COMPOUND RECOVERY TOWARDS CLEANER PRODUCTIONS 54

4.1 INTRODUCTION 55
4.2 MATERIALS AND METHODS 58
4.2.1 Experimental methods 58
4.2.2 Analytical methods 59
4.3 RESULTS AND DISCUSSION 60
4.3.1 Physical properties 60
4.3.2 Effect of acid on shell membrane and calcium content 60
4.3.3 Thermal analysis 62
4.3.4 Microstructural analysis 66
4.3.5 Recovery of collagen and other compounds 69
4.4 CONCLUSION 72

CHAPTER 5 SYNTHESIS AND ASSESSMENT OF ANTIMICROBIAL COMPOSITES OF AG NANOPARTICLES OR $AGNO_3$ AND EGG SHELL MEMBRANES 73

5.1 INTRODUCTION 74
5.2 MATERIALS AND METHODS 76
5.2.1 Preparation of Eggshell Membranes (ESM) 76
5.2.2 Synthesis of AgNPs 77

5.2.3 Detection and Characterization of AgNPs 77
5.2.4 Production of ESM Composites 78
5.2.5 Characterization of ESM Composites 78
5.2.6 Antimicrobial Activity of AgNPs, $AgNO_3$, and ESM Composites 79
5.3 RESULTS AND DISCUSSION 80
5.3.1 Synthesis and Characterization of AgNPs 80
5.3.2 Ag/ESM Composite Adsorption Optimization, Kinetics, and Equilibrium Behaviour 82
5.3.3 Characterization of Ag/ESM Composites 92
5.3.4 Antimicrobial Activity of Ag/ESM Composites 97
5.4 CONCLUSIONS 101

CHAPTER 6 CYTOTOXIC AG MODIFIED EGGSHELL MEMBRANE NANOCOMPOSITES AS BACTERICIDES IN CONCRETE MORTAR 102

6.1 INTRODUCTION 103
6.2 MATERIALS AND METHODS 106
6.2.1 Preparation of Ag Modified Eggshell membranes (Ag-EMs) 106
6.2.2 Preparation of Cement Mortar 107
6.2.3 Characterization of ESM Modified mortar. 108
6.2.4 Antimicrobial activity of ESM Modified mortar. 109
6.2.5 Mechanical Strength Test 110
6.3 RESULTS 112
6.3.1 Synthesis of AgNPs and production of ESM composites 112
6.3.2 Antimicrobial Activity of Mortar Composite 115
6.3.3 Mechanical Strength Characteristics of Mortar Composite 118
6.4 CONCLUSION 120

CHAPTER 7 CONCLUSIONS AND RECOMMENDATIONS 122

7.1 SIGNIFICANT FINDINGS 122
7.2 RECOMMENDATIONS FOR FUTURE STUDIES 124

REFERENCES … 126

APPENDIX ……. 159

CHAPTER 1 GENERAL INTRODUCTION

1.1 PREAMBLE

The adverse impacts of climate change are arguably the prime focus of global dialogues regarding the environment in the twenty-first century. Its impacts are real, demanding urgent and decisive action to address [1]. The focus of managing climate change has been and remains two-pronged. Firstly, learning to live with the adverse impacts of this phenomenon - the essence of adaptation and secondly, retarding or halting the increase of anthropogenic atmospheric greenhouse gases (GHGs) - the essence of mitigation. The major source of anthropogenic GHGs is the burning of fossil fuels for direct and indirect energy inputs in industrial and social activities resulting in the release of carbon monoxide (CO_2).

The global awareness for the reduction of CO_2 emissions has encouraged further investigations on the use of alternative cementitious materials or additives for concrete production [2]. It has been argued and estimated that the construction industry alone is responsible for approximately 80% of the world's pollution. The building industry is estimated to be responsible for about 40% of greenhouse gas emissions (GHGs) globally and 40% of global energy consumption [3]. The general pollution and (GHGs) emissions of the construction industry vary across the industry value chain. GHGs are the drivers of global warming which in turn drives climate change [3]. Since the industrial revolution, the concentration of anthropogenic GHGs in the atmosphere has increased leading to accelerated global warming and climate change. Ordinary Portland cement (OPC) has long been traditionally and widely used as a binder in the manufacture of concrete. However, using OPC as a primary construction material has been questioned extensively over the last decades due to the environmental impact of clinker production and the huge cost of maintenance incurred over the lifetime of the structure. The production of Portland cement clinker emits up to 1.5 billion tons of CO_2 annually, accounting for about 5% of the total man-made CO_2 emission [4]. As versatile as it is, one principal dilemma of concrete structures is its high cost of maintenance which has been seen to go as high as 45% of the total infrastructure budget in the UK and EU [5]. This expensive maintenance

has been necessitated due to environmental factors, human factors, use over time, and microbial attack (especially in wet conditions) [6].

Other sources of GHGs includes farming and waste management practices that rely on the traditional disposal of solid waste in dump sites. In these dumps, the waste decomposes thereby releasing methane - an extremely potent GHG. Contemporary approaches to managing waste involve recycling, alternative uses of some waste materials, and ultimately advocating a zero-waste community (circular economy) [7]. The last few decades have witnessed a tremendous increase in waste generation due to industrialization, automation, urbanization, and rapid development of economics [8]. According to Kaza et.al [9], global waste generation was estimated at 2.01 billion tons in 2016 with a projection of 3.40 billion tons by 2050. In South Africa, the Department of Environmental Affairs (currently known as the Department of Fisheries, Forestry and the Environment) [10] reported that 42 million tons of general waste was generated in 2017 and only 11% was recycled. The report further particularized that biomass waste (from the sugar mills, sawmills, and paper and pulp industry) is the largest contributor generating up to 35% of the country's waste niche. Organic waste shadows closely at 16%, followed by construction and demolition waste at 13%, scrap metals at 8%, and commercial and industrial waste at 7%. It is on this fatal increasing trend that the pursuit for a circular economy finds its anchor. Circular economy seeks to eliminate waste by the continual use of resources. It engages the principles of reuse, sharing, repair, renovation, remanufacturing and recycling to create a closed system, curtailing the use of resource input and the creation of waste, pollution and emissions [7], [11]. In essence, All "waste" should become "food" for another process [12]. Example of these wastes include paper, tin cans, plastics, scrap metals etc.

It is in this vein, that researchers in the concrete industry have invested enormously into reusing food, agricultural and industrial waste as prospective Cement Replacement Material (CRM) [2] or additive in concrete. These wastes include sugarcane bagasse ash [13], bottom ash [14], fly ash [15], ground granulated blast furnace slag [16], palm oil clinker powder [17], palm oil fuel ash [15], rice husk ash

[18], eggshells [19], phlogopite [20]. CRMs and additives do not only improve the environmental credibility of the industry but may also improve concrete strength and durability depending on the pozzolanic activity of the CRM and the concrete.

1.2 PROBLEM DEFINITION

Firstly, in a world that is seeking to manage the climate change phenomenon, the construction industry, like many other industries is seeking ways to reduce its carbon footprint. One of the proposed instruments to achieve this is reducing the carbon content of the industry's input goods and services. The highest carbon content input in the construction industry is ordinary Portland cement (OPC) which is a binder substance that sets, hardens, and adheres to other materials, binding them together. The cement industry accounts for approximately 5-8% of global carbon dioxide (CO_2) emissions [21]. The production of cement generates both direct and indirect GHG emissions. Half of the industry's GHG direct emissions are from a process called calcination. The process involves the heating of limestone, i.e. calcium carbonate, which when heated forms calcium oxide and carbon dioxide. Indirect emissions include the burning of fossil fuels to heat the industry kilns usually heated by coal, natural gas, or oil, and the combustion of these fuels all of which produce GHG emissions. This accounts for approximately 40% of cement emissions [3].

Secondly, As versatile as it is, another principal dilemma of concrete and concrete structures is their high cost of maintenance which has been seen to go as high as 45% of the total infrastructure budget in the UK and EU [5]. This expensive maintenance has been necessitated due to environmental factors, human factors, use over time, and microbial attack (especially in wet conditions) [6].

The need to prolong the life of concrete while reducing the cost of maintenance has therefore necessitated various research with some aimed at inhibiting bacterial growth and biofilm formation. Among many other antimicrobial agents, silver and silver nanoparticles (AgNPs) is one of the most promising bacteria inhibitors [6,22].

Lastly, the concerning upward trajectory of waste production provides the basis for the concept of a circular economy. Circular economy aims to eliminate waste through the perpetual use of resources. This approach involves implementing practices such

as reuse, sharing, repair, renovation, remanufacturing, and recycling to establish a closed system that minimizes the utilization of resources and the production of waste, pollution, and emissions [7,11]. Essentially, the idea is that all "waste" should become "food" for another process [12]. Example of these wastes include paper, tin cans, plastics, scrap metals etc.

One of such waste is the eggshell. Globally, whole chicken egg production continues to rise with each passing year and with this increase comes the need to manage the shell waste. In 2008, 62 million metric tons was recorded. This grew to 76.7 million metric tons in 2018 and 86.3 million metric tons in 2021 [19,23,24]. Worthy of note is the approximately 10 million metric tons increase recorded between 2018 and 2021 (4 years), an increase that previously took about 13 years. With a shared mix of 452,000 tons of eggs in 2018, the South African poultry industry is not left behind. With a 10.2% shell content, these figures calls for a fast and decisive action especially when all other waste are put into context [25].

If the construction industry is to increase its contribution to reducing global GHG emissions, it must tackle the issue of cement linked emissions, maintenance of concrete infrastructure and the reuse of waste materials. This research explores the interconnectivity of these three issues with the principal focus on eggshell waste and its valorisation. The use of eggshells in concrete will not only exemplify the reuse of waste materials but also lead to reduction in maintenance cost and the associated GHG emission.

1.3 OBJECTIVES

Given the aforementioned challenges, the research seeks to meet three specific objectives encapsulated in the overarching objective of improving the cement and concrete production process by the use of waste eggshells, eggshell membrane, silver, and silver nanoparticles (to be used as additives, fine aggregate replacement, and antimicrobial agents) thereby resulting in greener cement/concrete with improved value chain, and yet possessing properties that compare favourably with OPC or transcends it. These are:

(i) Optimized calcination of waste eggshells to produce calcium oxide (CaO) while also upcycling the shell by membrane separation and protein leaching before calcination.

(ii) Production of optimised antimicrobial nanocomposite of separated eggshell membrane and silver nanoparticles. This is essential to produce an antimicrobial concrete mortal to drive down concrete maintenance cost.

(iii) Production of a Cytotoxic concrete mortar from the antimicrobial eggshell membrane in objective (ii).

1.4 LIMITATIONS

Due to the broad nature of waste and concrete research, this study will be primarily focused on eggshell as a waste material and its valorisation. The shell waste will be separated from its membrane while recovering other compounds before calcination. The separated membrane will used to produce an antimicrobial nanocomposite which will further be incorporated into cement mortar to produce an antimicrobial mortar. This research is not focused on concrete nor improving its mechanical properties. However, the optimised antimicrobial mortar will ensure that mechanical strength is not sacrificed for antimicrobial properties.

1.5 FRAMEWORK OF THE THESIS

This thesis consists of 7 chapters, of which the literature review and four results chapters have been published. Chapter 2 was published in *CRC Press Book by Taylor & Francis Group*, Chapter 3 was published in *Chemical Engineering Transactions*, Chapter 4 was published in *Biointerface Research in Applied Chemistry*, Chapter 5 was published in *Molecules* and Chapter 6 was published in the *International Journal of Molecular Sciences*. As a result, the materials and methods section in each of the chapters may appear repetitious. The chapters are presented as they appear in the journals, so they are presented with brevity and limitation in tables and figures. Appendices have been used to expound the chapters in this case. *As an author of the journal articles already published, the publishers give me the right to fully use my*

articles in a thesis without requests for special permission. The thesis is arranged following the outline below.

Chapter 1 provides a brief introduction to the research study in terms of motivation, objectives, and framework.

Chapter 2 gives a comprehensive description of past literature focusing on eggshell and its membrane, membrane separation techniques, eggshell valorisation, waste valorisation, and circular economy.

Chapter 3 gives a brief insight into eggshell membrane separation through leaching, and shell calcination to produce calcium oxide.

Chapter 4 provides an in-depth look at eggshell valorisation via acid leaching and shell calcination, leaching and calcination optimisation, as well as the recovery of leached collagen and other valuable compounds.

Chapter 5 describes the production of silver nanoparticles, adsorption of the nanoparticles on eggshell membrane and evaluation of the toxicity of an eggshell membrane/nano silver composite on microbes.

Chapter 6 evaluates the possibility of producing an antimicrobial concrete mortar from the membrane/nano silver composite.

Chapter 7 presents the overarching conclusions and recommendations arising from the thesis.

CHAPTER 2 REVIEW OF LITERATURES

From Waste to Best: Valorisation and Upcycling of Chicken Eggshells

Published in Waste Management (CRC Press): Refer to; Aina, S. T., Du Plessis, B. J., Mjimba, V., & Brink, H. G. (2022). From Waste to Best Valorisation and Upcycling of Chicken Eggshells. In Waste Management (1st ed., pp. 140–155). CRC Press. https://doi.org/10.1201/9780429341106-8.

Chapter Abstract

As the concept of Circular Economy takes centre stage in the world of waste management, it has consequently become more evident that environmental sustainability requires conversion of the outputs of a process into inputs of other processes. Circular Economy elevates the principles of reuse, sharing, repair, renovation, remanufacturing, and recycling to create a closed system, curtailing the use of virgin inputs as well as the creation of waste, pollution, and emissions. In a nutshell, all "waste" should become "food" for other processes, or better put, "from waste to best".

One example of waste with enormous potential are eggshells produced by the domestic chicken (*Gallus gallus domesticus*); these eggshells had an annual production of 7.82 million metric tonnes globally in 2018. This chapter examines the formation, structure, and constituents of the eggshell. It further discusses methods of separation of the eggshell and its membrane as well as the valorisation of the shell and membrane. It was concluded that eggshells stand as one of the most recyclable and eco-friendly waste products with applications in bioremediation, agriculture, food processing, health, construction, and renewable energy. A call was also made for the effective collection and reuse of the waste product.

2.1 INTRODUCTION

Modern approaches to managing waste amidst the challenge of managing climate change advocate for the alternative and continual use of resources in a bid to eliminate waste. One such approach called the circular economy elevates the principles of reuse, sharing, repair, renovation, remanufacturing and recycling to create a closed

system, curtailing the use of virgin inputs and the creation of waste, pollution and emission [11,26]. The tenet of the approach is that all "waste" should become "food" for another process [12]. One such waste material is eggshell whose disposal creates an acute ecological hazard [26,27].

Calcareous, porous, and bioceramic in nature, eggs are the reproductive means of all birds and most reptiles. Oval in shape after years of adaptive evolution, the chicken egg is just strong enough to fight physical and pathogenic attacks from the environment and also not too hard to allow for the exchange of gas and water needed for the development of a growing embryo inside the shell [28,29].

An eggshell (Figure 2-1) is made up of a calcified component (the shell) and a double layer of shell membrane. It is one of the best and most abundant sources for naturally occurring calcium (Ca) and Strontium (Sr) with up to 401 mg/g of Ca and 372 µg/g of Sr [30].

With the publication of the chicken *(Gallus gallus)* genome sequence in 2004, investigations into the composition, structure, and interactions of cellular molecules of the avian species has proceeded to unprecedented levels. These studies include but not limited to its breeding, biology, and physiology [31]. In 2008, the world production of eggs from domesticated chickens *(Gallus gallus domesticus*) was estimated at 62 million tonnes [23]. Through deliberate human efforts, ten years later, this value has grown to 76.7 million metric tonnes in 2018 [32].

In this mix, the Chinese poultry industry is the largest producer of eggs globally with a yield of about 458 billion eggs annually accounting for 42% of global production, followed by the United States (7%) and India (6%) [33].

In South Africa, the production of eggs in 2018 was 452,000 tonnes [25]. With production constantly rising, disposal of the waste shells will always be of huge concern. The shell makes up approximately 10.2% of the whole egg.

Eggshell comprises about 98% calcium carbonate ($CaCO_3$) and other trace elements such as magnesium and phosphorus. Shell membranes comprises 69.2% protein, 2.7% fat, 1.5% moisture and 27.2% ash.

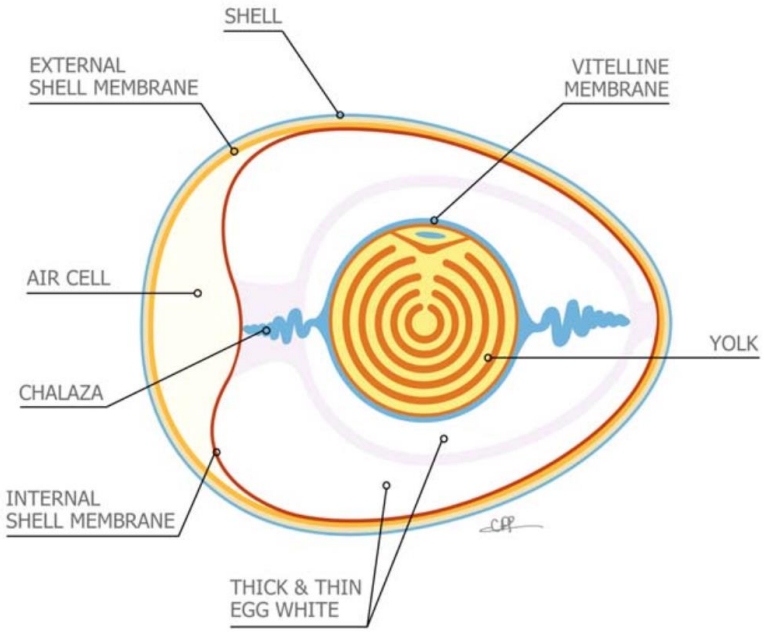

Figure 2-1: *Longitudinal section of a chicken egg [31].*

The membranes protein is about 10% collagen [28,31,34]. Eggshells have been effectively used as fertilizer in agriculture, soil stabilizer in construction, calcium supplement in health and medicine. Likewise, shell membrane collagen when extracted has diverse uses in medicine, biochemical, pharmaceutical, food and cosmetics industries. Collagen is a tough protein that connects and supports bodily tissues, such as skin, bone, tendons, muscles, and cartilage.

Traditionally collagen for industrial applications has primarily been extracted from swine skins, bovine and bones. However, following the outbreaks of bovine spongiform encephalopathy, foot and mouth disease, autoimmune and allergic reactions, restrictions on collagen usage from these sources have increased [31,35]. The fact that eggshell membrane collagen is very low in autoimmune and allergic reactions as well as high in biosafety but also has some of its characteristics similar to other mammalian collagen sources avails it to industrial application as an alternation to the traditional sources. An eggshell and its membrane can be separated by a wide variety of techniques including chemical, mechanical, steam, microwave and vacuum processes [29,34].

An interesting discovery is that calcium oxide can be produced through calcination of the shells. This avails eggshells as a plausible substitute for lime in cement

production and more important and relevant to this research, an alternative source of calcium addictive to geopolymer concrete with high early strength. This presents the possibility of a significant reduction in the cement-linked high carbon footprint of the construction industry. Elsewhere, results of studies carried out by [20,36–38] showed that eggshells proved to be a good alternative to conventional foaming agents in the production of foam glass.

Given the foregoing, this chapter examines the formation, structure, and constituents of the eggshell. It further discusses methods of separation of the eggshell and its membrane as well as the valorisation of the shell and membrane with applications in bioremediation, agriculture, food processing, health, construction, and renewable energy.

2.2 FORMATION AND STRUCTURE OF THE EGGSHELL

As stated earlier and perhaps commonly known, the eggshell is the outer covering of the avian egg as well as the shield for the growing embryo. Located at its centre is the yellowish yolk which is surrounded by the egg white, (known as albumen), inner and outer membrane, and the calcium-rich shell at the exterior [29,31]. Once ovulation takes place, the yolk moves through the oviduct to the uterus. The various components of the egg are added to the yolk during this journey [35,39] (Figure 2-1). The calcified shell which is made up of 98% $CaCO_3$ is a matrix of three distinctive layers [31] (Figure 2-2). The 100 µm thick mammillary layer initiates the formation of the calcified crystals. It is the innermost layer with an array of cones and infiltrates the outer membrane. Next is the palisade layer which is approximately 200 µm thick. This layer has pores which are responsible for the exchange of gases and water vapour. The calcite crystals or columns of the palisade layer are perpendicular to the shell membrane and eggshell surface [35,39].

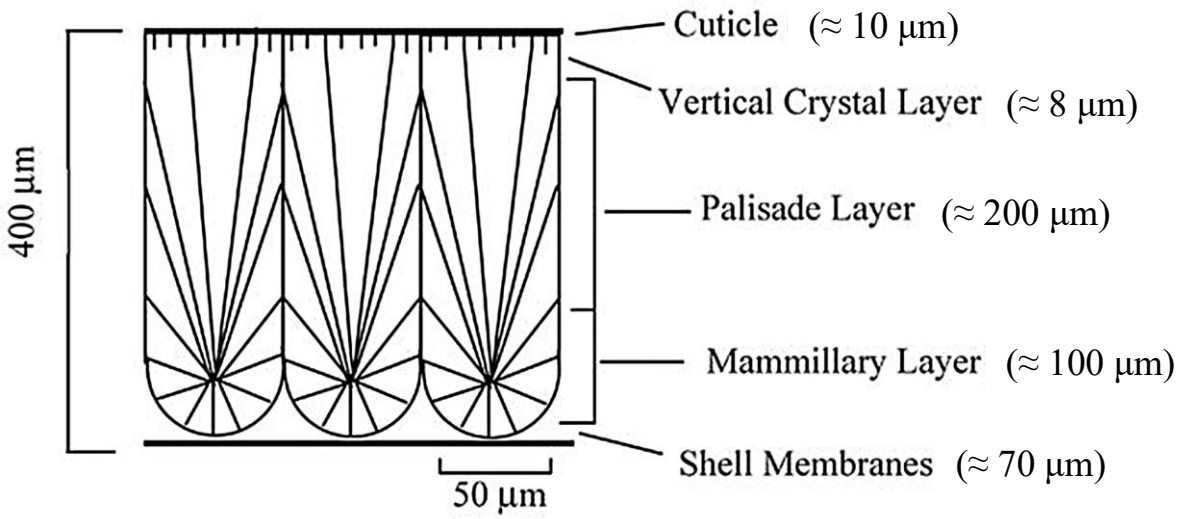

Figure 2-2: *Schematic diagram of the structure and different layers within the eggshell [39].*

The final outer layer of the shell which is also denser than the other two is the vertical crystal layer. It is a very thin layer of about 8 µm thick and provides a face for the development of the cuticle and also resists the propagation of cracks on the shell. The cuticle covers the eggshell. It is a thin organic proteinaceous layer, 10 – 30 µm thick, with protein content up to 90% [29,31].

An avian eggshell membrane is made up of collagen types I, V, and X [35]. The eggshell constitutes an inner and outer membrane. Each layer is a complex network of several layers of interwoven fibres. They are indispensable in the formation of the egg as they retain the albumen and prevent penetration of pathogens [28,39,40].

2.3 CONSTITUENTS OF EGGSHELL AND EGGSHELL MEMBRANE

A study by Balch and Cooke (1970) on the composition of eggshell membrane exemplifies the age-long interest in the make-up of eggshells. Elementally, an eggshell is about 98% $CaCO_3$ with up to 91.89% calcium (Ca) [41] and other elements as in Table 2-1. The membrane is known for its nitrogen content (Table 2-2). The calcined shell yields CaO with a purity as high as 98.3% (but 53.51% including loss on ignition) [26].

Table 2-1: *Percentage elemental composition of eggshells*

Element / Source	[42]	[43]	[44]	[45]	[41]	[46]
Ca	19.5	77.4	-	-	91.86	33.13
Al	-	0.4	-	-	1.45	-
Mg	-	0.24	-	-	-	0.36
O	57.3	12.9	29.46	27.32	-	-
Fe	-	-	-	-	-	-
K	-	8.6	-	-	0.52	0.04
Na	2.1	0.4	-	-	0.51	0.04
Si	1.1	0.06	-	-	4.32	-
C	6.3	-	13.09	10.61	-	-
S	-	-	0.03	-	-	-
N	11.6	-	0.54	-	-	-
Cl	1.1	-	-	-	-	-
P	1	-	-	-	-	0.07
H	-	-	0.35	0.71	-	-
F	-	-	-	-	0.44	-

Table 2-2: *Percentage elemental composition of eggshells membrane*

Element / Source	[42]	[44]	[45]
O	20.5	12.03	10.41
C	53.7	47.5	42.74
S	12.6	3	-
N	13.3	15.34	-
H	-	6.78	6.45

Beyond the elemental and oxide composition of eggshells, investigations into its biochemical and molecular component has been of great importance. The emergence of the chicken *(Gallus gallus)* genome sequence in 2004 created further success in understanding these components [29,31,35].

The chicken eggshell has been found to be a complex matrix of proteins and carbohydrates with 70% of it been proteins. Some of the amino acids (proteins) include ovalbumin, ovocleidin – 17, ovocleidin – 116, ovocalyxin – 25, ovocalyxin – 32, ovocalyxin – 36, osteopontin, clusterin, lysozyme, ovotransferrin and collagen with some of the composition proportions outlined in

Table **2-4**.

Table 2-3: *Percentage oxide composition of eggshells*

Oxide / Source	[47]	[48]	[49]	[26]
CaO	26.55	-	50.7	53.51
SiO2	0.11	-	0.09	0.02
Al2O3	0.03	0.207	0.03	0.01
MgO	0.01	-	0.01	0.66
Fe2O3	0.03	0.093	0.02	-
Na2O	0.14	-	0.19	0.12
P2O5	0.26	-	0.24	0.3
CaCO3	-	99.9	-	-
SO3	-	0.467	0.57	0.55
K2O	-	0.029	-	0.03
SrO	-	-	0.13	-
NiO	-	-	0.001	-
LOL	-	-	-	44.79

Table 2-4: *Amino acid composition of decalcified eggshell and eggshell membranes (Mol%)*

Amino acid	Eggshell	Inner shell membrane	Outer shell membrane [28]
Asx	8.1	8.4	8.8
Thr	6.2	6.9	6.9
Ser	9.7	9.2	9.2
Glx	11.8	11.1	11.9
Gly	13	11.1	10.6
Ala	6.9	4.6	4.1
Val	7.3	7.2	7.9
Met	2	2.3	2.3
Ile	2.6	3.3	3.4
Leu	6.1	5.6	4.8
Tyr	1.8	2.2	1.7
Phe	2.1	1.6	1.5
His	4.2	4.1	4.3
Lys	3.6	3.6	3.4
Arg	5.9	5.7	5.8
Pro	8.3	11.6	12
Hyp	0.3	1.5	1.4

Uronic acids, sialic acids, chondroitin sulphate A and B, dermatan sulphate, hyaluronic acids, and keratan sulphate are some of the polysaccharides (carbohydrates).

Ovalbumin, lysozyme, ovotransferrin are egg white proteins. Ovalbumin is reported to be confined to the mammillary layer of the shell while lysozyme and ovotransferrin can be found in both the mammillae and the shell membrane [29,50].

Ovocleidin – 17 is a homologous protein with composition as high as 40 µg/g in the shell. It was the first eggshell protein to be discovered. It is present throughout the shell matrix but concentrated in the mammillary layer. Ovocleidin – 116 is the first eggshell protein to be cloned and the most abundant (80 µg/g). Ovocleidin – 116 and Osteopontin are localized to the palisade region of the eggshell. Ovocalyxin – 32 is confined in the external region of the palisade layer, the cuticle, and the crystal layer of the eggshell. Ovocalyxin – 36 mostly occurs in the membrane and inner mammillary region of the shell [29,31,35,40,50]. Eggshells have also been found to contain certain hormones such as calcitonin and progesterone in nano measures [30].

2.4 SEPARATION OF EGGSHELL MEMBRANE AND EGGSHELL

The eggshell and its constituent membrane are proven store houses of several valuable bio-reactive compounds. Where these compounds are effectively harvested they are often put to profitable use thus accentuating the need for a means to efficiently separate the shell and its double layered membrane [51].

In [52], Inoue et al. patented a method and device for breaking and separating shell membrane from the eggshell with emphasis on taking advantage of the variation in the specific gravity of both materials. The shells are crushed in a pulveriser and separated by the centrifugal force of a liquid cyclone. The force pushes the shell to sink while the membrane floats to the upper part of the cyclone where it is collected. Monferrer and Pons, [53] secured a patent almost similar to that of [52]. The inventors demonstrated the use of a crusher to break the shells in a liquid medium with the option of employing additives. The liquid medium is then agitated to aid separation of the shell and membrane and also to force the separated shell to the bottom of the tank. The shell is collected from the bottom of the tank and the membrane from the top. The wet membrane and shell are then dried with the use of chemical or enzymes.

Another patent was published by MacNeil [51] seeking to increase the efficiency of the shell-membrane separation process and decrease energy intensity. This MacNeil approach, Figure 2-3, employs an abrading hopper to partially disrupt the linking structure between the shell and membrane, and also reduce the shell to sizes varying between 0.4mm and 0.5mm. The abraded constituents are then sent into a liquid tank, preferably water, where a sweep arm assembly (with the use of a motor) is used to stair the water and the slightly separated membrane-shell. This stirring completely separates the shell and membrane. The shell sinks to the bottom of the tank while the membrane floats at surface of the liquid medium.

The floating membrane is suctioned out of the tank, screened on a mesh belt to dewater it and subsequently dried and stored. The bottom shells are collected and transported to a second recovery device that involves drying after which the shells collected and use in a variety of applications.

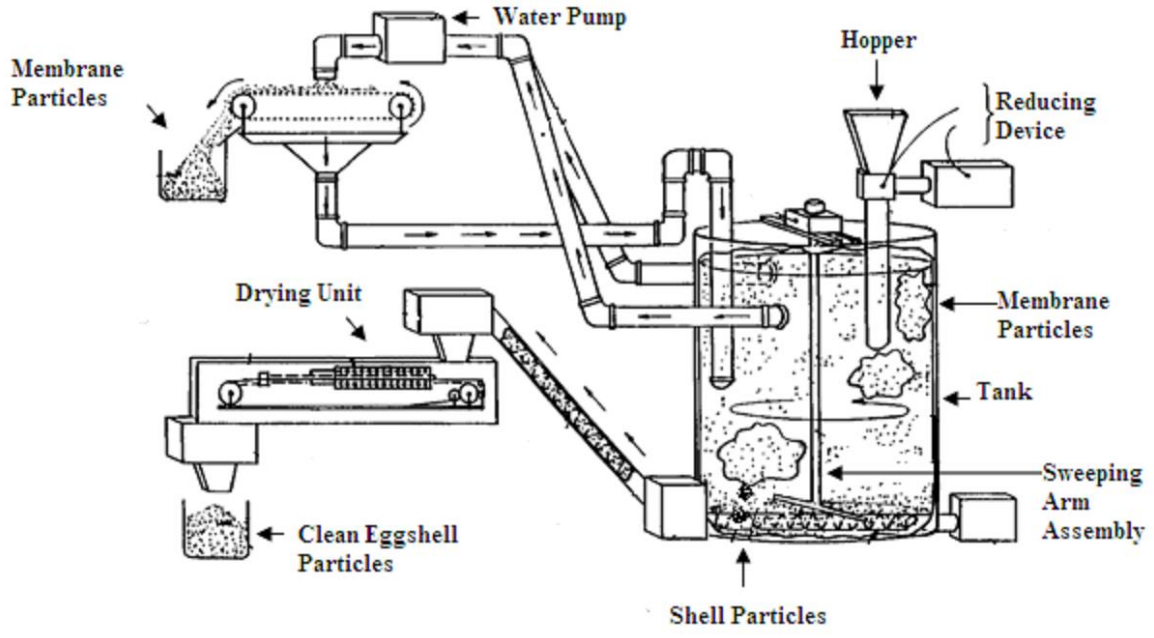

Figure 2-3: *Apparatus for separation of eggshell and membrane [51]*

Departing from the norm, Adams [54] patented another separation method emphasising the use of steam, mechanical abrasion and vacuum treatment. In his invention, Adams feeds broken eggshells to a processor which crushes the shells and employs steam to bake and moisturize the shells. At required moisture content, the

shell and membrane flakes are pulled by a vacuum into a cyclone device where the cyclonic action of the device forces the lighter membrane away from the heavier shells.

In 2011, Vlad and Ames [55] patented a method of separating eggshells and its membrane using acetic acid solution and cavitation force. The unseparated shells are placed in a fluid tank containing the acid solution. The acid solution weakens the bond between the shell and the membrane. Cavitation is then applied to the solution to pull the membranes away from the shell. The separated shell sink to the bottom of the tank where it is collected while the less dense membrane floats rises to the top where it is also collected. The method also includes a process of drying the separated shell and membrane and also grinding the shell before storage.

Following Vlad's [55] invention, Akikusa and Cao Qiu [56] also published a patent for a separation method with high recovery efficiency and without denaturation of the membrane proteins and also with a notable low energy consumption. The method begins by washing the eggshells to remove excess egg white and egg yolk. The washed shell is then immersed in a water tank and agitated. The agitation through a mixing blade causes turbulence in the tank, the water is pressurized with carbon dioxide to produce a concentrated aqueous solution. A microbubble generation process is used to produce microbubbles on the surface of the shells which in turn dissolves the papillary nucleus of the eggshell and weakens the bond between the shell and its membrane.

The combination of the turbulence from the mixing blade and papillary nucleus dissolution causes the membrane to separate from the shells. Separated membrane floats to the top of the tank and collected while the shells settle at the bottom and also collected. The method also provides for drying and storing the shells and membrane separately.

In 2013, another method of separation was patented by New, [57]. New's system used an airflow through a venturi to pulverize the eggshells and thereby separate the shell from the membrane. The process utilizes shock waves and pressure changes within the venturi to separate the brittle shells from the more elastic membrane. Separated

shells and membrane are then feed into a separation apparatus designed to collect the shells separately from the membrane.

The downside of these inventions includes energy intensity, high water consumption, incomplete separation, reduced usefulness of membrane due to milling, denaturalization and leaching of eggshell protein due to use of acid.

Moving away from patents, [29] proposed a method of separation of eggshell from its membrane using a microwave by taking advantage of the dielectric properties of the eggshell and membrane. In his research, Hussain discovered that shell membrane responds more to microwaves than the shells because the membrane has higher dielectric constant and loss. This in turn lead to the separation of both components.

The separation is premised on the fact that the membrane absorbs more electro-magnetic wave than the shell due to its high moisture content. This therefore causes a differential heating of the shell and membrane producing a weakening effect on the shell-membrane bond. The membrane is manually peeled off the shell.

The separated eggshells and its membrane have found tremendous application in construction, health, agriculture, food production, and remediation of water pollution. Six of these applications will be discussed in the next section.

2.5 VALORISATION OF EGGSHELL AND EGGSHELL MEMBRANE

2.5.1 Industrial Processes

Trends in industry-based research shows a growing focus on cost reduction, material sustainability and eco friendliness. In their research, Dwivedi et al. [58] investigated the use of carbonized waste eggshells in reinforcing 2014 aluminium alloy (AA2014) green metal matrix composites. The study showed that at a 12.5 wt.% addition, carbonized waste eggshells produced AA2014 alloy of better physical and mechanical properties when compared to AA2014 alloy reinforced with commercial $CaCO_3$. Likewise, Hayajneh et al. [27] examined the use of eggshells in the production of green metal composite. Eggshell particles were used to create an aluminium/eggshell green metal matrix composite. The outcomes revealed that the

aluminium-eggshell metal composite possess improved mechanical, microstructural, and tribological properties when compared to aluminium. At 3% addition of eggshell particles, wear resistance improved by 65%, compressive strength by 40%, and hardness increased by 15%. A similar study with corresponding result was also conducted by Shin et al. [59].

In the field of rubber technology, Bhagavatheswaran et al. [60] investigated the improvement of interactions between filler and acrylonitrile butadiene rubber (NBR) composite. The effect of two fillers (eggshell and $CaCO_3$) was studied. The addition of the functionalized filler resulted in an improvement in the maximum torque, Young's modulus, and elongation at break of the eggshell-NBR composite. A corroborating study earlier conducted by [61] exemplifies the use of eggshells as bio-filler in epoxidized natural rubber (ENR).

2.5.2 Agriculture

Due to its calcium and nitrogen content, ground eggshells have been identified as effective liming agent. This therefore makes eggshells an inexpensive and environmentally friendly fertilizer for plant growth [23,34,62]. According to PlantingScience.org [63], red clover plants showed a 10mm increase in growth when fertilized with eggshell powder as compared to other fertilizing agents. This fertilizing ability of eggshells was also confirmed by [23,64]. Oliveira, [9] also proposed a system for utilizing eggshells in the production of animal feed due to its high protein and calcium content.

2.5.3 Health and Food Production

Eggshell particles and its membrane are fast receiving wide acceptance in the health and food industry. Eggshells have been used as calcium supplements, treatment of osteoporosis, improvement of bone mineral density (BMD), [34,65,66]

Due to the numerous restrictions and difficulties accompanying the use of free enzyme, enzyme immobilization is a preferred alternative. In view of this and with

the aim of a cost effective immobilization technique, [67] studied the porogen effect of eggshell membrane powder as on the physicochemical structure and protease immobilization of chitosan-based macroparticles. It was observed that an addition of up to 20% eggshell membrane powder resulted into improved pore size of mesopores in chitosan which led into an increased diffusion of substrates into its internal spaces. Elizondo-Villarreal, [68] successfully synthesized hydroxyapatite (HAp) using CaO from eggshells and commercial calcium dibasic phosphate ($CaHPO_4.2H_2O$). Hydroxyapatite is an essential mineral in the human bone and teeth. These compounds are responsible for the rigidity of the teeth. Results shows that hydroxyapatite from eggshells is suitable for dental prosthesis applications. Similarly, [69] investigated the use of calcined eggshells in the synthesis of HAp using the wet chemical precipitation route. Their findings was in consonant with those of [23,68].

In [70], Ding eggshell membrane-templated gold nanoparticles was used as a flexible surface-enhanced Raman scattering (SERS) substrate for the detection of thiabendazole (TBZ) pesticide in Oolong tea. Due to its non-destructive nature and trace detection capability, SERS is gaining attention. The outcomes showed that eggshell membrane-templated gold nanoparticles were able to detect TBZ at a concentration of 0.1 ppm.

With focus on food preservation and post processing, [71] valorised eggshells into calcium chloride ($CaCl_2$) for the post processing of sweet potato chips. The eggshell $CaCl_2$ was used in comparison to commercial $CaCl_2$. The results showed that the eggshell $CaCl_2$ behaved similarly to the commercially sourced $CaCl_2$.

Collagen is a tough protein that connects and supports bodily tissues, such as skin, bone, tendons, muscles, and cartilage. Collagen has primarily been extracted from swine skins, bovine and bones. However, following the outbreaks of bovine spongiform encephalopathy, foot and mouth disease, autoimmune and allergic reactions, restrictions on collagen usage from these sources were enforced. Eggshell membrane collagen is very low in autoimmune and allergic reactions as well as high in biosafety and is of similar characteristics to other mammalian collagens. [29,34].

Collagen from eggshell membrane has found wide usage in production of adhesives [34], plastic surgery [72], improving skin health and joint pain relive [73], cosmetics and pharmaceutical industries [74]. Partial hydrolysis of collagen produces gelatine, a flavouring agent in food production [23,75,76].

2.5.4 Construction

The versatility and universality of concrete rests in its ability to withstand harsh environments, attain enormous strength and durability. It is obtained by mixing cementitious materials, water, aggregate and sometimes admixtures in required proportions [77]. Calcium oxide (quicklime) derived from the calcination of limestone has been proven to be responsible for the early strength development of concrete at room temperature. This is achieved by the hydration of CaO to form Calcium hydroxide causing evolution of heat and therefore high early strength [77,78].

The average value of quicklime in 2018 was $124.60 per tonne [79], resulting in a potential market value of eggshell derived quicklime of $550 million globally in 2018. The current lime production in South Africa is 1.2 million metric tonnes per year [79], meaning the local production of 452,000 tonnes of eggshells, potentially yielding 252,000 tonnes of lime, has the potential to substitute as much as 21% of the South African lime market. Currently, most of these waste eggshells are disposed of in landfills that have inherent high management cost [80]. According to [78], while the percentage composition of CaO in ordinary Portland cement can be as high as 66.89%, it ranges between 0.02% and 8.4% in cement replacement materials (CRMs) except for ground granulated blast furnace slag where it can be as high as 45.38%. This low composition of CaO has therefore necessitated the curing of geopolymer concrete at elevated temperatures ranging between 60 and 70 ℃. Research has shown that a 2% addition rate has an equivalent cure strength at 50 °F as plain concrete at 70 °F [81]. This claim was also backed up by Huang et al. [82] when he opined that up to 5% increase in calcium content of geopolymers will result in considerable increase in early strength development at room temperature. In addition, to substantial

increase in early strengths, calcium in chloride form improves workability, and reduces settlement [81,83].

Evaluating the quality of CaO derived from calcined eggshells, [26] lectured that calcium oxide from eggshells belonged to the most reactive class of lime (R5-60 °C in 10 min), which is the class of calcium oxide from limestone. Jaber, [84] realised the same using calcined and un-calcined eggshells as cement replacements in mortar. These results show that the replacement of cement with eggshells improves the strength and workability of the mortar. However, calcined eggshells, CaO gave more promising results.

In the same vein, Ofuyatan et al. [85] investigated the use of eggshell powder as a partial replacement for cement in self-compacting concrete. The results revealed that, at 20% partial replacement, compressive strength was 41 kN/mm^2 and flexural strength was 3.2 kN/mm^2 after 28 days.

Further, [86] explored the use of eggshell powder as a partial replacement for cement in a grade 20 concrete. Results showed that, at a 5% replacement level, the mechanical properties of the concrete improved. Compressive strength at 0% and 5% replacement was 21 and 26.30 N/mm^2 respectively after 28 days while the split tensile strength at 0% and 5% replacement was 2.45 N/mm^2 and 2.98 N/mm^2 respectively after 7 days.

Raji and Samuel [87] also examined the use of eggshell powders as full replacement of fine aggregate (sand). The result was not adequate for a normal weight concrete as compressive strengths were low. They concluded that eggshells should only be used as full replacement of fine aggregate where lightweight concrete is desired.

Cree and Pliya [88] investigated the use of eggshell powders for masonry applications and concluded in favour eggshell powder. They concluded that eggshell powder can be used as alternative supplementary cementitious material (SCM) in mortar at a replacement level as high as 20% and still be within ASTM standards.

Still in the move of valorising eggshells, Tiong et al. [48] effectively incorporated eggshells into lightweight foamed concrete. Lightweight concrete incorporated with

eggshell powder exhibited increased compressive strength and ultrasonic pulse velocity (UPV) at a replacement level of 7.5%.

In the field of transportation engineering, eggshell lime has been found to be an effective stabilizing agent. Bensaifi et al. [89] investigated the use of calcined eggshells in stabilizing marl. From there investigation, CaO form eggshells significantly improved the mechanical properties of marl. At 15% composition the stabilized soil had 22 times increase in CBR index and an improvement in cohesion and internal friction angle.

Casting the focus on dielectrics and high voltage insulation, Abdelmalik et al. [90] explored the use of eggshell composite polymer for power insulation. The composite polymer was mixture of eggshells and epoxy resin in contrast to a mixture of titanium oxide nanoparticles TiO_2 and epoxy resin. The eggshell composite displayed better dielectric and insulation properties than TiO_2 composite. The dielectric constant was directly proportional to the percentage of eggshell particles added with values as high as about 7 at 5% eggshell content. The insulation property was derived as a measure of the conductance of the composites. Eggshell composite had the lowest conductance (i.e. best insulation property) at 3% content with a conductance of about 2.70×10^{-9} S. The TiO_2 composite had a conductance of about 4.90×10^{-9} S. [42,43] and [91] also conducted a similar study with agreeing results.

Arunya [92] further testified to the reusability of eggshell powder in the bid of promoting circular economy and environmental friendliness of the construction industry.

2.5.5 Renewable Energy

As petroleum price continues to rise and the need for energy soars, there is a daring need for a cheap and sustainable source of energy [93–95].

In their research, Ajala et al. [93] used thermally modified chicken eggshells as heterogeneous catalyst for palm kernel biodiesel production. Employing a definitive screening design of optimization technique, 4% calcined eggshell as catalyst yielded a 97.10% pure biodiesel fuel. The produced biodiesel was found to be of ASTM

standard. In the same vein, Gupta and Rathod [94] derived a solid based catalyst for biodiesel production from eggshells and waste cooking oil. Results yielded up to 96.07% pure biodiesel under optimized conditions with a reusability of up to 5 cycles. Kavitha et al. [95] produced biodiesel from scum oil and nano calcined eggshell yielding 96% pure biodiesel in 3 hours with methanol: oil ratio of 6:1 and 2.4% by weight of catalyst at 65℃. The fuel had low NOx and high cetane number. Similarly, Wong and Ang [96] also produced a high quality biodiesel from used cooking oil and calcined waste eggshells. The yielded fuel was optimum at 65 ℃ temperature, 2% catalyst, and methanol oil ration of 4:1. Using eggshells as catalyst for biodiesel production has also been proposed by [23].

While the refining of petroleum has given rise to numerous valuable products, it is also responsible for a number of harmful ones. Among these are volatile organic compounds (VOCs). These carcinogenic gases are not only poisonous to humans but also detrimental to the environment. They have been found partly responsible for greenhouse effects and stratospheric ozone depletion [97]. In the bid of solving the problem of VOCs, Li investigated the use of eggshells $CaCO_3$ as a catalyst with Co_3O_4 in the oxidation of VOCs in comparison with commercial $CaCO_3$. Results revealed that the catalyst produced using eggshells had higher VOC oxidation power than commercial $CaCO_3$.

2.5.6 Bioremediation, and Removal of Metals and Non-Metals.

Rapid industrialization and improvements in mining technology came with the problem of various forms of contamination of water bodies and the soil [45]. The removal of these toxic pollutants has been extensively researched. The research is centred around the use of various methods including osmosis, adsorption, precipitation, photodegradation, and electro-dialysis, among others. Irrespective of the method, the process of decontamination can be very expensive [45,98]. This raises the impetus for finding low-cost decontaminants.

Seeking to alleviate the problem dye pollution from textile industries, Tsai et al. [44] evaluated the adsorption properties of eggshells and shell membrane on basic blue 9

(Methylene blue). The eggshell particle was able to take up to 0.80 mg/g while the membrane had lower adsorption of 0.24 mg/g. A similar investigation was carried out by [99]. The authors examined the use of eggshells in the removal of direct blue 78 dye form wastewater. The eggshell adsorbent was 95% effective at pH 5. Maximum capacity of adsorption was 13 mg/g. In 2018, Al-Ghouti and Khan [100] investigated the application of eggshell wastes for boron remediation from water. Results showed that calcined eggshells had the best boron removal property of 96.3% at pH 6. Additionally, Borhade [101] further examined the use of eggshells calcined at 120 ℃ for 2 hours in the removal of Rhodamine B, Eriochrome black T and Murexide dyes from aqueous solutions. The results showed that calcined eggshells can be used as adsorbents for the dyes with an adsorption capacity of 2 mg/L. As photocatalysis continues to gain a wider usage spectrum, Sree et al. [102] successfully valorized eggshells for use in photodegradation. Nanoparticles of CaO from calcined eggshells were synthesized and examined for photocatalytic dye degradation of Methylene blue and Toluidine blue solution. The investigation revealed that at pH 7, 50 mg of catalyst loading, and 20 ppm dye concentration, CaO nanoparticles optimally degraded Methylene blue within 15 min and Toluidine blue within 10 min.

Likewise, the adsorption properties of sonicated raw eggshells was found impressive by Ahmad et al. [103]. The adsorption capabilities of sonicated raw eggshells for Sulphur dioxide (SO_2) and Hydrogen sulphide (H_2S) was studied. At a constant gas flow rate of 300 ml/min, 80 ℃ sonication temperature and 3 hours contact time, sonicated raw eggshells adsorbed 2.4 mg/g of SO_2 and 1.85 mg/g of H_2S.

The concern for the treatment of waterbodies and soils contaminated with heavy metals is globally gaining attention due to its adverse effect on the life of humans, plants and microorganisms [104]. In this regard, Ashrafi et al. [105] studied the effect of using eggshell and banana stem amendments to immobilize lead (Pb), cadmium (Cd) and zinc (Zn) in a contaminated soil. The study revealed that eggshell powder was able to reduce the concentration of Pb, Cd, and Zn in the contaminated soils by transforming their readily available forms to less accessible fractions while banana stem reduced only Cd. These claims have also been backed up by [106,107].

Mashangwa, [86] and his team demonstrated the adsorption power of eggshells over Pb, Zn, copper (Cu), nickel (Ni), and other heavy metals. At pH 7, 7 g adsorbent, 100 ppm metal ion and 360 min contact time. Pb, Zn, Cu, and Ni had percentage adsorption of 97%, 80%, 95%, and 94% respectively. Other metals such as aluminium (Al), iron (Fe), and potassium (K) recorded adsorptions of over 75%. Rahmani-Sani, [87] on the other hand employed chicken feathers and eggshells in the synthesys of a novel magnetized activated carbon for sorption of heavy metal ions. The results on the sorption of Pb^{2+}, Cd^{2+}, Cu^{2+}, Zn^{2+}, and Ni^{2+} ions testified of the adsorption efficiency of eggshells. Furthermore, Oke et al. [108] examined the adsorption kinetics for arsenic removal from aqueous solutions by untreated powdered eggshell. The result revealed that 63 µm eggshell powder at a pH of 7.2 removed up to 99.6% of 1.5 mg/L of arsenic ion in synthetic water in 6 hours. 100% removal was recorded in 8 hours. It was also observed that particle size affected the rate of arsenic removal and smaller particles yielded a faster rate of removal.

Using a hybrid system of calcined eggshells and microalgae *(Chlorella vulgaris)*, Choi and Lee [41] demonstrated the removal of heavy metals form acid mine drainage (AMD). The hybrid system in an optical panel photobioreactor had a biomass productivity of more than 8 times its initial concentration and light transmittance of 95 % at a depth of 305 mm. Iron (Fe), Cu, Zn, Cd, Arsenic (As), and Manganese (Mn) was effectively removed from the AMD. Calcined eggshells had about 80% removal capacity while the hybrid system reported as high as 100% removal efficiency of the metals. Following the growing concern for the depletion and irreplaceable nature of phosphorus, [109] discovered a Novel eggshell based adsorbent for the removal of phosphorus from liquid effluents. The adsorbent showed 50% efficiency in an acid to neutral environment.

Other studies on the valorisation of eggshells includes, co-precipitation of chromium (Cr) VI [110], oxidation of methane [111], and water/wastewater decontamination [45].

The continuous use of eggshell and its membrane in all these applications pose an eminence benefit environmentally and economically.

2.6 CALCIUM SILICATE HYDRATE GEL

The main reaction product of cement hydration is the Calcium Silicate Hydrate (CSH) gel with chemical formula $Ca_5Si_6O_{18}H_2.nH_2O$, which constitutes over 60% of the volume of hydrated Portland cement [112,113]. This gel plays a crucial role in the durability and strength of both cement and concrete. Despite its widespread presence, the structure of CSH is not completely understood. The varying stoichiometry poses challenges in accurately characterizing its nanostructure. However, it has been reported that CSH gels exhibit a three-dimensional atomic structure resembling naturally occurring tobermorite. This structure features a layered geometry primarily composed of calcium silicate sheets, containing chain units of silicates connected by calcium ions [112,114]. CSH is a porous gel with gel pores ranging from 5 Å to 100 Å and capillary pores exceeding 100 Å. These pores function as conduits for the transportation of water molecules and ions [115].

The efficacy of concrete depends on the nanoscale organizational structure of the hydration products constituting concrete, as opposed to the material itself. Consequently, it is plausible to enhance concrete performance by controlling the nanoscale structures of cement hydration products. This adjustment alters the mechanical properties and durability of concrete without escalating the cement content. In essence, it reduces the need for cement while ensuring the desired performance, showcasing significant potential for reducing the carbon footprint in the concrete industry [116,117].

2.7 CONCLUSION

After examining the developments in egg production and applications, it is evident that the production will increase to meet growing global demand. Simultaneously, waste from the industry will grow. The demonstrated alternative uses of all the components of eggshells offers avails opportunities to minimise the number of eggshells that are disposed of in municipal waste dumps or other disposal sites. These uses inter alia include application in aluminium alloys and rubber production, uses in

the agriculture industry, in the energy sector, and the use of eggshells and membrane to remove various metals, non-metals, and dyes from wastewater.

From these and other uses, it is evident that eggshells are not just a waste material. Instead, they are and can be a useful input material in many industries. This is the essence of the circular economy concept. In this context this fact gives eggshells a monetary value to companies that generate this waste. The value is in the collection, treating and use of this material. Industries in these activities can provide employment and other industrial innovations that aid economic development. Also important is that the shells have an environmental management value in that they reduce the use of carbon-intensive materials in some industrial process most prominently in the production of cement. This is key to the demands of sustainable development- a growing requirement of the 21st century.

In this milieu, players in the egg industry (producers and consumers) are therefore called upon for strategic collaboration among themselves to aid effective collection and delivery of eggshells to organisations that use this 'waste' material as a raw material. To this end, governments are also critical is formulating policies that can direct the management of this product.

CHAPTER 3 EFFECT OF MEMBRANE REMOVAL ON THE PRODUCTION OF CALCIUM OXIDE FROM EGGSHELLS VIA CALCINATION

Published in Chemical Engineering Transactions: Refer to; Aina, S. T., Du-Plessis, B. J., Mjimba, V., & Brink, H. G. (2020). Effect of Membrane Removal on The Production of Calcium Oxide from Eggshells Via Calcination. Chemical Engineering Transactions, 81, 1069–1074. https://doi.org/10.3303/CET2081179.

Chapter Abstract

In the pursuit of a circular economy and against a background of viable alternative uses of avian eggshells and eggshell membranes, this research investigated the effect of domesticated chicken eggshell membrane separation on the calcination process and quality of Calcium Oxide (CaO) produced. Acetic acid was used to leach the eggshells for 60 min to aid separation of the shell membrane. X-ray diffraction, red, green, blue colour model, and thermogravimetric analyses were used to characterize the calcined shells. Leached and separated shells produced CaO of comparable quality and crystallinity to unseparated shells after calcination. Results showed that while leaching and membrane separation did not affect calcination temperature, residual ash from the membrane left impurities in the unseparated shells after calcination. It was concluded that leaching and separating the membranes from eggshells prior to calcination serves to upcycle eggshells by facilitating improved CaO production and membrane value extraction.

3.1 INTRODUCTION

The adverse impacts of climate change are arguably the prime focus of the twenty-first century's global dialogues seeking to improve human economic and social wellbeing. Climate change influences almost all human activities demanding urgent and decisive action to address the adverse impacts while simultaneously exploiting any opportunities to advance human wellbeing [1]. The focus of managing climate

change has been and remains two-pronged: learning to live with the adverse impacts of this phenomenon – the essence of adaptation on one hand – and retarding or halting the increase of anthropogenic atmospheric greenhouse gases (GHGs) – the essence of mitigation on the other hand.

A major source of anthropogenic GHGs (also called carbon emissions) is the burning of fossil fuels for direct and indirect energy supply in commercial and social activities. Other sources include farming and waste management practices that rely on the traditional disposal of solid waste in dump areas. In these dumps, the waste decomposes releasing methane - an extremely potent GHG. The contemporary approach to managing waste and (tacitly) climate change encourages recycling, alternative uses of some waste materials [1], and ultimately advocating a zero-waste community (circular economy).

The global awareness for the need to reduce carbon emissions has encouraged investigations on the use of alternative cementitious materials for concrete production [2].This focus arises from the realisation that the production of Portland cement clinker emits up to 1.5 Gt carbon (often expressed as carbon dioxide – CO_2) annually. These emissions account for approximately 5 % of the total man-made CO_2 global emissions [4,118]. CO_2 in the atmosphere is now above 400 ppm and by far exceeds the pre-industrial benchmark levels [119]. Simultaneously, the last few decades have witnessed a tremendous increase in waste generation due to increased industrialization and urbanization [8]. According to [9], global waste generation was estimated at 2.01 Gt in 2016 with a projection of 3.4 Gt by 2050. In South Africa, [10], the Department of Environmental Affairs reported that 42 Mt of general waste was generated in 2017.

Traditional approaches to the management of waste are disposal in dumpsite or incineration. Both methods contribute to GHG emissions. Modern philosophies of managing waste and the challenges of managing climate change advocates for the continual optimization of resource utilisation in the bid to eliminate waste. One such approach, called the Circular economy, elevates the principles of reuse, sharing, repair, renovation, remanufacturing, and recycling to create a closed system,

curtailing the use of virgin inputs and the creation of waste, pollution, and emission [11]. The tenet of the approach is that all "waste" should become "food" for another process [12].

Currently, the major contribution of CO_2 in the production of Portland Cement is the calcination of $CaCO_3$ to quick lime (CaO), releasing one mole of CO_2 per mole of CaO produced (786g CO_2/kg CaO produced). A plausible alternative binder to cement is a class of alkali alumino-silicates called geopolymers or alkali-activated materials (AAM) [120]. AAMs presents a dual advantage. Firstly, they help reduce the carbon footprint of the construction industry as a result of their production from agricultural and industrial by-products and secondly, they aid in reducing the cost associated with waste management and disposal. However, because of their low calcium oxide content, geopolymers need to be processed at high temperatures to achieve comparably high early strength to conventional cement used in the construction industry. Where this heating process is fossil fuel-driven, the process directly contributes to GHG emission. Therefore, it remains necessary to find a means of reducing or eradicating this heating process. Investigations by [78] showed that CaO is responsible for the early strength development of conventional concrete at room temperature. In the same vein, [77] opined that the addition of CaO to geopolymers aids early strength development in room temperature.

The production of CaO through the calcination of eggshells makes it a plausible substitute for lime in general. The world production of eggs from domesticated chickens (*Gallus gallus domesticus*) was estimated at 76.7 Mt in 2018 [19] while the local South African production of eggs in 2018 was 452,000 t [25]. The calcified eggshell and double layer membrane of the egg makes up approximately 10.2 % of the whole egg (i.e. 7.82 Mt globally and 46,100 t locally in 2018). The average value of quicklime in 2018 was $124.60/t [79], meaning a potential market value of eggshell derived quicklime of $550 M globally in 2018. The current lime production in South Africa is 1.2 Mt/y [79], meaning the local production of 452,000 t of eggshells, potentially yielding 252,000 t of lime, has the potential to substitute as much as 21 % of the South African lime market. Currently, the majority of these

waste eggshells are landfilled with a high associated management cost [80]. However, research works involving the calcination of eggshells have often been done by calcinating the entire shell [121], including its constituent proteins and membrane [122].

Eggshells consist of about 98 % calcium carbonate and other trace elements such as magnesium and phosphorus. The remaining mass consists of the shell membrane comprising of 69.2 % protein, 2.7 % fat, 1.5 % moisture and 27.2 % ash. The membrane protein consists of about 10 % collagen [34]. Eggshells have been used as fine aggregate in concrete [87], fertilizer in agriculture, soil stabilizer in construction, and calcium supplements in health and medicine. Likewise, extracted shell membrane collagen has diverse uses in medicine, biochemical, pharmaceutical, food, and cosmetics industries. Collagen is a tough protein that connects and supports bodily tissues, such as skin, bone, tendons, muscles, and cartilage. Collagen has primarily been extracted from swine or bovine skins, hooves, and bones. However, following the outbreaks of bovine spongiform encephalopathy, foot and mouth disease, and autoimmune and allergic reactions, restrictions on collagen usage from these sources were enforced. Eggshell membrane collagen is very low in autoimmune and allergic reactions as well as high in biosafety and is of similar characteristics to other mammalian collagens [34]. Eggshells and its membrane can be separated by a wide variety of techniques including chemical, mechanical, steam, microwave, and vacuum processes [29].

Against the backdrop of the importance of CaO to the construction industry and alternative use of eggshell membranes, this research seeks to evaluate the potential of producing CaO from eggshells via acetic acid leaching and calcination, simultaneously upcycling the eggshell by separating its membrane for other uses before calcination. The process was evaluated and characterized by pH, X-ray diffraction (XRD), red, green, blue colour model- (RGB), and thermogravimetric (TGA) analyses to assess how membrane separation and leaching affects the calcination and subsequent CaO quality.

3.2 MATERIALS AND METHODS

3.2.1 Experimental Methods

Eggshells were collected from eateries within the Hatfield campus of the University of Pretoria and the Hatfield Plaza mall, in Pretoria, South Africa. To decontaminate the shells, they were washed repeatedly in ultra-pure water, dried at 60 °C for 60 min in an EcoTherm oven and stored within 24 h of collection.

For the leaching rate experiments, 20 g of eggshells were leaching in 13 sacrificial reactors containing 500 mL of 1 mol Acetic acid each. After pH measurement, the entire contents of each reactor were sieved and washed with distilled water and dried to constant weight at 60 °C. The pH of a 14^{th} reactor was measured in parallel for 180 min to monitor the $CaCO_3$ loss over time.

For the calcination experiments, 1 mol of acetic acid was used to leach the shells and aid membrane separation using 250 g of eggshells in 1,000 mL of the solution under gentle stir in a plastic jug. Leaching was carried out for 60 min at room temperature. The membrane separation was done by removing the membrane from its shell by hand. Samples of 20 g shells (unseparated and separated by leaching for 60 min) were calcined using a Carbolite CWF1100 furnace in the presence of oxygen at 700 °C and 900 °C for 30 min, 1 h, 3 h and 5 h. Unseparated shells and shells separated after 60 min are hereafter referred to as US, and S60.

3.2.2 Analytical Methods

The pH was measured instantaneously using GOnDO software (GOnDO Electronic) with a special purpose pH probe connected to an Ezodo PL-700PC meter. The change in mass was determined by the difference in the initial and final mass for each sacrificial reactor. Thermal analysis was conducted with the use of TGA5500 thermogravimetric analyser. The change in mass was measured with an increase in temperature from room temperature to 950 °C at a heating rate of 10 °C/min in the presence of nitrogen.

RGB colour analysis was performed using Image J software to observe the colour change in the samples due to change in temperature. A 13-megapixel digital camera was used to take pictures of the samples after calcination at constant distance and lightning condition. The software separated the images into their red, green, and blue colour spectrum. The red component was used for the analysis due to the additive nature of the colours; a value of 255 indicates a pure white sample.

The raw shells and samples calcined for 5 h at 900 °C was subjected to X-ray diffraction (XRD) analysis to determine the mineralogy of the shells before and after calcination. The samples were prepared according to the standardized Panalytical backloading system, which provides a nearly random distribution of the particles. The samples were analysed using a Panalytical X'Pert Pro powder diffractometer in θ–θ configuration with an X'Celerator detector and variable divergence - and fixed receiving slits with Fe filtered Co-Kα radiation (λ=1.789Å). The mineralogy was determined by selecting the best–fitting pattern from the ICSD database to the measured diffraction pattern, using X'Pert High score plus software. The relative phase amounts (weight% of the crystalline portion) were estimated using the Rietveld method using Autoquan/BGMN software employing Fundamental Parameter Approach.

3.2.3 Chemical Model used to Estimate $CaCO_3$ Mass Leached

The model assumed that all reactions in the leaching process were limited by the rate of $CaCO_3$ dissolution to the medium (reaction 3.1):

$$CaCO_3 \rightarrow Ca^{2+} + CO_3^{2-} \quad (3.1)$$

Therefore, it was assumed that the interactions between the carbonic species, the acetic species, and the medium were at pseudo equilibrium conditions (Eq 3.2-3.4):

$$HAc \rightleftharpoons H^+ + Ac^-, pK_A = 4.76 \quad (3.2)$$

$$HCO_3^- \rightleftharpoons H^+ + CO_3^{2-}, pK_A = 10.25 \quad (3.3)$$

$$H_2CO_3 \rightleftharpoons H^+ + HCO_3^-, pK_A = 3.60 \quad (3.4)$$

The system of equations used to predict the amount of $CaCO_3$ leached at each time step are shown in equations:

$$\frac{[Ac]}{[HAc]} = 10^{-4.76+pH} \quad (3.5)$$

$$\frac{[CO_3^{2-}]}{[HCO_3^-]} = 10^{-10.25+pH} \quad (3.6)$$

$$\frac{[HCO_3^-]}{[H_2CO_3]} = 10^{-3.60+pH} \quad (3.7)$$

$$[Ca^{2+}] = [CO_3^{2-}] + [HCO_3^-] + [H_2CO_3] \quad (3.8)$$

The concentration of calcium in solution would be equivalent to the amount of $CaCO_3$ leached (in molar units) and was therefore used to determine the mass of $CaCO_3$ leached from the eggshells.

3.3 RESULTS AND DISCUSSION

As expected, 1M Acetic acid leaches $CaCO_3$ from the shell into the solution and this results into an increase in pH and mass loss in the eggshell. The mass loss was measured over 60 min and plotted with the change in pH as seen in Figure 3-1a.

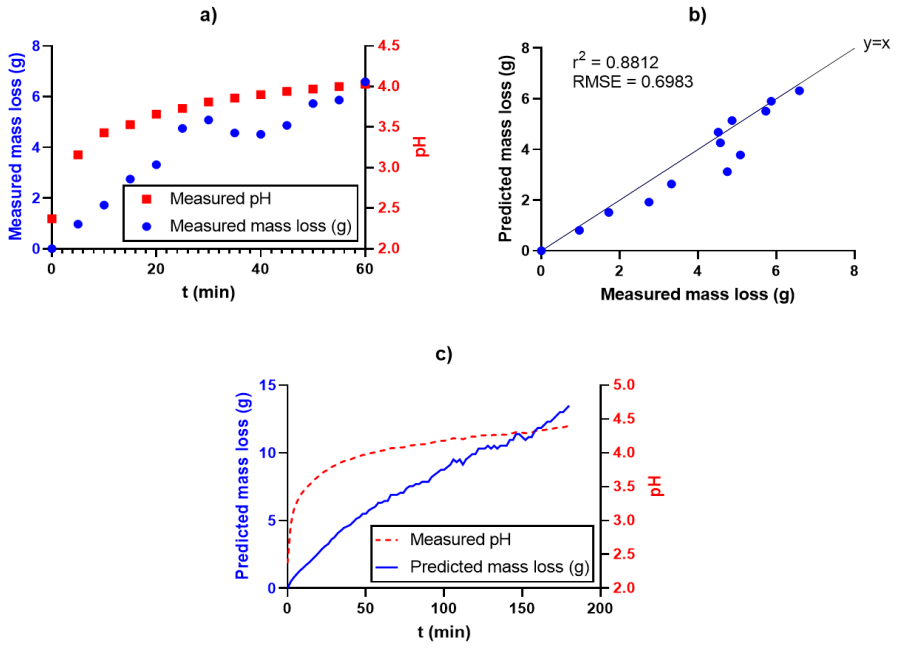

Figure 3-1: *Leaching kinetics. a) Change in pH and measured mass loss of eggshell in acetic acid, b) Parity plot of the measured mass loss and the predicted mass loss*

using Eq 3.5-3.8, c) Predicted mass loss estimated from the measured pH using Eq 3.5-3.8.

This reveals that after 60 min of leaching, about 6 g (30 %) of $CaCO_3$ was dissolved into the solution. The predicted amount of $CaCO_3$ lost using Eq (3.5) – Eq (3.8) correlated well with the m easured values as shown in Figure 3-1b. The pH and predicted $CaCO_3$ mass loss Eq (3.5) – Eq (3.8) from the measured pH values are shown in Figure 3-1c revealing that about 15 g (75 %) of $CaCO_3$ was dissolved in the solution after 180 min of leaching. These results show that one of the most potentially significant limitations of the leaching method for membrane removal would be the amount of $CaCO_3$ lost to the solution as a result of the leaching.

Thermal analysis plots comprising of the TG spectra of US and S60 shells, as well as the membrane, are seen in Figure 3-2. US and S60 samples began with a linear reduction in weight due to loss of moisture up to 300 °C after which US samples records a nonlinear reduction due to the volatilization of its membrane constituent. Both shell samples continued the linear path until about 650 °C. All water, protein, and carbon constituents of the shells are evaporated, and actual calcination sets in. As seen in the plot, separated shells were fully calcined at 720°C while unseparated shells became fully calcined at 735 °C. On the other hand, the shell membrane which is less dense than the shells turn completely into ash after 300 °C, leaving approximately 10% weight at >700°C. A potential source of impurities in the US samples.

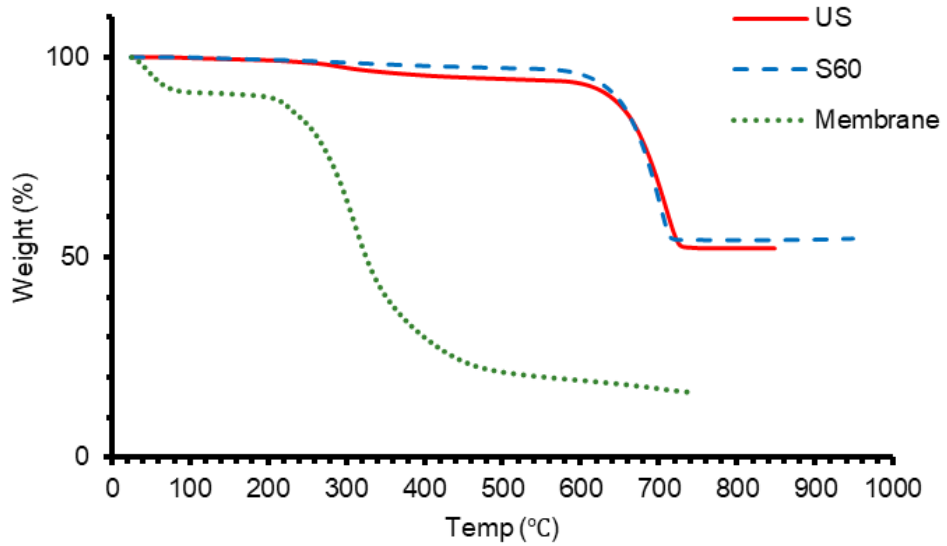

Figure 3-2: *Thermogravimetric analysis of the US, S60, and membrane only in the presence of nitrogen*

RGB results in Figure 3-3 shows the trend of the colour change of the calcined US shells from light brown (242) to dark brown (127), grey (148), and finally, light grey (245) at 900 °C; the carbon in the samples undergo carbonization during the initial stages of calcination (darkening) followed by combustion to CO_2 (whitening). In contrast, it was observed that the samples leached for 60 minutes did not get as dark as the US samples at either 700 °C or 900 °C. This can be due to the reduced carbon content of the S60 samples. Both US and S60 eventually attained a "white" colour spectrum at 900 °C; S60 had an RGB value of 253 while US samples measured 248 after 5 hours at 900 °C. The observation that neither samples became "white" at 700 °C indicates incomplete calcination (supported by Figure 3-2).

The XRD qualitative results in Figure 3-4 demonstrates that before calcination, US and S60 shells indicated only the presence of $CaCO_3$. After calcination, shells leached for 60 min had slightly higher CaO intensity compared to the unseparated shells. Quantitative results in Figure 3-5 reveals that both separated and unseparated shells had about 99% CaO content after calcination. This implies that leaching and membrane separation did not impact the quality of CaO product. It should be noted that the US samples showed significantly more additional peaks, potentially the result of residual impurities from membrane ash remaining in the sample.

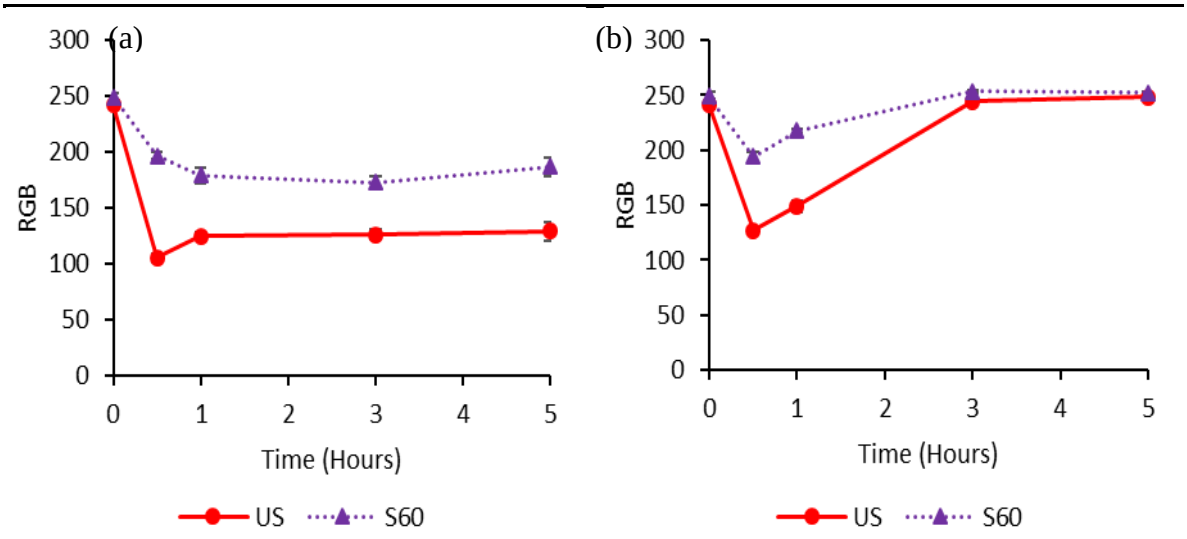

Figure 3-3: *RGB colour analysis of calcined eggshells. (a) at 700 ℃; (b) at 900 ℃.*

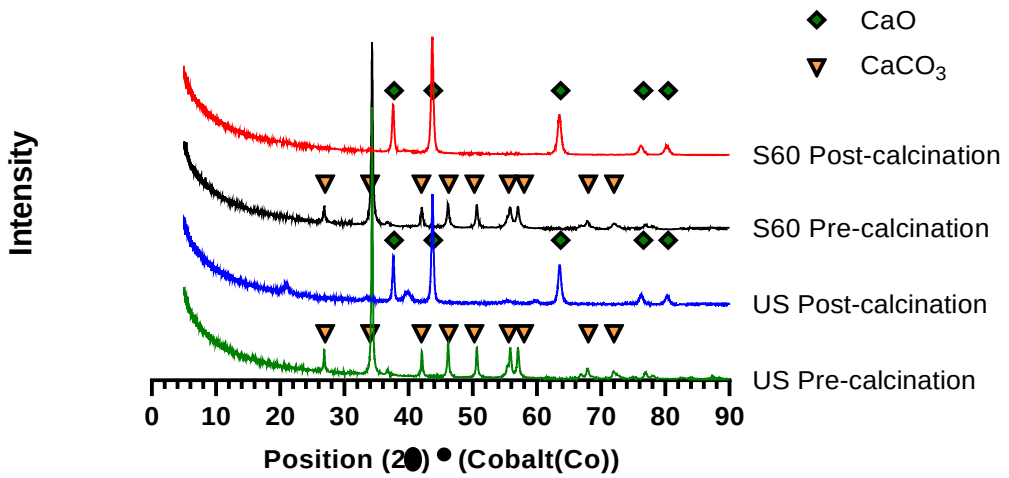

Figure 3-4: *XRD pattern of eggshell after calcination at 900°C*

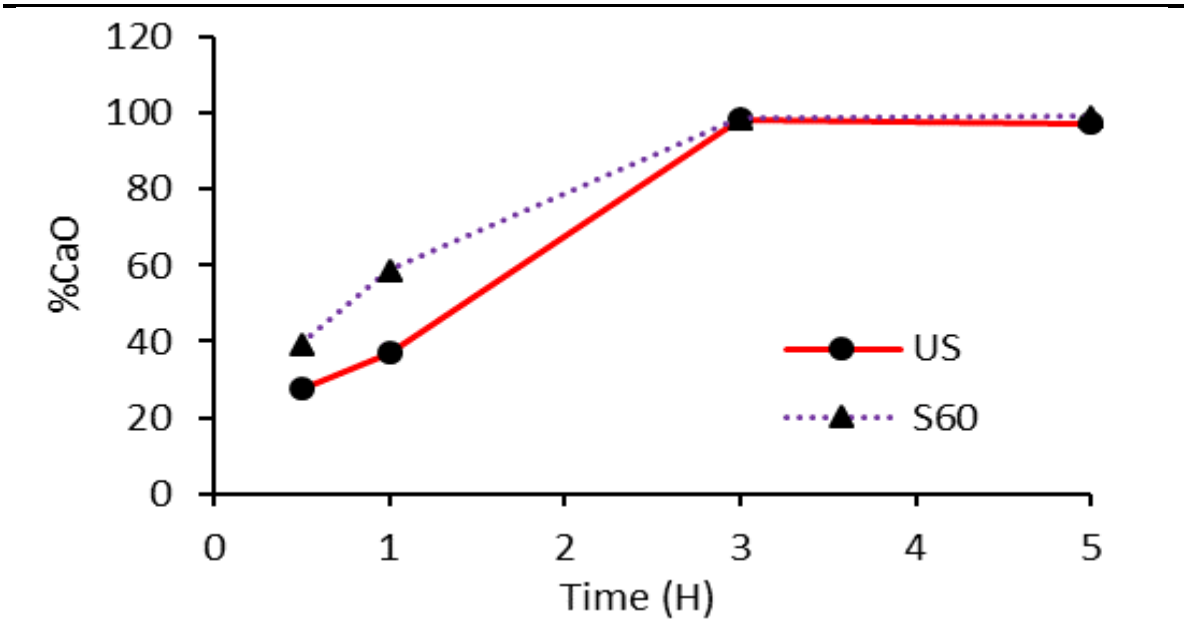

***Figure 3-5**: XRD quantitative analysis of calcined eggshells at 900°C*

3.4 CONCLUSIONS AND RECOMMENDATION

From the experimental results and analysis carried out, it was concluded that acetic acid effectively weakened the bond between eggshells and its membrane thereby aiding separation of the membrane and valorisation of the eggshells to CaO thereby facilitating the profitable use of shell membrane and constituent protein. Additionally, the separation of the eggshell membrane before calcination does not harm the quality of CaO produced. Results revealed that both separated and unseparated shells yielded CaO of similar purity and crystallinity at a similar temperature. It should be, however, noted that eggshell membrane turns to ash above 300 °C consequently becoming an impurity (<1%) in the CaO produced from the unseparated shells.

Further research is recommended to optimize the process for maximum $CaCO_3$, membrane, and constituent protein recovery. Besides, the optimized process should be costed to assess the economic scalability.

CHAPTER 4 EGGSHELL VALORISATION: MEMBRANE REMOVAL, CALCIUM OXIDE SYNTHESIS, AND BIOCHEMICAL COMPOUND RECOVERY TOWARDS CLEANER PRODUCTIONS

Published in Biointerface Research in Applied Chemistry: Refer to; Aina, S., du Plessis, B., Mjimba, V., & Brink, H. (2021). Eggshell Valorisation: Membrane Removal, Calcium Oxide Synthesis, and Biochemical Compound Recovery towards Cleaner Productions. Biointerface Research in Applied Chemistry, 12(5), 5870–5883. https://doi.org/10.33263/BRIAC125.58705883

Chapter Abstract

As climate change continues to rank high among issues of global concern, industries such as agriculture and construction continue to unearth possible ways to curb carbon dioxide generation and encourage the use or reuse of a variety of by-products and waste materials thereby fostering the implementation of cleaner technologies. Eggshells form a notable component of this waste making up more than 7.6 million metric tonnes annually. Research works involving the calcination of eggshells have often been done by burning both shell and its constituent proteins and membrane to produce calcium oxide, CaO. This research investigated a cleaner means of CaO synthesis through the recovery of the shell membrane and some valuable chemical compounds from eggshells before calcination. Atomic absorption (AA), thermogravimetric analysis (TGA), scanning electron microscope (SEM), X-ray fluorescence analysis (XRF), X-ray diffraction (XRD), Ultra-performance-liquid chromatography quadrupole-time-of-flight mass spectrometry (UPLC-Q-TOF-MS), and RGB colour analysis were all employed. Acetic and Nitric acid was used to weaken the shell-membrane bond thereby aiding membrane separation. Shell membrane was easily separated after 17 minutes of soaking time. Calcium oxide,

CaO was synthesized from separated shells after calcination for 3 hours at 900 °C. 99% CaO with an RGB value of 253 was produced. Collagen, as well as other chemical compounds, were recovered. Eggshell was successfully valorised for CaO production. The shell membrane, collagen, and other recovered compounds which would have been burnt off and left as an impurity in the CaO can now the put to more profitable use.

4.1 INTRODUCTION

Global discourse in the twenty-first century is more than ever before aimed at adapting to and mitigating the effects of climate change with the improvement of human economic and social wellbeing at its core. This is because the effects of climate change impact almost all human activities and thus demand urgent and decisive action to address the adverse impacts simultaneously with the exploitation of any arising opportunities to advance human wellbeing [1]. The focus of managing climate change has been and remains two-pronged: learning to live with the adverse impacts of this phenomenon - the essence of adaptation on one hand – and retarding or halting the increase of anthropogenic atmospheric greenhouse gases (GHGs) – the essence of mitigation on the other hand [123–125]. A major source of anthropogenic GHGs (also called carbon emissions) is the burning of fossil fuels for direct and indirect energy supply in commercial and social activities. Other sources include farming and waste management practices that rely on the traditional disposal of solid waste in dump areas. In these dumps, the waste decomposes releasing methane - an extremely potent GHG. Contemporary approaches to managing waste and (tacitly) climate change encourages; recycling, alternative uses of some waste materials and ultimately advocating a zero-waste community (circular economy) [12,126–128].

The global awareness of the need to reduce carbon emissions has encouraged investigations on the use of alternative cementitious materials for concrete production [2]. This focus arises from the realisation that the production of Portland cement clinker emits up to 1.5 billion tons of carbon (often noted as carbon dioxide- CO_2

annually. This accounts for about 5% of the total man-made CO_2 emission [4]. Simultaneously, the last few decades have witnessed a tremendous increase in waste generation due to increased industrialization and urbanization [8,129,130]. According to Kaza et.al, [9], global waste generation was estimated at 2.01 billion tonnes in 2016 with a projection of 3.40 billion tonnes by 2050. In South Africa, reports show that 42 million tons of general waste were generated in 2017 [131]. 62 million tonnes of eggs were produced from domesticated chickens *(Gallus gallus domesticus)* in 2008 [23]. Over ten years, this statistic grew to 76.7 million metric tonnes in 2018 [19]. In this mix, the South African poultry industry produced 452,000 tonnes of eggs in 2018 [25]. With shells comprising about 10.2% of the whole egg and a constant increase in production, disposal of the waste shells will always be of huge concern.

The traditional approaches to the management of waste are disposal in dumpsite or incineration. Both approaches contribute to GHG emissions. Modern approaches to managing waste again the challenge of managing climate change advocates for the continual use of resources in the bid to eliminate waste. One such approach called the Circular economy elevates the principles of reuse, sharing, repair, renovation, remanufacturing and recycling to create a closed system, curtailing the use of virgin inputs and the creation of waste, pollution and emission [7,11]. The tenet of the approach is that all “waste” should become “food” for another process [12,127].

Calcareous, porous, and bioceramic in nature, eggs are the reproductive means of all birds and most reptiles. Oval in shape after years of adaptive evolution, the chicken egg is just strong enough to fight physical and pathogenic attacks from the environment and also not too hard to allow for the exchange of gas and water needed for the development of a growing embryo inside the shell [28,29]

An eggshell is made up of a calcified shell and a double layer of shell membrane. It is one of the best and most abundant sources of naturally occurring calcium (Ca) and Strontium (Sr) with up to 401 mg/g of Ca and 372 µg/g of Sr [30]. Eggshell comprises about 98% calcium carbonate and other trace elements such as magnesium and phosphorus. Shell membranes comprise 69.2% protein, 2.7% fat, 1.5% moisture and

27.2% ash. The membranes protein is about 10% collagen [28,31,34]. Beyond the elemental and oxide composition of eggshells, investigations into their biochemical and molecular component have been of great importance. The emergence of the chicken *(Gallus gallus)* genome sequence in 2004 created further success in understanding these components [29,31,35].

The chicken eggshell is a complex matrix of proteins and carbohydrates with 70% of it been proteins. Some of the amino acids (proteins) include ovalbumin, ovocleidin – 17, ovocleidin – 116, ovocalyxin – 25, ovocalyxin – 32, ovocalyxin – 36, osteopontin, clusterin, lysozyme, ovotransferrin and collagen. Uronic acids, sialic acids, chondroitin sulphate A and B, dermatan sulphate, hyaluronic acids, and keratan sulphate are some of the polysaccharides (carbohydrates).

Eggshells have been effectively used as fertilizer in agriculture, soil stabilizer in construction, calcium supplement construction, health and medicine. Likewise, shell membrane collagen when extracted has diverse uses in the health, biochemical, pharmaceutical, food and cosmetics industries. Collagen is a tough protein that connects and supports bodily tissues, such as skin, bone, tendons, muscles, and cartilage [132‑136].

Collagen is mainly extracted from pigskin, cowhide and bone skin. However, with the outbreak of mad cow disease, foot-and-mouth disease, autoimmune and allergic reactions, the use of collagen from these sources has been restricted. Eggshell membrane collagen has very low autoimmune and allergic reactions, high biological safety, and has similar properties to other mammalian collagen. Eggshells and their membranes can be separated by a variety of techniques, including chemical, mechanical, steam, microwave, and vacuum processes. [29,34,137].

Calcium oxide derived from the calcination of limestone has been proved to be responsible for the early strength development of concrete at room temperature. This is achieved by the hydration of calcium oxide (CaO) to form Calcium hydroxide causing the evolution of heat and therefore high early strength [77,78]. This process

of decomposing limestone to form calcium oxide is responsible for 70% of the total CO_2 generated at cement plants [138,139].

An interesting observation is that calcium oxide can be produced through the calcination of the eggshells [135]. This avails a plausible substitute for lime in cement production while also halting the depletion of natural limestone resources and presenting the possibility of a significant reduction in the cement-linked high carbon footprint of the construction industry [140–142].

Against this backdrop, this research seeks to produce CaO from eggshells separated from its membrane by a chemical process as well as to recover substances leached from the shells during membrane separation. Leachate characterization was carried out with the use of UPLCMS and AA analysis while XRD, XRF, RGB, TGA, and SEM analysis were used to aid microstructural characterization of the separated/unseparated shells and membrane.

This research is novel in that it examines the recovery of eggshell membranes and other valuable compounds from the shell before the calcination of the shells to produce CaO for the construction industry.

4.2 MATERIALS AND METHODS

4.2.1 Experimental methods

Eggshells were collected from eateries within the Hatfield surrounds, including the University of Pretoria, in Pretoria, South Africa. To decontaminate the shells, they were washed repeatedly in ultra-pure water, dried at 60°C for 60 minutes in an EcoTherm oven and refrigerated at 4°C within 24 hours of collection.

1M of acetic and nitric acid was used to leach the shells and aid membrane separation as outlined in [143]. Membrane separation was possible after 17 min of leaching yet, leaching was carried out for up to 60 min. The separation was done by peeling off the membrane from its shell by hand.

Three groups of 20 g shells (unseparated, separated after 17 minutes, and separated after 60 minutes) were calcined using a Carbolite CWF1100 furnace in the presence of oxygen at 300, 500, 700, and 900 degrees for 30 minutes, 1 hour, 3 hours and 5 hours. Unseparated shells, shells separated after 17 minutes, and shells separated after 60 minutes are hereafter regarded as US, S17, and S60, respectively.

To determine the leaching rate, 20 g of eggshells were leached in 13 sacrificial reactors containing 500 ml of 1 mol Acetic acid each. After pH measurement, the entire contents of each reactor were sieved and washed with distilled water and dried to constant weight at 60 °C. The pH of a 14th reactor was measured in parallel for 180 min to monitor the $CaCO_3$ loss over time.

4.2.2 Analytical methods

Instantaneous pH measurement was carried out to evaluate the rate at which $CaCO_3$ and other shell constituents were being leached into the acid medium. Looking specifically at the concentration of calcium in the leached liquid, an atomic absorption spectrometer (AA) (Perkin Elmer AAnalyst 400, Waltham, Massachusetts) was used to measure the concentration of calcium in the leached liquid with an SJ hollow calcium lamp. $CaCl_2$ was used to generate the standard linear calibration curve while 1M KCl was used to inhibit ionization of Ca in water. The samples were diluted with ultra-pure water to the Ca concentration within the instrument's 5 mg/l linear range. The analysis was carried out using 3 different eggshell particle sizes for 17- and 60-minutes soaking time.

Thermal analysis (TGA) was conducted to examine the change in mass with an increase in temperature during the calcination process. Image J software was also simultaneously being used to monitor the change in colour with an increase in temperature.

A scanning electron microscope (SEM) was used to understand the morphology of the calcined and uncalcined shells and membranes. Oxide compositions were

obtained using X-ray fluorescence (XRF) analysis while X-ray diffraction (XRD) was used to determine the mineralogy of the shells.

Ultra-performance-liquid chromatography quadrupole-time-of-flight mass spectrometry (UPLC-Q-TOF-MS) with MassLynx V4.1 software was used to identify collagen in the leachate.

4.3 RESULTS AND DISCUSSION

4.3.1 Physical properties

Results in Table 4-1 are inconsonant with the findings of [29,122]. The density was measured using the Archimedes principle. The reduced density is due to the removal of the highly porous membrane layer. However, this porosity is responsible for its use as a dye absorbent [44,144].

Table 4-1: *Characteristics of Eggshell and membrane*

Characteristics	Value
% Composition of the shell	96.65%
% Composition of the membrane	3.35%
Density of unseparated shell (g/cm^3)	2.01
Density of separated shell (g/cm^3)	1.53

4.3.2 Effect of acid on shell membrane and calcium content

Acetic and nitric acid was used to weaken the bond between the shell and its membrane. Conversely, while the bond was getting weakened, eggshell calcium was gradually being leached into the acid medium. An atomic absorption spectrometer (AA) was used to measure the concentration of calcium in the leached liquid using 3 different eggshell particle sizes for 17 and 60 minutes soaking time.

It was evident that smaller particles released their calcium content much faster than bigger ones as expected (Figure 4-1). In addition to this, nitric acid (N) leached as much as twice the amount of calcium leached by acetic acid (A).

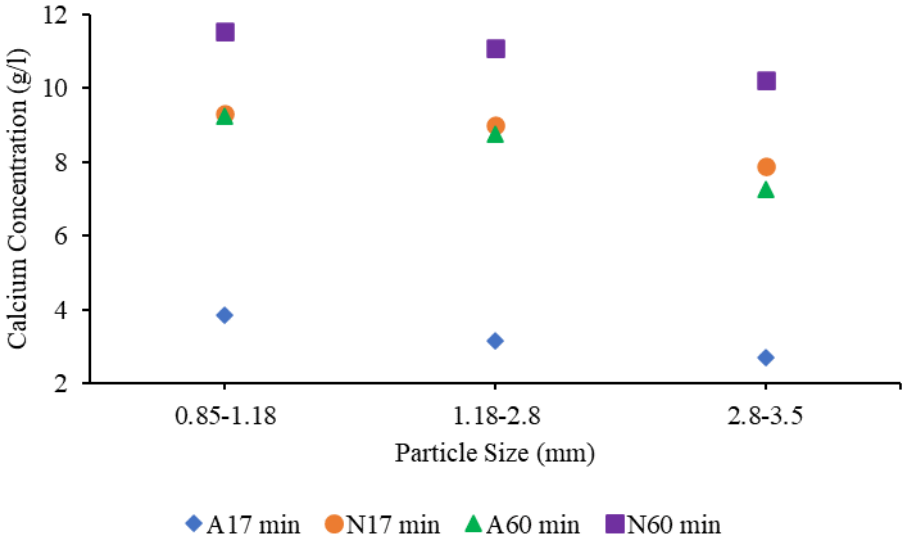

***Figure* 4-1:** *Calcium concentration in acid leachate. A17: acetic acid 17 minutes; N17: nitric acid 17 minutes; A60: acetic acid 60 minutes; N60: nitric acid 60 minutes.*

Due high leaching rate of nitric acid, acetic acid was adopted for further study. The AA analysis result was also corroborated by pH experimental analysis in Figure 4-2 About 6 g (30%) and 15 g (75 %) of $CaCO_3$ was dissolved into the medium after 60 and 180 minutes of leaching, respectively.

Equation (4.1) depicts the model that governs the rate at which calcium is dissolved into the acidic medium. This gives an insight into the mass loss of $CaCO_3$ during the leaching process for up to 180 minutes. The model is further explained in [143].

$$[Ca^{2+}] = [CO_3^{2-}] + [HCO_3^-] + [H_2CO_3] \quad (4.1)$$

These results demonstrate that the amount of $CaCO_3$ lost in the solution is the most significant limitation to the leaching method and agent for membrane removal [143]. This observation will be crucial in recommending an optimum leaching time.

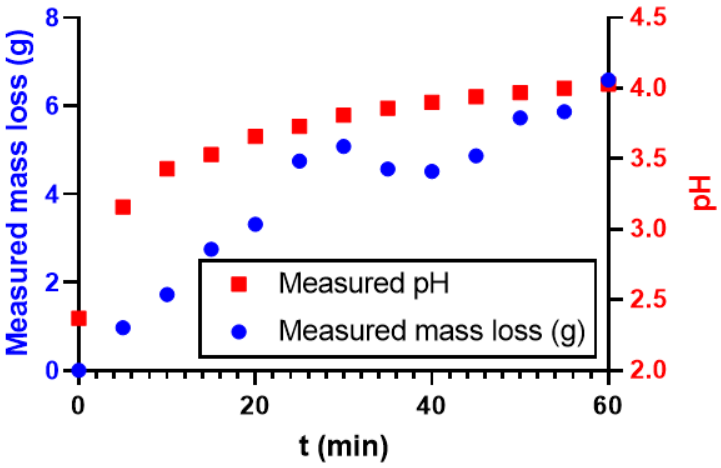

Figure 4-2: *Change in pH and measured mass loss of eggshell in acetic acid*

4.3.3 Thermal analysis

A TGA5500 thermogravimetric analyser was used to study the effect of increased temperature on the separated and unseparated eggshells as well as the shell membrane. The change in mass was measured with an increase in temperature from room temperature to 950 °C at a heating rate of 10 °C/min in the presence of nitrogen.

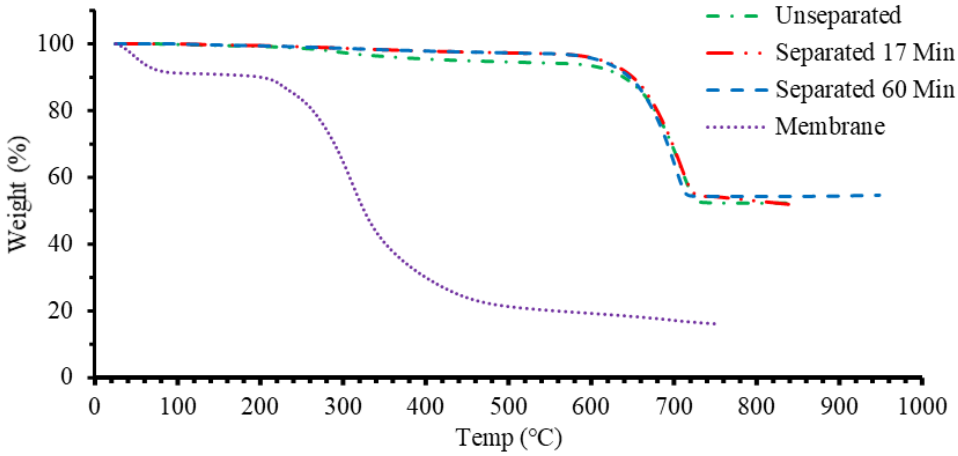

Figure 4-3: *Thermogravimetric analysis.*

Thermal analysis plots comprising of the TG spectra of US, S17 and S60 shells, as well as the membrane, are seen in Figure 4-3. The three shell samples began with a linear reduction in weight due to loss of moisture up to 300 °C after which US samples

records a nonlinear reduction due to the volatilization of its membrane constituent. All shells samples continued the linear path until about 650 °C at which point water, protein, and carbon constituents of the shells are evaporated, and actual calcination sets in. As seen in the plot, separated shells were fully calcined at about 720°C while unseparated shells became fully calcined at 735 °C. On the other hand, the shell membrane which is less dense than the shells turn completely into ash after 300 °C, leaving approximately 10% weight at >700°C which eventually becomes a potential source of impurities in the US samples.

Calcination was carried out in a carbolite CWF1100 furnace at 300, 500, 700, and 900 degrees for 30 minutes, 1 hour, 3 hours and 5 hours. Mass loss with an increase in temperature was recorded and plotted in Figure 4-4. (a), (b), and (c), logged a wide difference between the leached and unseparated samples. This is due to the presence of shell membrane which burns out faster in the unseparated samples. Nevertheless, this disparity was largely decreased at 900 °C with the formation of membrane ash. Unseparated shells had a 47% mass loss while separated samples lost 45% of their initial mass. This is consistent with readings from the TGA analysis.

While calcination was carried out, Image J was used to conduct an RGB colour analysis of the calcined shells. Pictures of the calcined shells were taken with a 13-megapixel camera at a constant distance and illumination (Figure 4-5).

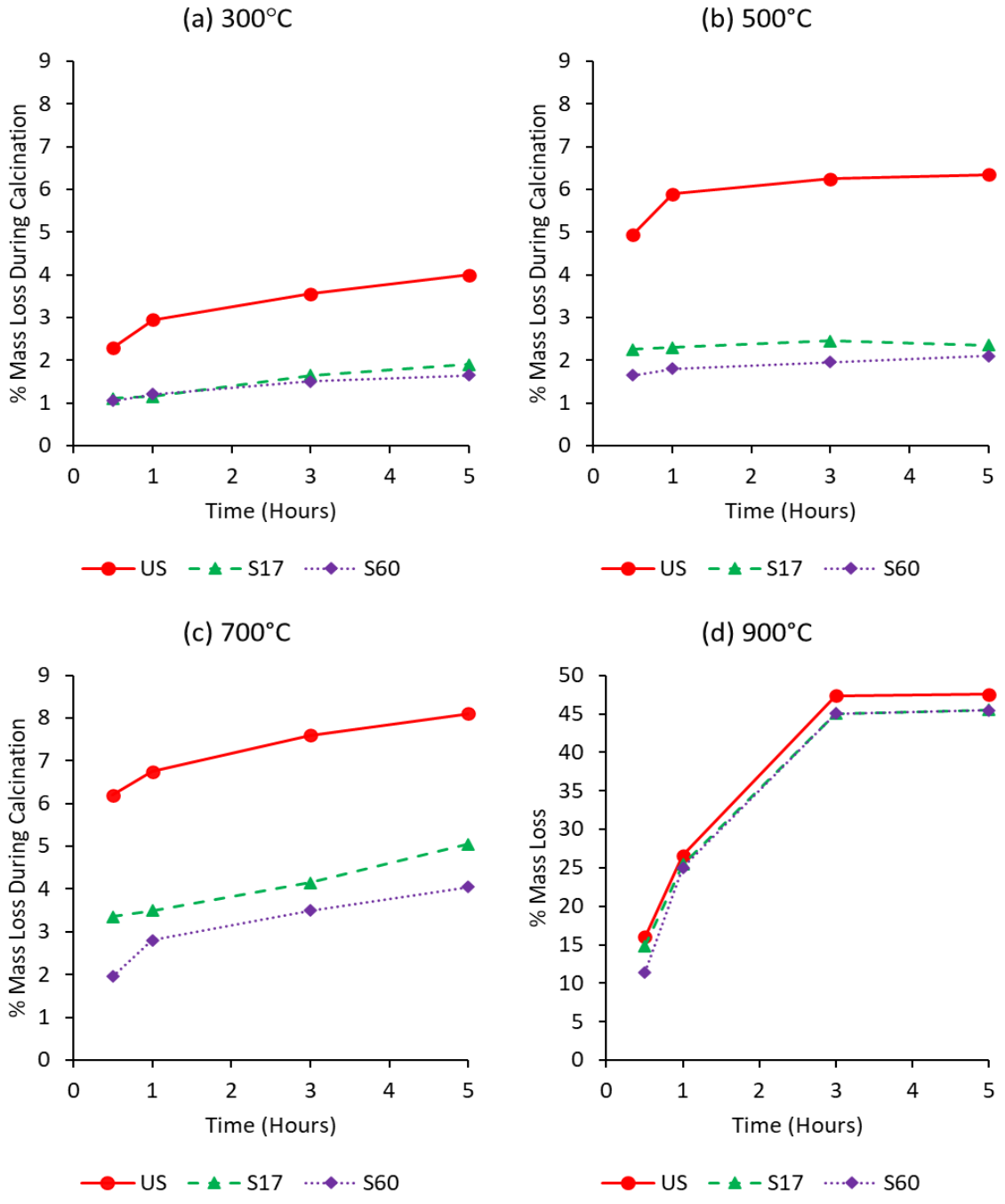

Figure 4-4: *Calcination analysis*

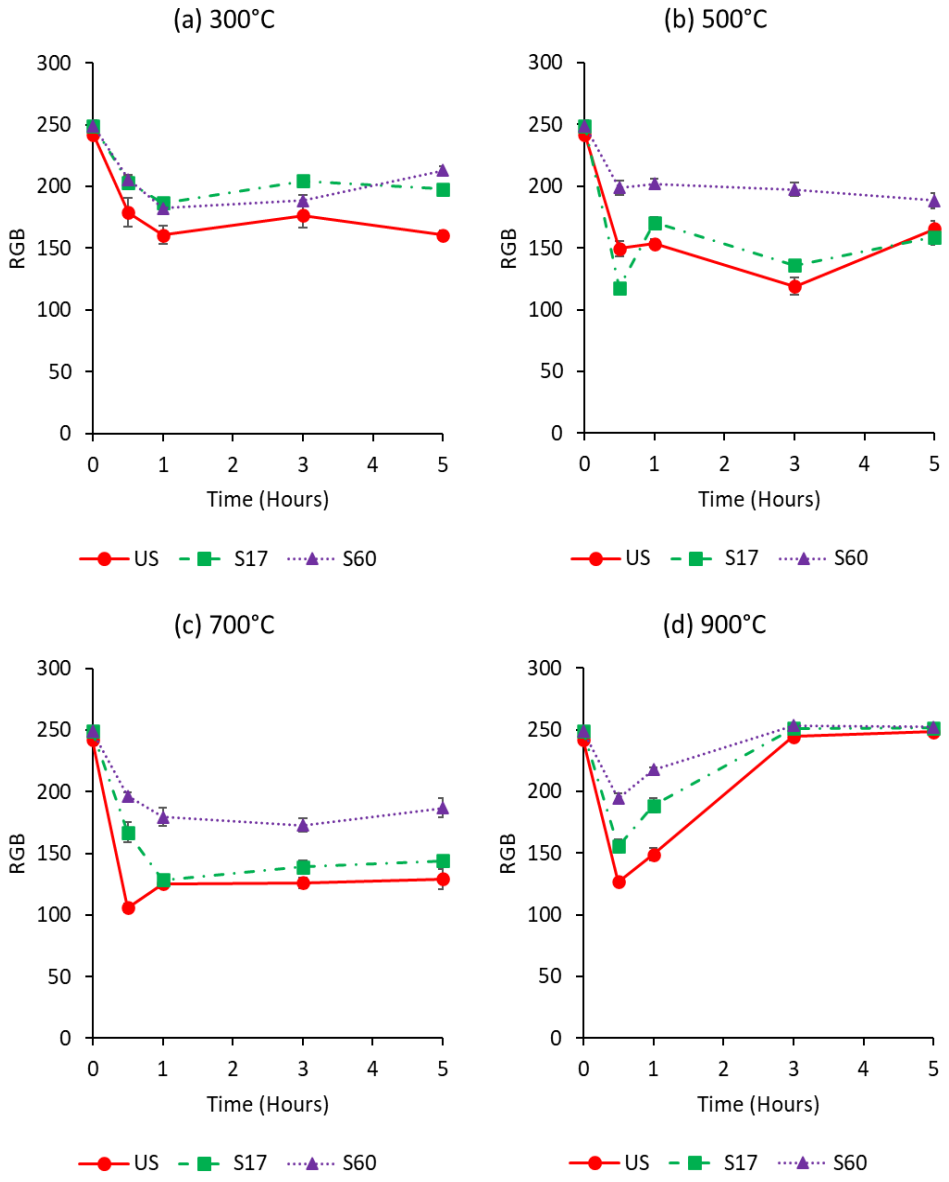

Figure 4-5: *RGB colour analysis*

The data revealed the trend of colour change from brown at 300 °C to dark brown, grey, and finally white at 900 °C [122]. It was also detected that the samples leached for 60 minutes did not get as dark as much as the raw samples and those leached for 17 minutes. This can be due to the reduced carbon content of the S60 samples. All three categories of samples attained a constant white colour spectrum after 3 hours of calcination. The lack of white colour at 700 °C and the result of the XRD analysis imply that calcination was only optimum at 900 °C [121,122]. S17 samples were

observed to behave similarly to S60 samples while calcination was complete after 3 hours. Leaching beyond 17 minutes and more than 3 hours of calcination, therefore, seems not to aid calcination.

4.3.4 Microstructural analysis

The morphology of the shell and membrane samples was studied in a Zeiss Ultra PLUS FEG scanning electron microscope (SEM). Samples were dried before being sputter-coated with carbon in a Quorum Q150T ES coater for imaging. The morphology results as seen in Figure 4-6(a-c) disclosed that the eggshell is porous, crystalline in nature, and characterized by an angular pattern. The formation of agglomerates was also observed [145]. CaO on the other hand as spotted in (d-f) exhibits a honey-comb like porous surface with rod-like particles [107,146]. SEM image of the shell membrane revealed that the membrane has an enormous surface with fibre-like pores. This porous fibril structure makes the shell membrane a good adsorbing agent [147].

Oxide composition of shells calcined at 900 °C for 3 hours was investigated by X-ray Florescence (XRF) analysis and outlined in Table 4-2. The Thermo Fisher ARL Perform'X Sequential instrument with Uniquant software was employed. The samples were roasted in alumina refractory crucibles at 1000 °C to determine Loss on Ignition (LOI). 1 g roasted sample was then placed together with 6 g of $Li_2B_4O_7$ into a Pt/Au crucible and fused into a glass bead at 1050 °C. The software analysed for all elements in the periodic table between Na and U, but only elements found above the detection limits were reported. The results were normalised, to include LOI for the sample to indicate crystal water and/or oxidation state changes. Blank and certified reference materials are analysed with each batch of samples.

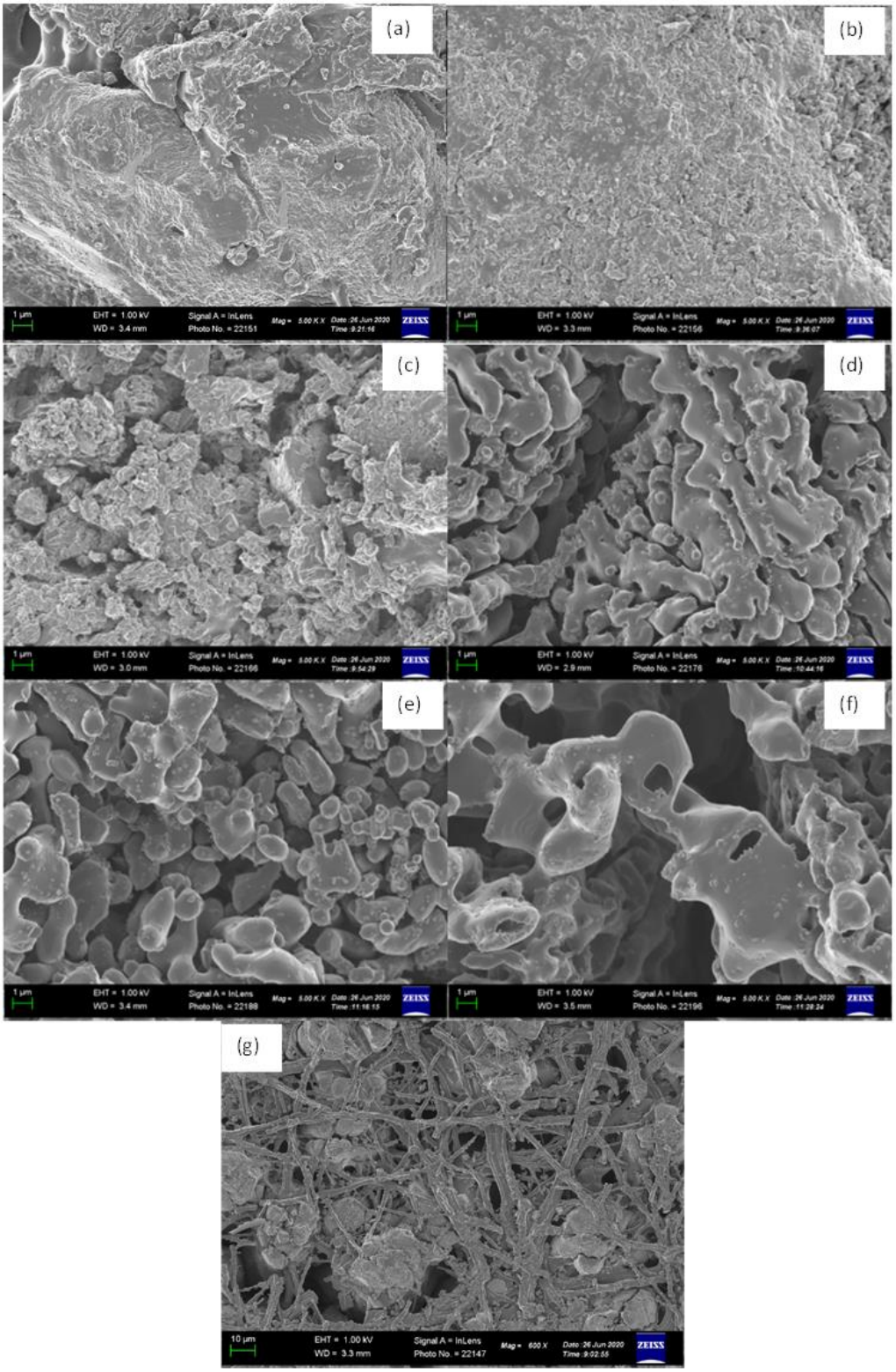

Figure 4-6: *SEM image of eggshell, CaO, and membrane. (a)US shells, (b) S17 shells, (c) S60 shells, (d) US CaO, (e) S17 CaO, (f) S60 CaO, (g) membrane*

Table 4-2: *Oxide composition of the calcinated shell*

Oxides	US	S17	S60
MgO	1.366	1.279	1.138
P_2O_5	0.618	0.419	0.416
CaO	97.435	97.663	97.700
SO_3	0.023	0.039	0.052
SrO	0.025	0.021	0.022
BaO	0.237	0.211	0.256

Oxide composition from the XRF analysis in

Table **4-2** as well as the XRD quantitative analysis results in Figure 4-7 both gave similar data of CaO composition to be about 98% after 17 minutes soaking time and 3 hours calcination. Calcination therefore, effectively transforms $CaCO_3$ into CaO [121,122].

X-ray diffraction (XRD) analysis was used to determine the mineralogy of the shells before and after calcination. The samples were prepared according to the standardized Panalytical post-loading system, which provides a nearly random particle distribution. The PANalytical X`Pert Pro powder diffractometer was used to analyze the sample in the θ-θ configuration, which is equipped with an X`Celerator detector and variable divergence and fixed receiver tank, with Fe filtered CoKα radiation (λ = 1,789Å). The mineralogy is determined by using the X`Pert Highscore plus software to select the most suitable pattern for measuring the diffraction pattern from the ICSD database. The relative amount of phase (weight% of the crystalline part) was estimated using the Rietveld method by utilizing the basic parameter method of the Autoquan/BGMN software.

Figure 4-7 and Figure 4-8 exemplifies the transformation of CaCO3 in uncalcined shells to CaO after 3 hours of calcination. Uncalcined shells were characterized by peaks of $CaCO_3$ though, unseparated shells showed slightly higher peaks compared to separated ones. After calcination, peaks of CaO were observed. Due to the hygroscopic nature of CaO, faint peaks of portlandite, $Ca(OH)_2$ identified. Soaking time had no significance in the formation of CaO in S17 and S60 samples.

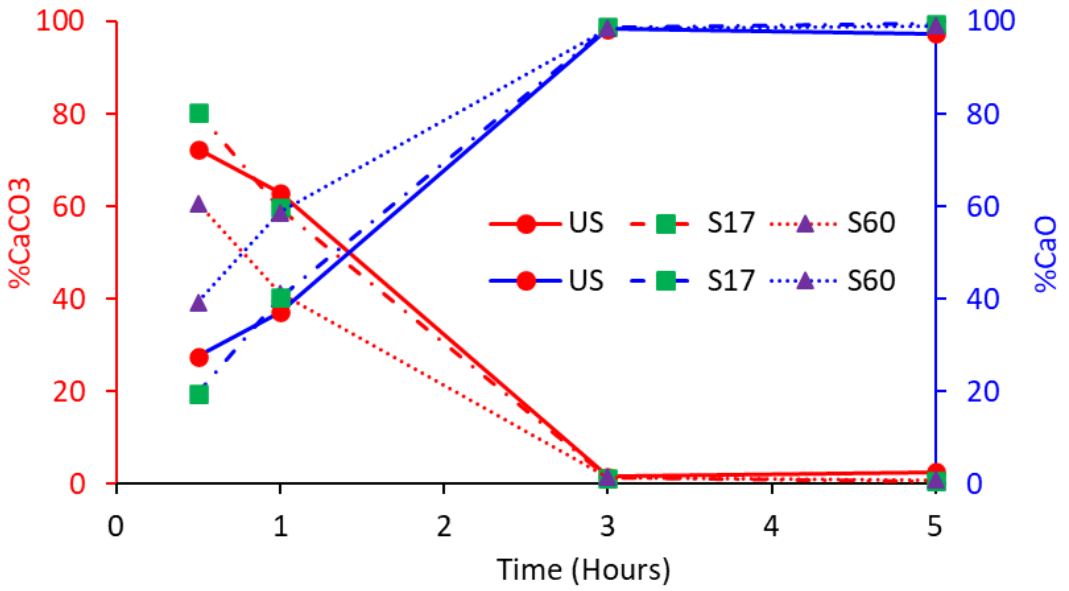

Figure 4-7: *XRD quantitative analysis*

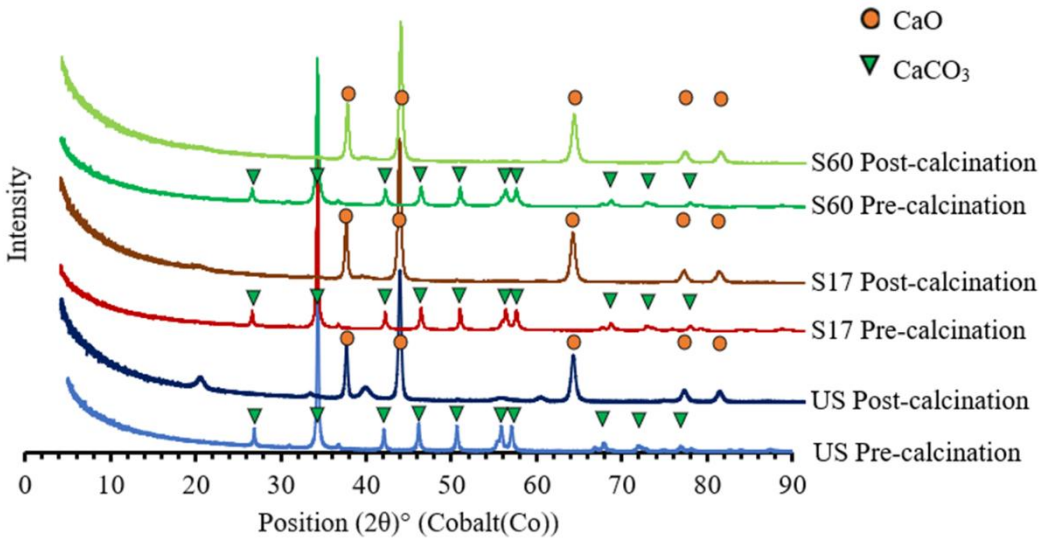

Figure 4-8: *XRD pattern of eggshell before and after calcination*

4.3.5 Recovery of collagen and other compounds

UPLC was performed using a Waters Acquity UPLC system (Waters Corp., MA USA) equipped with a binary solvent delivery system and an autosampler. The Waters Synapt G2 high-resolution QTOF mass spectrometer equipped with an ESI

source is used to acquire negative and positive ion data. The system was powered by MassLynx V 4.1 software (Waters Inc., Milford, Massachusetts, USA) for data acquisition. By generating molecular formulas from MassLynx V 4.1 based on iFit values and comparing MS / MS fragmentation patterns with those of matching compounds from the PubChem, ChemSpider, and Massbank libraries, the compounds were initially identified. Furthermore, the precise masses obtained are compared with the precise masses of known compounds in the compound database.

All the compounds listed in

Table **4-3** were identified in Nitric acid leached shells while, compounds 6, 8, and 11 were not identified in shells leached with acetic acid. This can be associated with the already observed high leaching power of nitric acid. It should however be noted that other forms of these compounds (5,7,10) were identified in acetic and nitric acid leached shells.

Collagen was identified in both S17 and S60 samples in both positive and negative modes. Three forms of collagen were observed as in

Table **4-3**. This illustrates the possibility of recovering eggshell collagen and other valuable compounds before calcining the shell for CaO.

Table 4-3: *Identified compounds.*

S/No	Name	Molecular formula	Molecular mass, (g/mol)	Presence in Nitric acid leached effluent	Presence in Acetic acid leached effluent	Reference
1	Collagen	$C_8H_7FO_3$	170.1378	+	+	[148]
2	Collagen ointment	$C_{18}H_{28}N_2O$	288.4277	+	+	[149]
3	Collagen (type II fragment)	$C_{13}H_{24}N_4O_4$	300.3541	+	+	[150,151]
4	lysozyme	$C_{36}H_{61}N_7O_{19}$	895.4022	+	+	[152]
5	Uronic acid	$C_6H_{11}NO_6$	193.0586	+	+	[153]
6	Uronic acid	$C_{12}H_{17}Cl_3O_9$	411.6170	+	-	[154]
7	Sialic acid	$C_{11}H_{19}NO_9$	309.2699	+	+	[155]
8	Sialic acid	$C_{20}H_{36}N_2O_{17}$	576.5030	+	-	[156]
9	Chondroitin sulphate A	$C_{14}H_{23}NO_{15}S$	477.3951	+	+	[157]
10	Dermatan sulphate	$C_{14}H_{21}NO_{15}S^{-2}$	475.3792	+	+	[158]
11	Dermatan sulphate	$C_{18}H_{31}NO_{14}S$	517.5020	+	-	[159]
12	Hyaluronic acid	$C_{33}H_{54}N_2O_{23}$	846.7815	+	+	[160]
13	Keratan sulphate	$C_{28}H_{48}N_2O_{32}S_4$	1052.9349	+	+	[161]

4.4 CONCLUSION

The evidence provided in this article has shown that firstly, acetic acid efficiently weakened the bond between the eggshell and its membrane as opposed to nitric acid thereby aiding membrane separation. Similarly, 17 minutes socking time is just enough to minimise loss of calcium into the solution. Membrane separation before calcination serves to valorise the eggshell as the membrane can be put to more beneficial use. Secondly, the process of leaching and membrane separation does not impair the quality of CaO produced after calcination, instead, it validates it as the supposed membrane impurities have been eliminated. Finally, collagen and other compounds identified in the leachate gives rise to more research as to how they can be efficiently salvaged before calcination.

CHAPTER 5 SYNTHESIS AND ASSESSMENT OF ANTIMICROBIAL COMPOSITES OF AG NANOPARTICLES OR $AgNO_3$ AND EGG SHELL MEMBRANES

Published in Molecules: Refer to; Aina, S. T., Kyomuhimbo, H. D., Ramjee, S., Du Plessis, B., Mjimba, V., Maged, A., Haneklaus, N., & Brink, H. G. (2023). Synthesis and Assessment of Antimicrobial Composites of Ag Nanoparticles or $AgNO_3$ and Egg Shell Membranes. Molecules, 28(12), 4654. https://doi.org/10.3390/molecules28124654

Chapter Abstract

Engineering research has been expanded by the advent of material fusion, which has led to the development of composites that are more reliable and cost-effective. This investigation aims to utilise this concept to promote a circular economy by maximizing the adsorption of silver nanoparticles and silver nitrate onto recycled chicken eggshell membranes, resulting in optimized antimicrobial silver/eggshell membrane composites. The pH, time, concentration, and adsorption temperatures were optimized. It was confirmed that these composites were excellent candidates for use in antimicrobial applications. The silver nanoparticles were produced through chemical synthesis using sodium borohydride as a reducing agent and through adsorption/surface reduction of silver nitrate on eggshell membranes. The composites were thoroughly characterized by various techniques, including spectrophotometry, atomic absorption spectrometry, scanning electron microscopy, transmission electron microscopy, Fourier transform infrared spectroscopy, and X-ray photoelectron spectroscopy, as well as agar well diffusion and MTT assay. The results indicate that silver/eggshell membrane composites with excellent antimicrobial properties were produced using both silver nanoparticles and silver nitrate at a pH of 6, 25°C, and after 48 hours of agitation. These materials exhibited remarkable antimicrobial activity against *Pseudomonas aeruginosa* and *Bacillus subtilis*, resulting in 27.77% and 15.34% cell death, respectively.

5.1 INTRODUCTION

Composites are now a highly regarded material due to their ability to combine two or more distinct materials, creating a superior product that embodies the strengths of each constituent material [162‑164]. To further enhance the benefits of these materials, engineers and scientists seek to minimize the drawbacks of each material during the fusion process, resulting in a final product that optimizes the advantages of the individual materials [162,165,166]. Consequently, composites have enabled the engineering of materials with tailored physical, microstructural, chemical, and mechanical properties, making them ideal for a broad range of applications [162,165,167].

Metal nanoparticles possess unique physicochemical properties due to their surface area-to-volume ratios and shapes, making them highly sought after for their antimicrobial, anti-cancer, chemical stability, electronic, magnetic, catalytic, and optical properties [168‑170]. There are several types of metal nanoparticles currently available, including mercury, iron, gold, cerium, silver, platinum, and thallium. Among these, silver nanoparticles (AgNPs) are the most extensively researched and utilized in various applications, owing to their desirable characteristics such as a high surface area-to-volume ratio, exceptional surface plasmon resonance, ease of functionalization and modification, potent toxicity against pathogens and cancer cells, and catalytic capabilities [171‑177].

Silver nanoparticles (AgNPs) have been observed to occur in different shapes, including oval, spherical, cubic, cylindrical, and triangular, which are influenced by the synthesis method employed [167,178]. There are various methods of synthesizing AgNPs, including physical, chemical, and green techniques. The chemical approach involves the use of reducing agents and stabilizers such as formaldehyde, hydrazine, and sodium borohydride [168].

Over the past decade, the South African poultry industry has continued to enjoy consistent growth. Statistic has revealed that domestic chickens (*Gallus gallus domesticus*) generated sixty-two million tons of eggs in 2008, and 10 years later, this

figure has grown to 76.7 million metric tons [19,23]. With a shared mix of 452,000 tons of eggs in 2018 and a 10.2% shell content, the management of this domestic waste now raises concern [25].

Eggshells are characterized by their oval, porous, bioceramic, and calcareous nature. Chicken eggs possess adequate strength to resist physical and pathogenic attacks while also facilitating the exchange of water and gases, which are critical for embryo development [28,29,179]. The nutritional profile of eggshells is complex, with approximately 70% amino acids and several polysaccharides. Some of the proteins found in eggshells are ovalbumin, ovocleidin-17, ovocleidin-116, ovocalyxin-25, ovocalyxin-32, ovocalyxin-36, osteopontin, clusterin, lysozyme, ovo-transferrin, and collagen. The carbohydrates present include uronic acids, sialic acids, chondroitin sulphate A and B, dermatan sulphate, hyaluronic acids, and keratan sulphate [29,31,35]. Of these amino acids, ovocalyxin-36 is particularly noteworthy as it is primarily responsible for the antimicrobial properties of the eggshell [180,181].

According to research [182], the ability of ESM to adsorb metal ions is due to the presence of electrostatic, hydrogen bonding, and van der Waals forces that come into play when ESM is immersed in these ions. Additionally, ESM is a fibrous biomaterial that possesses a high surface area and desirable adhesion ability, making it a suitable candidate for use in composite materials. One particular protein found in ESM, OCX-36, has been identified as having bactericidal properties similar to lipopolysaccharide-binding protein (LBP) and palate, lung, and nasal epithelium clone (PLUNC) proteins [180]. Its ability to resist microbial growth makes it an attractive component for developing antimicrobial materials.

Several studies have demonstrated the utility of composites, eggshells, eggshell membranes, and metal nanoparticles. For instance, Shin et al., Hayajneh et al., and Dwivedi et al. utilized eggshells to produce green aluminum metal composites with exceptional microstructural, tribological, physical, and mechanical properties when compared to pure aluminum, as reported in [27,58,59]. Additionally, an eggshell–rubber composite has been shown to surpass natural rubber in terms of maximum torque, Young’s modulus, and elongation, as discussed in [60]. In [70], a composite

of eggshell membrane-templated gold nanoparticles was employed to detect thiabendazole pesticides in Oolong tea.

ES and ESM have been utilized in construction applications, including full or partial replacement of fine aggregate, masonry, production of lightweight foamed concrete, aggregate stabilization, and power insulation [42,48,85–90]. Additionally, these materials have been employed in renewable energy as a catalyst for palm kernel biodiesel production [93,95,183] and an oxidizing agent for volatile organic compounds [97]. Moreover, eggshells and their membrane have been utilized in conjunction with osmosis, adsorption, precipitation, photodegradation, and electrodialysis, among other techniques, to decontaminate water bodies polluted with metals and non-metals. ESM has been found to have a high affinity for certain metals such as silver and mercury [44,47,98,102,144].

Given the constant drive for progress and change within the field of materials science, the combination of materials will continue to be significant. Consequently, this study proposes a novel ESM/Nanosilver antimicrobial composite. This research also aims to enhance the adsorption efficiency of chemically produced AgNPs and $AgNO_3$ by utilizing the eggshell membrane.

5.2 MATERIALS AND METHODS

5.2.1 Preparation of Eggshell Membranes (ESM)

Eggshells were sourced from eateries within the University of Pretoria and its surroundings. Within 24 h of collection, all shells were washed and dried at 60°C for 60 minutes. Decontaminated shells were stored in plastic bags until separation. To aid membrane separation, the shell was soaked in 1 mol/L acetic acid for 17 minutes, and thereafter, the ESM was removed from the shell by hand [219]. All separated membranes were washed in deionized water, dried, and stored.

5.2.2 Synthesis of AgNPs

AgNPs were synthesized by chemical reduction of $AgNO_3$ with sodium borohydride ($NaBH_4$) as well as by direct membrane reduction.

The method described in [180] was employed to carry out the chemical reduction. $NaBH_4$ functioned as a reducing agent, while trisodium citrate dihydrate ($Na_3C_6H_5O_7 \cdot 2H_2O$) was used as a ligand. Initially, 100 mL of $Na_3C_6H_5O_7 \cdot 2H_2O$ solution (0.01 M), 50 mL silver nitrate ($AgNO_3$) solution (0.01 M), and 50 mL 0.01 M $NaBH_4$ were prepared in deionized water. Then, 20 mL of deionized water, 1 mL of $AgNO_3$, and 1 mL of $Na_3C_6H_5O_7 \cdot 2H_2O$ from the prepared solution were added to a 100 mL beaker placed in an ice bath. To prepare a nanosilver solution, the $AgNO_3$-$Na_3C_6H_5O_7$ solution was stirred for 5 min using a magnetic stirrer, and then 1.2 mL of $NaBH_4$ was added dropwise until the colour of suspension changed to bright yellow. The reactor was stirred continuously for two hours to ensure a complete reduction reaction.

5.2.3 Detection and Characterization of AgNPs

The synthesized silver nanoparticles were characterized using a spectrophotometer, atomic absorption spectrometry (AA), scanning electron microscope (SEM), transmission electron microscopy (TEM), and Fourier transform infrared spectroscopy (FTIR).

The UV-vis absorbance spectra of the nanoparticles were measured from 300 nm to 600 nm with the use of the VWR UV-1600PC spectrophotometer. The Zetasizer Nano-ZS90 instrument (Malvern Instruments, Malvern, UK) was used for particle-size analysis.

An atomic absorption spectrometer (Perkin Elmer AAnalyst 400, Waltham, MA, USA) was used to measure silver concentration with an SJ hollow silver lamp. $AgNO_3$ was used to generate the standard linear calibration curve. The samples were

diluted with Distilled-deionized water to the Ag concentration within the instrument's 1 mg/l linear range. The analysis was conducted in triplicates.

5.2.4 Production of ESM Composites

Both synthesized AgNPs and $AgNO_3$ were adsorbed into ESM. Dried ESM of particle sizes ranging from 1 mm to 5 mm were placed in 40 mL glass Polytops containing double diluted AgNPs or $AgNO_3$ and agitated in an oscillator for adsorption to take place. The process was optimized using UV-vis absorbance spectra and AA analysis for pH (6.0–9.0), reaction time (30 min–48 h), temperature (25–65°C), and concentration. pH was adjusted using HNO_3 (0.1 M) or NaOH (0.1 M). The concentration range for the AgNPs was limited by the concentration AgNPs synthesized using the method described in Section 3.2, i.e., 35.5 mg/L. The concentration range of $AgNO_3$ was limited by the solubility limit of $AgNO_3$ in water. Transmission electron microscopy (TEM) images were obtained for post-adsorption nanoparticle size determination. The Jeol 2100F FEG TEM with an EDS detector and an accelerating voltage of 30 kV was used.

5.2.5 Characterization of ESM Composites

The morphology of the membranes before and after adsorption of the nanoparticles was studied in a Zeiss Ultra PLUS FEG scanning electron microscope (SEM). Samples were dried before being sputter-coated with carbon in a Quorum Q150T ES coater for imaging. SEM energy dispersive X-ray analysis (EDX) was also conducted to understand the distribution and elemental composition of the nanoparticles on the membranes.

The Bruker ALPHA II Compact FT-IR Spectrometer using the OPUS 7.0 software was employed to determine all functional groups likely to be found in the ESM/$AgNO_3$ composite. All samples were dried and grounded prior to the analysis. The chemical state of Ag absorbed on ESM was analyzed using X-ray photoelectron

spectroscopy (XPS, Thermo ESCAlab 250Xi, Monochromatic Al kα, 300W, Thermo Fisher Scientific, Waltham, MA, USA).

5.2.6 Antimicrobial Activity of AgNPs, $AgNO_3$, and ESM Composites

The antimicrobial activities against *Bacillus subtilis* and *Pseudomonas aeruginosa* were determined using the agar well diffusion method and MTT assay. For agar well diffusion, 8mm diameter holes were punched in agar plates containing the desired bacteria and filled with 100 µL of 100 µg/L of AgNPs, $AgNO_3$, AgNPs/ESM, and $AgNO_3$/ESM solution. Note the AgNPs/ESM and $AgNO_3$/ESM were the composites obtained at the maximum adsorption capacities, i.e., *circa* 0.6 mg/g and *circa* 16 mg/g, respectively. The agar plates were then incubated at 37 °C for 24 hours. Streptomycin and ampicillin were used as positive controls for *B. subtilis* and *P. aeruginosa,* respectively. Distilled water was used as a negative control.

MTT (3-(4,5-dimethylthiazolyl-2)-2,5-diphenyltetrazolium bromide) assay is a dependable and responsive colorimetric assay used to evaluate the metabolic activity of cells. This tetrazolium dye can be reduced into a purple-coloured insoluble compound known as formazan by specific bacterium enzymes. The concentration of formazan is determined by measuring its absorbance using a spectrometer within the 500 to 700 nm range. As the number of viable bacteria increases, the concentration of formazan also increases, resulting in a more intense purple colour and a higher absorbance value [220‑222]. Overnight cultures of bacteria were grown in nutrient broth at 37 °C while shaking at 150 rpm until an optical density of 0.4 was obtained. The cultures were centrifuged, the supernatant was washed twice with distilled water and resuspended in distilled water, and optical density was adjusted to ~1. Exposures of bacteria (OD600 = 0.2) to AgNPs, $AgNO_3$, AgNPs/ESM, $AgNO_3$/ESM, ESM, residual $AgNO_3$ solution after ESM adsorption and residual AgNPs solution after ESM adsorption was carried out in 96 well plates at a concentration 10 µL while shaking at 85 rpm for 3 h. 10 µL of MTT solution was added to 90 µL of exposed bacteria and incubated for 1 h in a thermostatic shaker at 37 °C for 200 rpm in the

dark. 100 µL of DMSO was then added to the mixture and incubated at room temperature for 1 hour in the dark while shaking at 70 rpm. The absorbance was measured at 560 and 700 nm using a microplate reader. A stock solution of 5 mg/mL of MTT in 0.1 M PBS (pH 7) was used.

5.3 RESULTS AND DISCUSSION

5.3.1 Synthesis and Characterization of AgNPs

The synthesized nanoparticle suspension was light yellow in colour (Figure 5-1a) and had a conspicuous UV-vis absorbance peak at 390–400 nm, indicating the successful synthesis of AgNPs (Figure 5-1b). The strong peaks recorded around 390 nm is a function of surface plasmon resonance (SPR) vis-à-vis the absence of particle aggregation [180,184]. The $AgNO_3$ resulted in a clear solution (Figure 5-1c) and demonstrated maximum adsorption at around 300 nm in solution consistent with results from the literature [185,186] (Figure 5-1d).

The particle size distribution of the synthesized AgNPs is shown in Figure 5-2. The data were analysed as per [187], and the results are summarized in Table 5-1. It can be seen that the AgNPs exhibited a multi-modal distribution with an overall average particles size (d_{50}) of 29.8 nm (Z-average particles size of 14.3 nm measured by the Zetasizer)—the discrepancy between the d_{50} calculated from the distribution curves and the Z-average value relates to the limitations of the Zeta-sizer which requires that the sample be mono-modal, near-spherical particles, in a narrow size distribution [188]. However, TEM imaging of the AgNPs (Figure A5.1) confirmed that the AgNPs were mostly in sub 50 nm range. According to [189], this particle size makes it suitable for antimicrobial purposes.

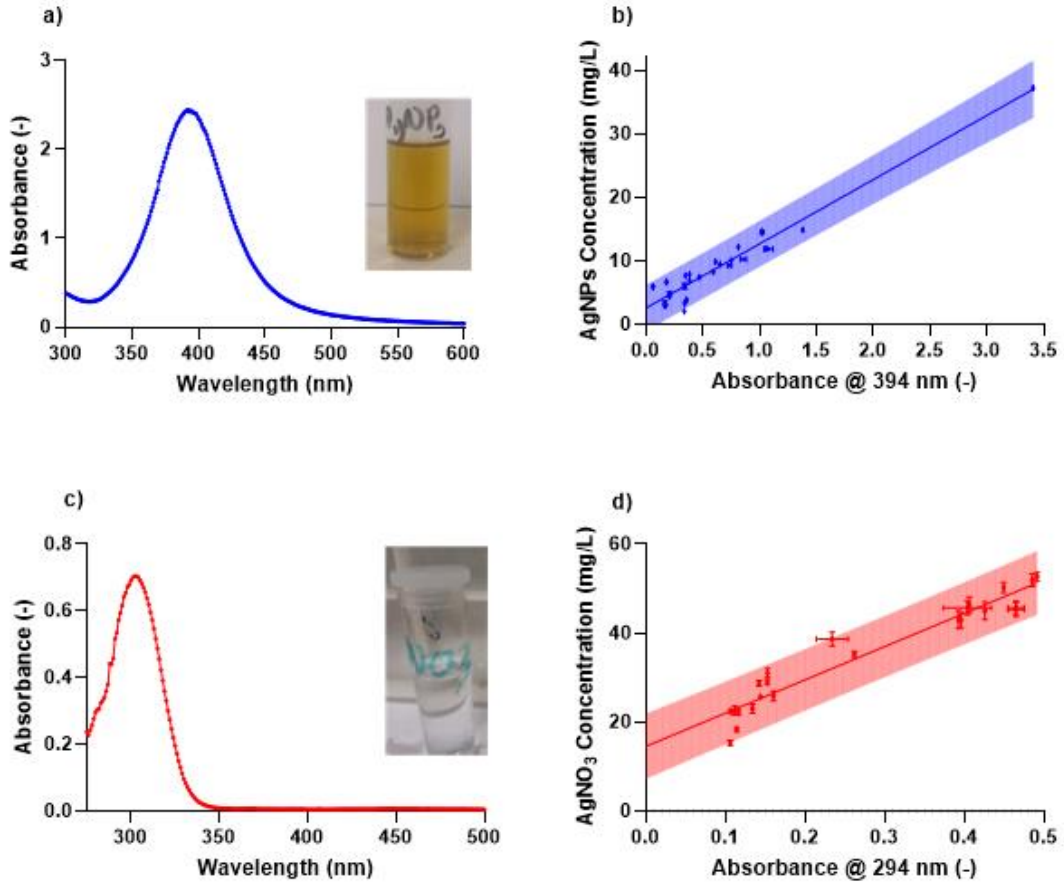

Figure 5-1. *UV–vis absorbance spectrometry of AgNPs and $AgNO_3$ (**a**) Synthesized AgNPs and UV–vis absorbance spectrometry of AgNPs, (**b**) UV–vis absorbance spectrometry of synthesized AgNPs solution, (**c**) The dissolved $AgNO_3$ before adsorption and UV-Vis adsorption spectrum of the $AgNO_3$, (**d**) the UV-Vis adsorption spectrum of the $AgNO_3$ prior to adsorption.*

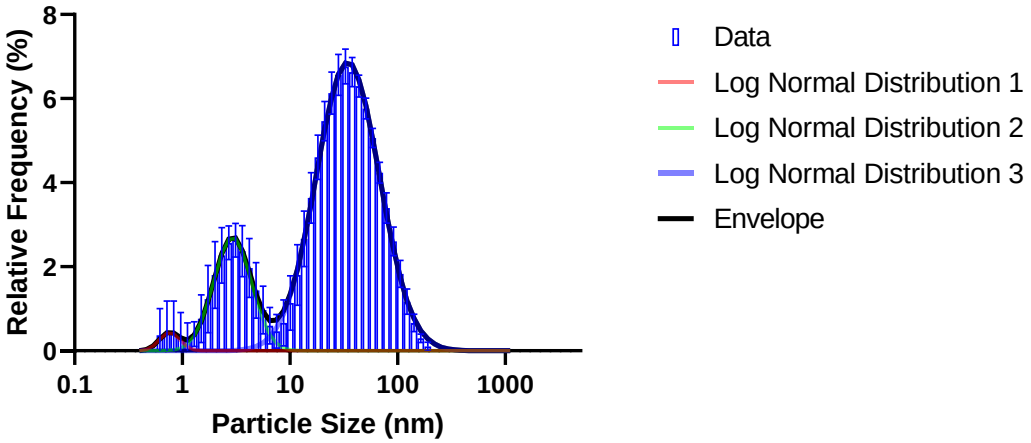

Figure 5-2. *Log-normal distribution for the AgNPs in suspension.*

Table 5-1. *Distribution properties of synthesised AgNPs.*

Distribution 1 (Red Peak)		Distribution 2 (Green Peak)		Distribution 3 (Blue Peak)		Total Distribution (Dashed Line/Bars)	
% of Total	d_{50} (nm) Predicted [1]	% of Total	d_{50} (nm) Predicted [1]	% of Total	d_{50} (nm) Predicted [1]	d_{50} (nm) Predicted [1]	*Z*-average (nm) Measured [2]
1.62	0.82	18.7	3.15	79.4	37.1	29.8	14.3

[1] As predicted from the distribution curves;

[2] As measured directly by the Zetasizer.

5.3.2 Ag/ESM Composite Adsorption Optimization, Kinetics, and Equilibrium Behaviour

The adsorption process was optimized for the mass of ESM required per 10 ml of solution, concentration, agitation time, pH, and temperature. This process was carried out for both AgNPs and $AgNO_3$. The slower adsorption of AgNPs compared to $AgNO_3$ was evident, possibly because of reduced interactions caused by the uncharged state of the AgNPs.

AgNPs became lighter in colour with increases in ESM load until 0.7 g, after which the solution became colourless and no longer returned a peak at around 400 nm. This change in colour indicates increased absorption, signified by a reduction in absorbance (Figure 5-3a). $AgNO_3$, on the other hand, was a colourless solution after

preparation. However, with every increase in ESM mass, the solution became colloidal with increased absorbance up until 0.4g (Figure 5-4a).

As observed in Figure 5-3c,d, increasing the concentration of AgNPs in solution before absorption decreased the relative Ag removal linearly after absorption. In contrast, the $AgNO_3$ saw an increased removal with increased initial concentrations as illustrated in Figure 5-4c,d.

Figure 5-3e,f demonstrate that the adsorption of AgNPs initially increased rapidly, with more than 60% of the adsorption taking place within the first 5 hours; this was followed by a much slower phase in which the remainder of the adsorption towards equilibrium took until 36 to 48 h. In contrast, the adsorption of $AgNO_3$ reached equilibrium within the initial 5 hours with negligible further adsorption after this time. The pH of the stock AgNPs was 6. This was adjusted from 4 to 10, and the effect on absorption was plotted in Figure 5-3h. The optimization was limited to this range because AgNPs turned dark grey and aggregated at pH less than 4 while it returned no peaks at pH greater than 10. The aggregation at low pH is likely caused by the high concentration of H^+ ions which lead to the protonation of the AgNP surfaces. The weaker surface charge reduces repulsion, which may lead to aggregation and precipitation. Absorbance and concentration readings were irregular at pH 4 and 5. This is most likely because of how close the solution is to that of the aggregation pH. However, at pH 6 and beyond, the change in pH had no effect on AgNPs absorption. This is indicative of a chemical absorption attributed to the surface charge of the ESM matrix and the ionic strength of the AgNPs [18,47]. The optimal absorption pH range for $AgNO_3$ was between 4 and 7. The solution returned no peak below pH 4 and aggregated with a grey colour above pH 7 (likely Ag(OH)). Nevertheless, $AgNO_3$ was immune to pH changes, as reported in Figure 5-4g,h.

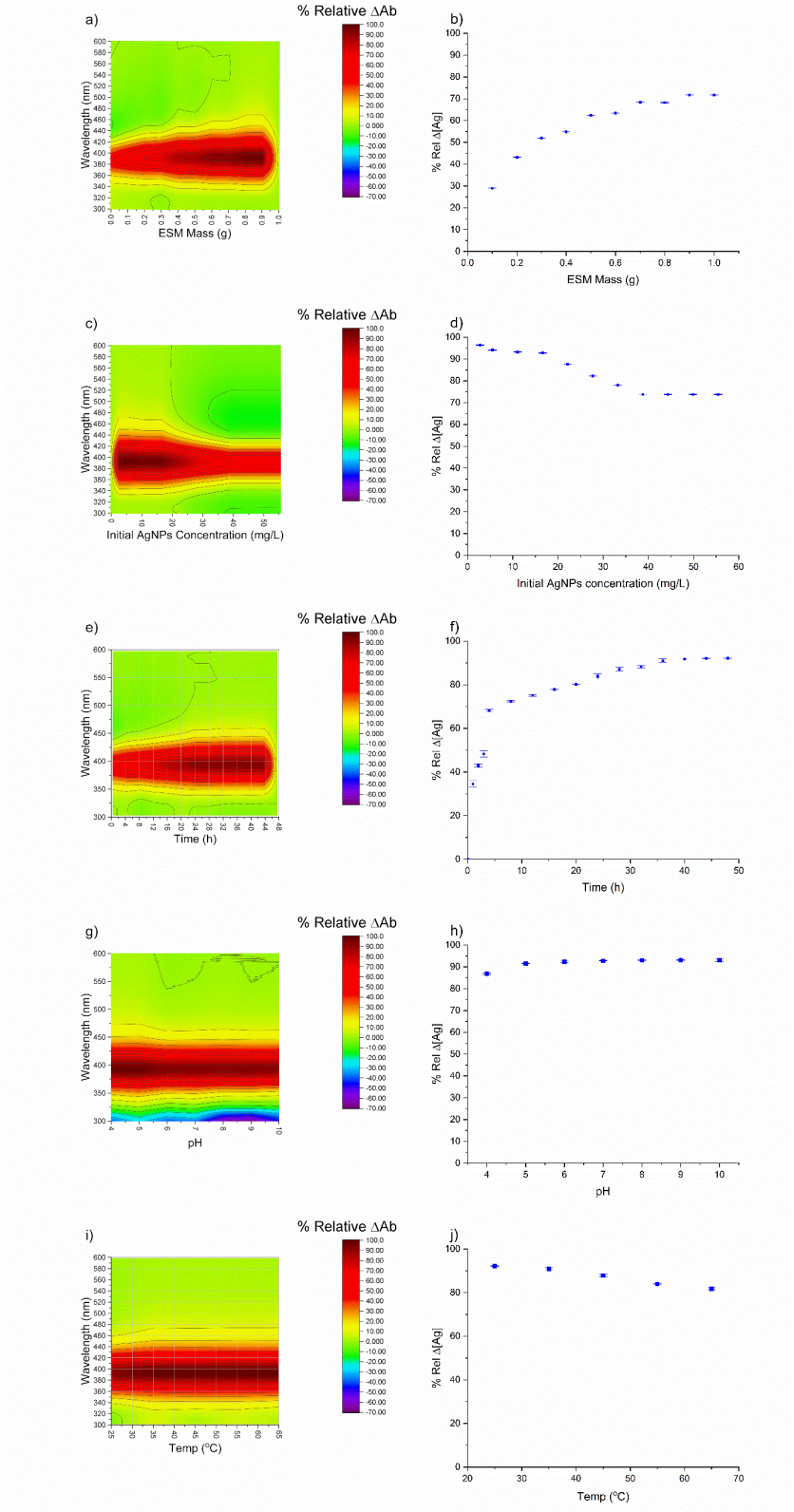

Figure 5-3. *AgNPs/ESM absorption parameters at 394 nm. (**a**) Contour plot of UV–vis absorbance spectrometry of $AgNO_3$ solution with change in ESM mass. (**b**) Effect of change in ESM mass on absorption. (**c**) Contour plot of UV–vis absorbance*

*spectrometry of AgNPs solution with change in initial AgNPs concentration. (**d**) Effect of change in ESM mass on absorption. (**e**) Contour plot of UV–vis absorbance spectrometry of AgNPs solution with change in agitation time. (**f**) absorption with change in agitation time. (**g**) Contour plot of UV–vis absorbance spectrometry of AgNPs solution with change in pH. (**h**) effect of change in pH on absorption. (**i**) Contour plot of UV–vis absorbance spectrometry of AgNPs solution with change in temperature. (**j**) effect of change in temperature on absorption.*

The adsorption temperature was varied from 25℃ to 65℃. The results (Figure 5-3i,j) revealed that absorption remained constant after 35℃. However, the concentration of Ag in the solution increased with an increase in temperature. This signifies the conversion of AgNPs to Ag^{+} at temperatures higher than 25℃. This is consonant with the know properties of AgNPs and why they are always prepared in an ice bath and stored at cool temperatures [180,190]. $AgNO_3$ behaved opposite to the AgNPs, the ESM turned dark brown at 45, 55, and 65 ℃, and the concentrations of Ag in solution significantly decreased with increased temperature (Figure 5-4i,j).

It was important to understand the kinetic behaviour of ESM absorption. The kinetic models tested and the corresponding fitted kinetic parameters are summarized in Table 5-2 and Table 5-3, respectively. The results of the fittings are shown in Figure 5-5.

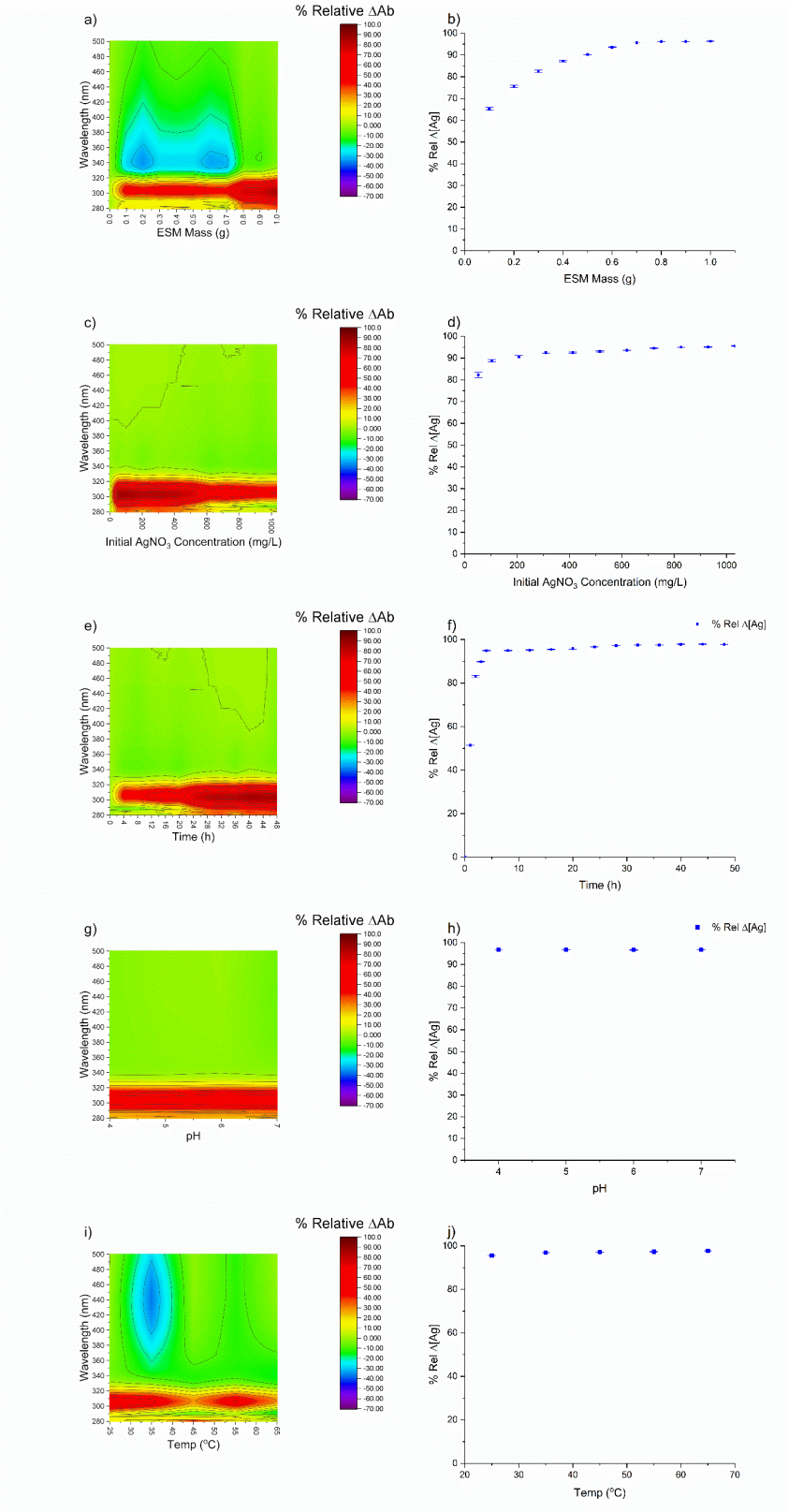

Figure 5-4. *$AgNO_3$/ESM absorption parameter at 294 nm. (**a**) Contour plot of UV–vis absorbance spectrometry of $AgNO_3$ solution with change in ESM mass. (**b**) Effect of change in ESM mass on absorption. (**c**) Contour plot of UV–vis absorbance*

*spectrometry of AgNO3 solution with change in initial $AgNO_3$ concentration. (**d**) Effect of change in ESM mass on absorption. (**e**) Contour plot of UV–vis absorbance spectrometry of $AgNO_3$ solution with change in agitation time (**f**) absorption with change in agitation time. (**g**) Contour plot of UV–vis absorbance spectrometry of $AgNO_3$ solution with change in pH. (**h**) effect of change in pH on absorption. (**i**) Contour plot of UV–vis absorbance spectrometry of $AgNO_3$ solution with change in temperature. (**j**) effect of change in temperature on absorption.*

The results for the kinetics model fits demonstrate that the AgNPs adsorption was best described by a 2-PA process with an R^2 = 0.982 (fast and slow adsorption in parallel [191,192]); this likely indicates heterogeneous interactions between the adsorbate and the adsorbent surface sites [191,192]. The adsorption kinetics of $AgNO_3$ is best described by the PFO model (R^2 = 0.990); this is supported by the observation that the 2-PA model reduces to a PFO model with the same R^2 value. This means that the system is likely significantly far from the saturation conditions, and therefore, the system behaves effectively irreversibly, and the adsorbate–adsorbent behaviour involves a single surface site per adsorbate molecule [193,194]. The CIMT model predicted an effective diffusivity value (D_e) of 2.78 × 10^{-11} $m^2.s^{-1}$ for the AgNPs. This does not compare well with results from the literature (D_{AgNPs} = 8.8 × 10^{-12}–9.34 × 10^{-12} [195], 9 × 10^{-17}–4.67 × 10^{-14} [196]); however, it should be noted that due to the size and characteristics of nanoparticles, these tend to behave more like particles than molecules and, therefore, more readily correspond to Brownian motion predicted by the Einstein–Stokes equation (Equation 5.1) [197]:

$$D = \frac{k_B.T}{6\pi\eta r} \qquad (5.1)$$

with D the diffusion coefficient ($m^2 \cdot s^{-1}$), k_B the Boltzmann constant (1.380649 × 10^{-23} $J \cdot K^{-1}$), T the absolute temperature (K), η the dynamic viscosity (Pa· s), r the radius of the particle (m).

Table 5-2. *Kinetic models for the adsorption of AgNPs and $AgNO_3$ by ESM.*

Kinetic Law	Differential Form *	Analytical Form *
Pseudo-first order (PFO) [198]	$\frac{dQ_t}{dt} = k_1(Q_e - Q_t)$	$Q_t = Q_e(1 - e^{-k_1 t})$
Pseudo-second order (PSO) [198]	$\frac{dQ_t}{dt} = k_1(Q_e - Q_t)^2$	$Q_t = \frac{(k_2 Q_e^2)t}{1 + k_2 Q_e t}$
Two-phase adsorption (2-PA) [191,192,199,200]	$\frac{dQ_{t,slow}}{dt} = k_{slow}\left((1-\phi)Q_e - Q_{t,sloe}\right)$ $\frac{dQ_{t,fast}}{dt} = k_{fast}\left(\phi Q_e - Q_{t,fast}\right)$ $\frac{dQ_t}{dt} = \frac{dQ_{t,slow}}{dt} + \frac{dQ_{t,fast}}{dt}$	$Q_t = Q_e\left((1-\phi)\left(1 - e^{-k_{fast}t}\right) + \phi(1 - e^{-k_{slow}t})\right)$ [201]
Crank internal mass transfer model (CIMT) [198]	$\frac{\partial Q_t}{\partial t} = \frac{D_e}{r^2}\frac{\partial}{\partial r}\left(\frac{r^2 \partial Q_t}{\partial r}\right)$	$\frac{Q}{Q_{max}} = \begin{cases} 6\left(\frac{D_e t}{R^2}\right)^{\frac{1}{2}}\left[\pi^{-\frac{1}{2}} - \left(\frac{1}{2}\right)\left(\frac{-D_e t}{R^2}\right)^{\frac{1}{2}}\right], & \frac{Q}{Q_{max}} < 0.8 \\ 1 - \frac{6}{\pi^2}\exp\left(\frac{-D_e \pi^2 t}{R^2}\right), & \frac{Q}{Q_{max}} \geq 0.8 \end{cases}$ [201]
Weber and Morris (W&M) [198,202]		$Q_t = k_{WM,i} t^{\frac{1}{2}} + C, k_{WM,i} = \frac{D_{e,i}}{r^2}$ [203]

* The definitions of the kinetic model parameters: General parameters: *Qt*—amount of dye adsorbed per unit of adsorbent at time t (mg· g−1), *Qe*—equilibrium adsorption capacity of adsorbent (mg· g−1), *r* = the average radius of the adsorbent particles (a conservative estimate of 16 μm was used as all particle diameters < 32 μm). Pseudo-first order (PFO) kinetics: *k1*—the PFO rate constant (min−1) Pseudo-second order (PSO) kinetics: *k2*—the PSO rate constant (g· mg−1· min−1), Two-phase adsorption (TPA) kinetics: *kfast*—the rate constant for the fast TPA adsorption (min−1), *kslow*—the rate constant for the slow TPA adsorption (min−1), ϕ—the fraction of adsorption taking place during the fast adsorption step (dimensionless) Crank internal mass transfer kinetic model: *De*—the effective diffusivity of the adsorbate in the system (m2· s−1) Weber and Morris kinetic model: *KWM,i*—the Weber–Morris intra-particle diffusion rate constant for adsorption phase *i* (mg· g−1), *De,i*—the effective diffusivity of the adsorbate during adsorption phase *i* (m2· s−1).

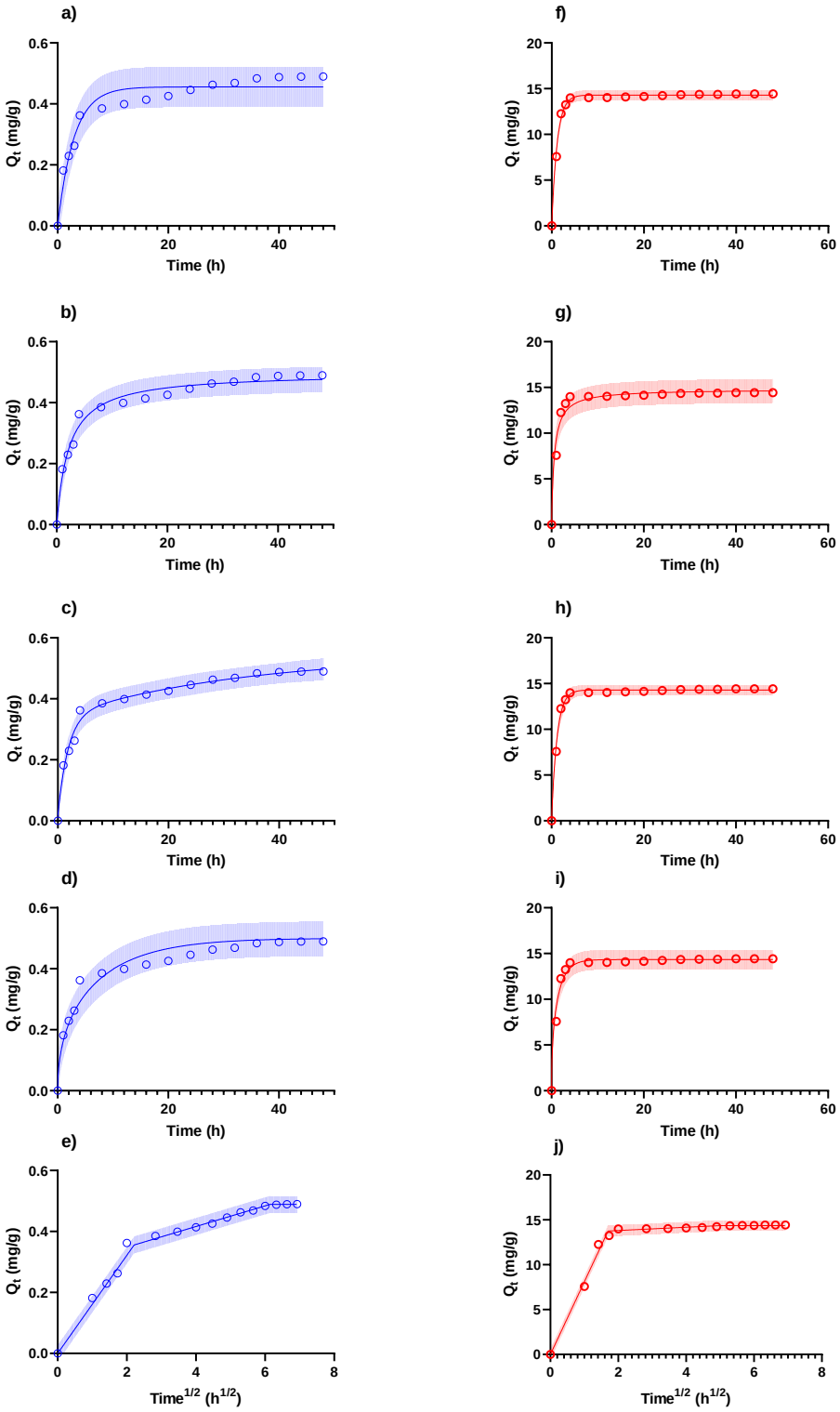

Figure 5-5. *Kinetics of adsorption (**a**–**f**) AgNPs, (**g**–**j**) $AgNO_3$. The model fits were (**a**,**f**) PFO, (**b**,**g**) PSO, (**c**,**h**) 2-PA, (**d**,**i**) CIMT, (**e**,**j**) W&M. The shaded areas represent the 95% prediction intervals* [203].

Table 5-3. *Fitted kinetic and goodness-of-fit parameters for kinetic models presented in Table 5-1.*

Kinetic Law	AgNPs		$AgNO_3$	
	Fitted Parameters	**R^2/RMSE**	**Fitted Parameters**	**R^2/RMSE**
PFO	k_1 = 0.339 min^{-1}	0.922/0.0316 $mg \cdot g^{-1}$	k_1 = 0.848 min^{-1}	0.990/0.261 $mg \cdot g^{-1}$
PSO	k_2 = 0.921 $g.mg^{-1} \cdot min^{-1}$	0.970/0.0196 $mg \cdot g^{-1}$	k_2 = 0.113 $g \cdot mg^{-1}.min^{-1}$	0.942/0.634 $mg \cdot g^{-1}$
2-PA	k_{fast} = 0.540 min^{-1}	0.982/0.0154 $mg \cdot g^{-1}$	$k_{fast} = k_{slow}$ = 0.848 min^{-1}	0.990/0.261 $mg \cdot g^{-1}$
	k_{slow} = 0.0297 min^{-1}		ϕ = N/A	
	ϕ = 0.616			
CIMT	$\frac{De}{r^2}$ = 0.0111 h^{-1}	0.940/ 0.0278 $mg \cdot g^{-1}$	$\frac{De}{r^2}$ = 0.0565 h^{-1}	0.963/ 0.509 $mg \cdot g^{-1}$
	D_e = 2.78 × 10^{-11} $m^2 \cdot s^{-1}$		D_e = 1.41 × 10^{-10} $m^2 \cdot s^{-1}$	
W&M	D_{e1} = 2.78 × 10^{-11} $m^2 \cdot s^{-1}$	0.986/0.0133 $mg \cdot g^{-1}$	D_{e1} = 1.41 × 10^{-10} $m^2 \cdot s^{-1}$	0.989/0.276 $mg \cdot g^{-1}$
	D_{e2} = 1.24 × 10^{-12} $m^2 \cdot s^{-1}$		D_{e2} = 2.80 × 10^{-14} $m^2 \cdot s^{-1}$	
	D_{e3} = 0 $m^2 \cdot s^{-1}$		D_{e3} = 0 $m^2 \cdot s^{-1}$	

For the system under consideration, values for D = 1.65 × 10^{-11} m^2/s for d_p = 29.8 nm (the d_{50} determined from the particle size distribution—Table 5-1) and D = 3.42 × 10^{-11} m^2/s (the *Z-average* measured by the Zetasizer—Table 5-1) were calculated using Equation 1. From these results can be seen that the D_e = 2.78 × 10^{-11} $m^2 \cdot s^{-1}$ falls comfortably within the predicted range, and therefore, the diffusivity of the nanoparticles is not significantly affected by the adsorbent particle characteristics [204]. The effective diffusivity of the $AgNO_3$ was determined as D_e = 1.41 × 10^{-10} $m^2 \cdot s^{-1}$, significantly lower than the molecular diffusivity for $AgNO_3$ of 1.71 × 10^{-9} $m^2 \cdot s^{-1}$ [205]; this indicates that the $AgNO_3$ was significantly limited by the internal structure of the adsorbent. The initial phase of the W&M models corresponded well with the predictions made by the CIMT models for both the AgNPs and $AgNO_3$, thereby supporting the observation made for the CIMT model [206].

To elucidate the equilibrium data for the AgNPs and $AgNO_3$ adsorption, isotherm models were fitted to the data, as summarized in Table 5-4 The resulting fitted graphical fits are shown in Figure 5-6.

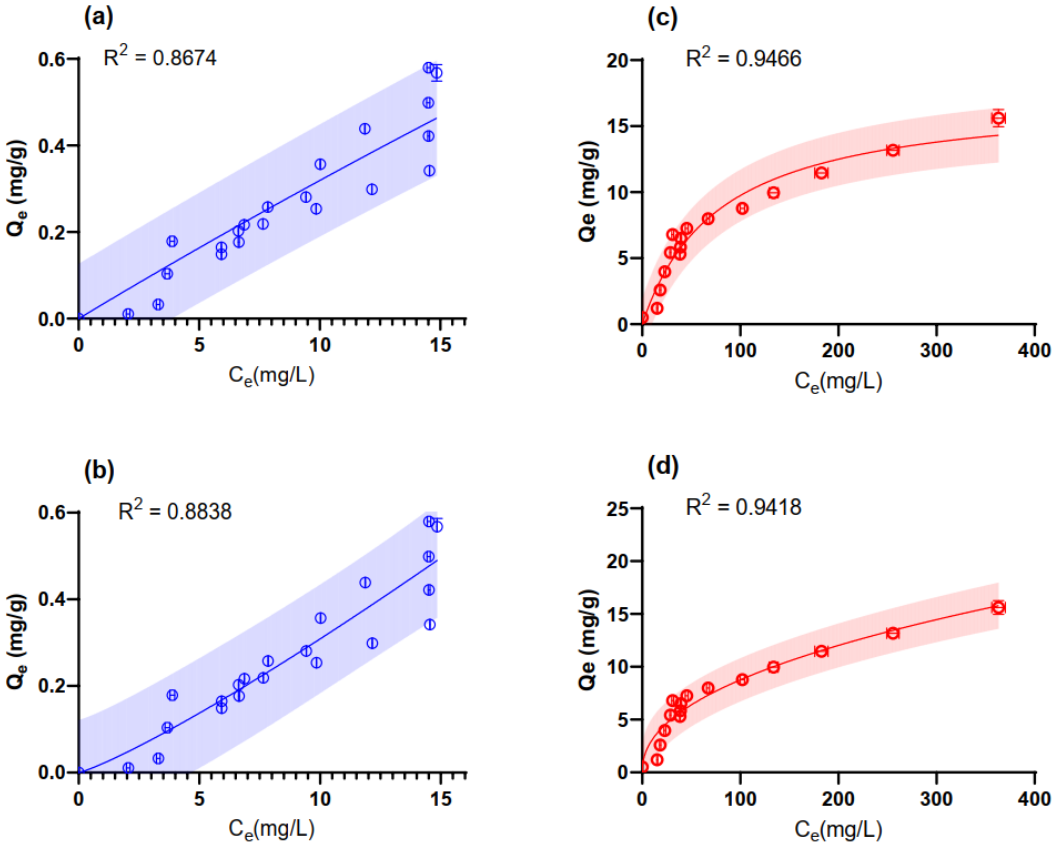

Figure 5-6: *The isotherm model fits for (**a**,**b**) AgNPs and (**c**,**d**) $AgNO_3$. The models fitted were (**a**,**c**) Langmuir, (**b**,**d**) Freundlich. The shaded areas represent the 95% prediction intervals.*

Table 5-4: *Isotherm models for the adsorption of AgNPs and $AgNO_3$ by ESM.*

Isotherm	Non-Linear Form *	AgNPs		$AgNO_3$	
		Fitted Parameters	R^2/RMSE	Fitted Parameters	R^2/RMSE
Langmuir [198,207,208]	$Q_e = \frac{k_L Q_{max,L} C_e}{1 + k_L C_e}$,	$k_L = 0.0050\ \mathrm{L \cdot mg^{-1}}$ $Q_{max} = 6.71\ \mathrm{mg \cdot g^{-1}}$	0.867/ 0.060 mg·g^{-1}	$k_L = 0.0127\ \mathrm{L \cdot mg^{-1}}$ $Q_{max} = 17.41\ \mathrm{mg \cdot g^{-1}}$	0.947/ 0.935 mg·g^{-1}
Freundlich [208]	$Q_e = K_F C_e^{\frac{1}{n_F}}$	$K_F = 0.0209\ \mathrm{mg \cdot g^{-1}(L \cdot mg^{-1})^{\frac{1}{n_F}}}$ $n_F = 0.856$	0.884/ 0.067 mg·g^{-1}	$K_F = 1.07\ \mathrm{mg \cdot g^{-1}(L \cdot mg^{-1})^{\frac{1}{n_F}}}$ $n_F = 2.19$	0.942/ 0.977 mg·g^{-1}

* The definitions of the isotherm parameters: Langmuir isotherm: *kL*—the Langmuir equilibrium constant (L· mg−1), *Qmax,L*—the Langmuir maximum adsorption capacity (mg· g−1); Freundlich isotherm: *KF*—the Freundlich intensity parameter ((mg· g−1)(L· mg−1)1/nF), *nF*—Freundlich isotherm exponent (dimensionless).

The isotherm data for the AgNPs exhibited significant variation, likely because of the variability in the AgNPs sizes (Figure 5-2) and the heterogeneity of the surface interactions. The data fitted the Freundlich model most closely supporting the

heterogenous surface interactions reported for the kinetic data (2-PA model). It is interesting to note that a Freundlich exponent of 0.856 was fitted, indicating an upward-sloping isotherm with increasing adsorption as the concentration rises. These results likely indicate multi-layer adsorption as previously reported for biosorption of Cu-ions by *Pseudomonas syringae* [209].

The isotherm data for the $AgNO_3$ appeared to reach an initial maximum at a maximum adsorption capacity of ≈ 17 mg/g. This shape is characteristic of the Langmuir isotherm model in which the surface is saturated with a monolayer of adsorbate (consistent with the observations reported in the kinetic runs).

5.3.3 Characterization of Ag/ESM Composites

The fibre-like structures of ESM composites were analysed using SEM-EDS (Figure 5-7 and appendix Figures A5.2 – A5.4). This porous fibril structure responsible for ESM's absorption capacity [51] proved effective. As observed in the EDS map image in Figure 5-7d,f (and appendix Figures A5.2 and A5.3), $AgNO_3$ and AgNPs were evenly absorbed on the surface of the membrane. Both Ag solutions were significantly absorbed into the ESM with weighted compositions of 15.68% and 4.87% for $AgNO_3$ and AgNPs, respectively (Table 5-5).

Table 5-5: *EDS elemental analysis of ESM composites.*

Element	ESM (Wt%)	$AgNO_3$/ESM (Wt%)	AgNPs/ESM (Wt%)
Ag	-	15.68	4.87
S	46.42	30.52	36.05
O	49.97	53.19	57.62
Si	0.85	-	-
Ca	2.77	0.61	1.45

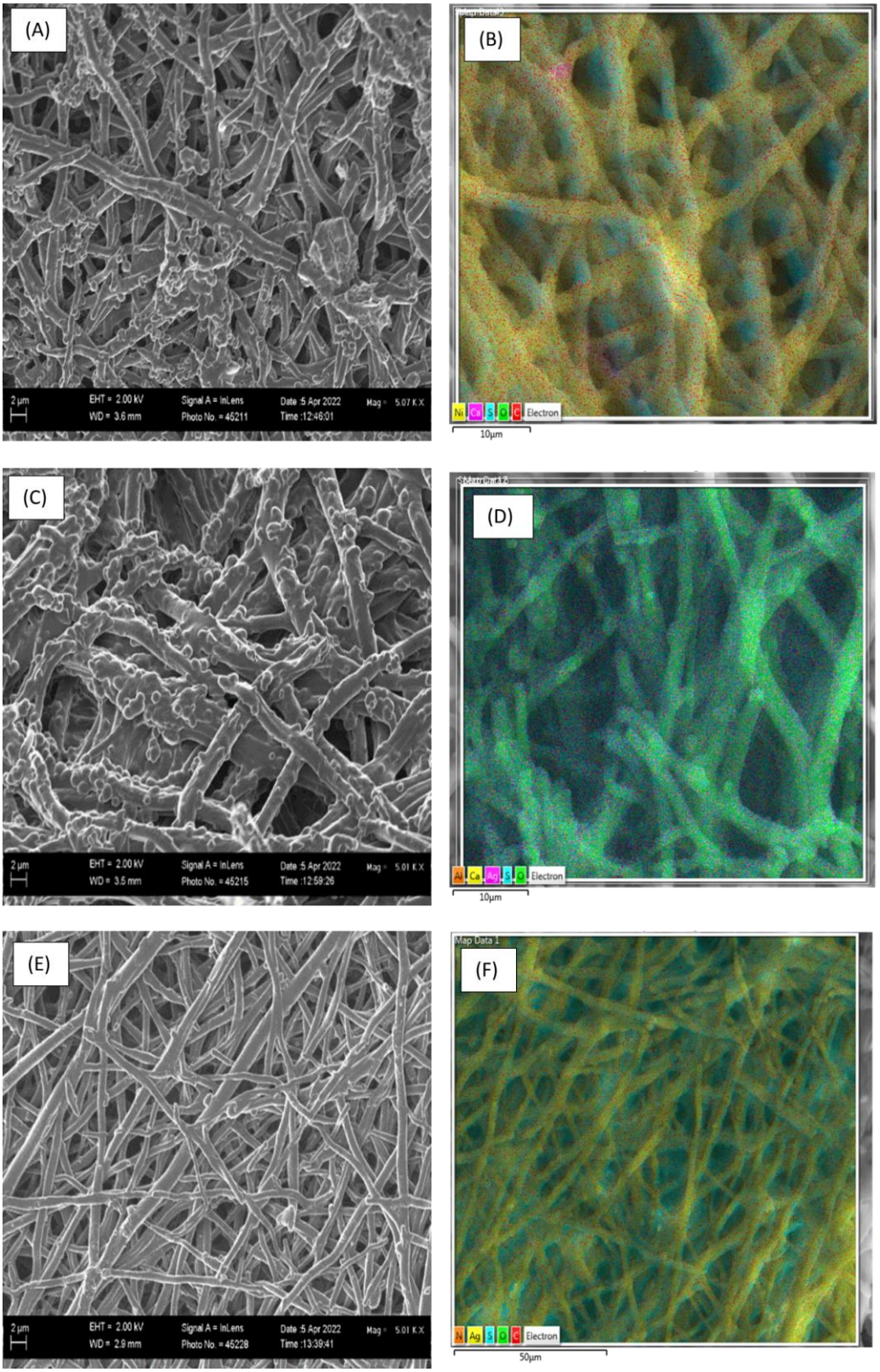

Figure 5-7: *SEM images (**a**,**c**,**e**) EDS maps (**b**,**d**,**f**) of ESM composite. (**a**,**b**) ESM. (**c**,**d**) AgNO3/ESM. (**e**,**f**) AgNPs/ESM.*

The AgNPs ESM structure shows a much more even distribution of the coated Ag, which dominates the surface composition; this is indicative of a slower, more controlled deposition (Figure 5-7d and A5.2). The $AgNO_3$ ESM shows nodules on the fibre surface. This suggests compounds are absorbed, producing a rougher texture, with predominantly oxygen on the surface; this is observed via the cyan-like colour as a mixture of green (oxygen) and magenta (silver), as shown in Figure 5-7f and A5.3. This suggests the presence of AgO as the form of Ag absorbed. This supports the notion that $AgNO_3$ is reduced to AgO as part of the absorption process. This rough surface is likely a product of the high rates of absorption. The absorption occurred on both the ESM matrix as well as previously absorbed material. In this mechanism, the growth of crystallites is favoured over nucleation. This suggests an abundance of absorption sites; the same conclusion is reached through modelling.

All materials exhibited broad FTIR absorption peaks at 3275 and 2927 cm^{-1} corresponding to O-H and N-H groups stretching mode. Peaks of C=O (amide I), CN/NH (amide II), and CN/NH (amide III) modes were prominent at 1638, 1517, and 1442 absorption bands. This corresponds to reports from [147] with similar peaks. The 1235 cm^{-1} is often correlated with the stretching vibration of C-O bonds and interaction with some amino acids. The shifts and/or changes in the intensity of these peaks indicate an interaction of the nanoparticles with the protein structure.

The bands at 1077, 875, and 556 cm^{-1} correspond to the C-O stretching modes, CH_2 deformation, and unknown peaks in the fingerprint region. The higher intensity of these peaks in the Ag/ESM samples compared to ESM indicates the absorption of $AgNO_3$ and AgNPs to ESM. Likewise, peak shifts were identified in these bands between ESM and the composite samples, which were also indicative of the absorption process [147] (Figure 5-8 and Table 5-6).

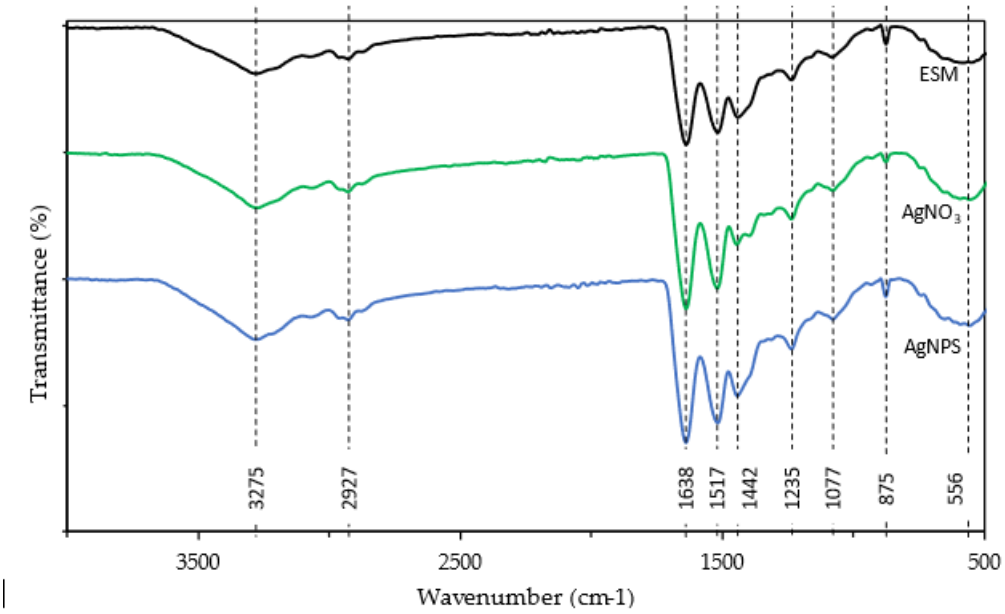

Figure 5-8: *FTIR spectra of ESM, $AgNO_3$/ESM, and AgNPs/ESM.*

Table 5-6: *FTIR spectra of ESM composites.*

Species	O-H	N-H	C=O (Amide I)	CN/NH (Amide II)	CN/NH (Amide III)	C-O	C-O Stretching	CH_2 Deformation
ESM	3274.36	2926.90	1637.21	1517.58	1439.67	1235.67	1080.33	874.94
$AgNO_3$/ESM	3269.37	2927.48	1637.56	1518.81	1444.05	1235.26	1078.68	875.19
AgNPs/ESM	3275.56	2927.09	1638.14	1517.33	1442.24	1235.33	1077.26	875.50

The results from FTIR suggest a strong interaction of the silver compounds with the amine groups present in the eggshell membrane. The interaction with the proteins may have led to the absorption of nanoparticles to the surface, likely through van der Waals forces. Similarly, proteins (glycine, lysine, or cysteine) may have contributed to the reduction of $AgNO_3$ to AgO.

X-ray photoelectron spectroscopy (XPS) was used to investigate the valence state and chemical composition of Ag absorbed on ESM, as seen in Figure 9 and Table 3. Elemental signals of O1s, C1s, N1s, and $CaCO_3$ compounds were detected on ESM, $AgNO_3$/ESM, and AgNPs/ESM samples. The ESM sample had no trace of silver, as expected. $AgNO_3$/ESM sample had signals of both elemental silver ($3d_{5/2}$ Ag0 and $3d_{3/2}$ Ag^0 with peaks at 368.08 and 374.77, respectively) and silver oxide ($3d_{3/2}$ AgO with peaks at 364.41 and 370.41). AgNPs/ESM, on the other hand, only had signals

of elemental silver ($3d_{5/2}$ Ag^0 and $3d_{3/2}$ Ag^0 with peaks at 367.89 and 373.91, respectively) with similar peaks as those found in the $AgNO_3$/ESM composite. These AgNPs peaks are similar to those already reported by [22], signifying the successful absorption of AgNPs on ESM. The similar Ag^0 peaks found in both $AgNO_3$/ESM and AgNPs/ESM also signify the reduction of $AgNO_3$ to nanoparticles by ESM during the adsorption process.

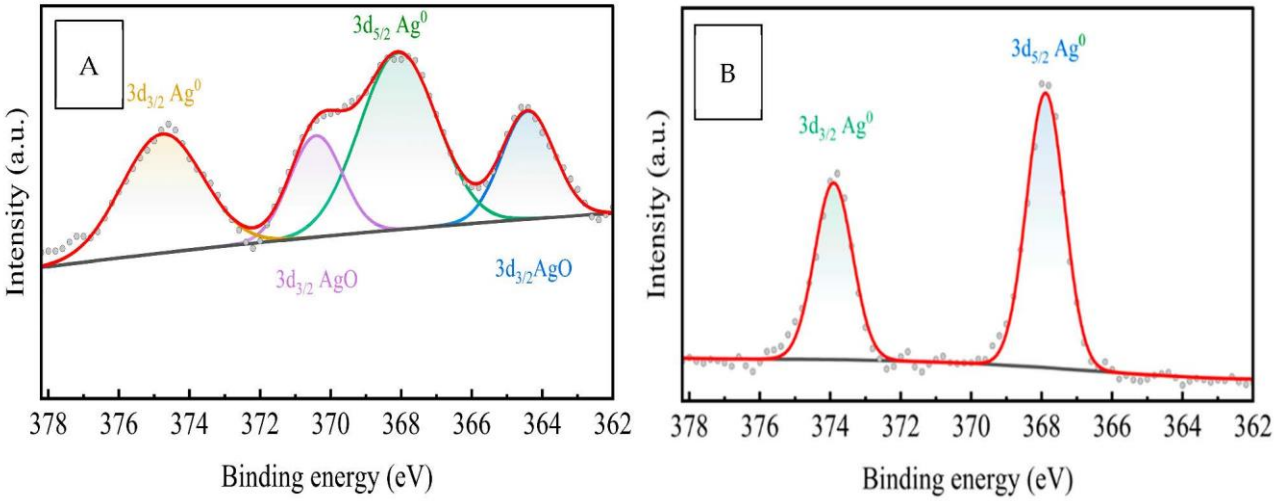

Figure 5-9: *XPS spectrum for (A) $AgNO_3$/ESM and (B) AgNPs/ESM.*

The results indicate that the adsorption mechanism is dictated by surface interactions between the AgNPs/$AgNO_3$ and the ESM. According to Xin et al. [210], the interactions of heavy metals and ESM is strongly affected by surface species. In contrast, however, the lack of pH effects on either AgNPs or $AgNO_3$ adsorption negates the likelihood of significant electrostatic or ion exchange mechanisms present in the Ag/ESM adsorption—as proposed by Xin et al. [210]. It is clear from the shifts in FTIR peaks (Table 5-7) that significant interactions between the Ag species and the O-H, NH, C=O (amide I), CN/NH (amide II), and CN/NH (amide III). C-O bond, C-O stretching, and CH_2 deformation with significant shifts observed. This is confirmed by the Ag distribution observed in the SEM-EDS (Figure 5-7) and the significant shifts in the O1s and N1s peaks in the XPS results (Table 5-7).

Table 5-7: *XPS analysis of ESM composites.*

	ESM	AgNO3/ESM	AgNPs/ESM
O1s	531.40 and 532.35	531.79 and 533.48	531.32 and 532.15
N1s	399.76	399.86	399.70
3d Ag0	-	368.08 and 374.77	367.89 and 373.91
3d AgO	-	364.41 and 370.41	-
Ca 2p	347.22 and 350.80	347.19 and 350.75	347.21 and 350.78
C1s	284.57, 285.50, 287.75, and 288.57	284.56, 285.31, 287.45, and 288.74	284.54, 285.11, 287.5, and 288.4

5.3.4 Antimicrobial Activity of Ag/ESM Composites

P. aeruginosa is an opportunistic gram-negative pathogen that is common and highly adaptive to various environmental conditions, including aquatic environments [211]. It is highly resistant to antimicrobials, with a percentage resistance of 33.9%. This makes it vital to treat concrete, especially in aquatic environments [212,213]. On the other hand, *B. subtilis,* though gram-positive, can survive harsh conditions such as high temperature, UV, and ɣ-radiation. It is also found in various environments and broadly adapted to grow in diverse settings within the biosphere, from soil to marine habitats [214,215]. *B. subtilis* has shown the highest occurrence in hospital settings compared to other bacteria groups, with the biggest percentage of multiple resistant strains to antimicrobials. Their ability to survive harsh conditions makes them a problem for cleaning and disinfection [216].

For purposes of consistency, concentrations were based on the concentration of Ag in the sample, and the mass of ESM was determined from the mass that could provide 100 µg/L of AgNPs. The agar well diffusion showed clear halos of varying diameters, indicating antimicrobial properties for AgNPs, AgNPs/ESM, and $AgNO_3$, as shown in Figure 5-10. This is evidenced by both bacteria and the strength of the antimicrobial activity depending on the component tested. These results were fitted into the zone of inhibition bar charts, as shown in Figure 5-11

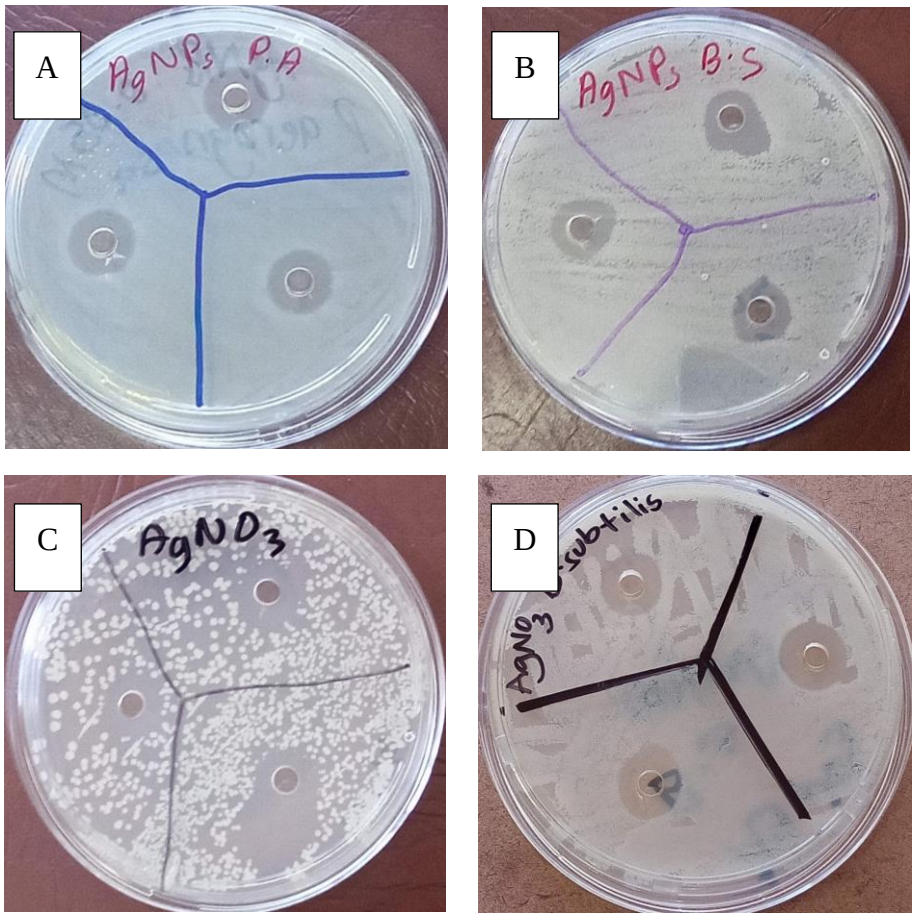

Figure 5-10: *Agar well diffusion images. (**A**) AgNPs with P. aeruginosa, (**B**) AgNPs with B. subtilis, (**C**) $AgNO_3$ with P. aeruginosa, (**D**) $AgNO_3$ with B. subtilis.*

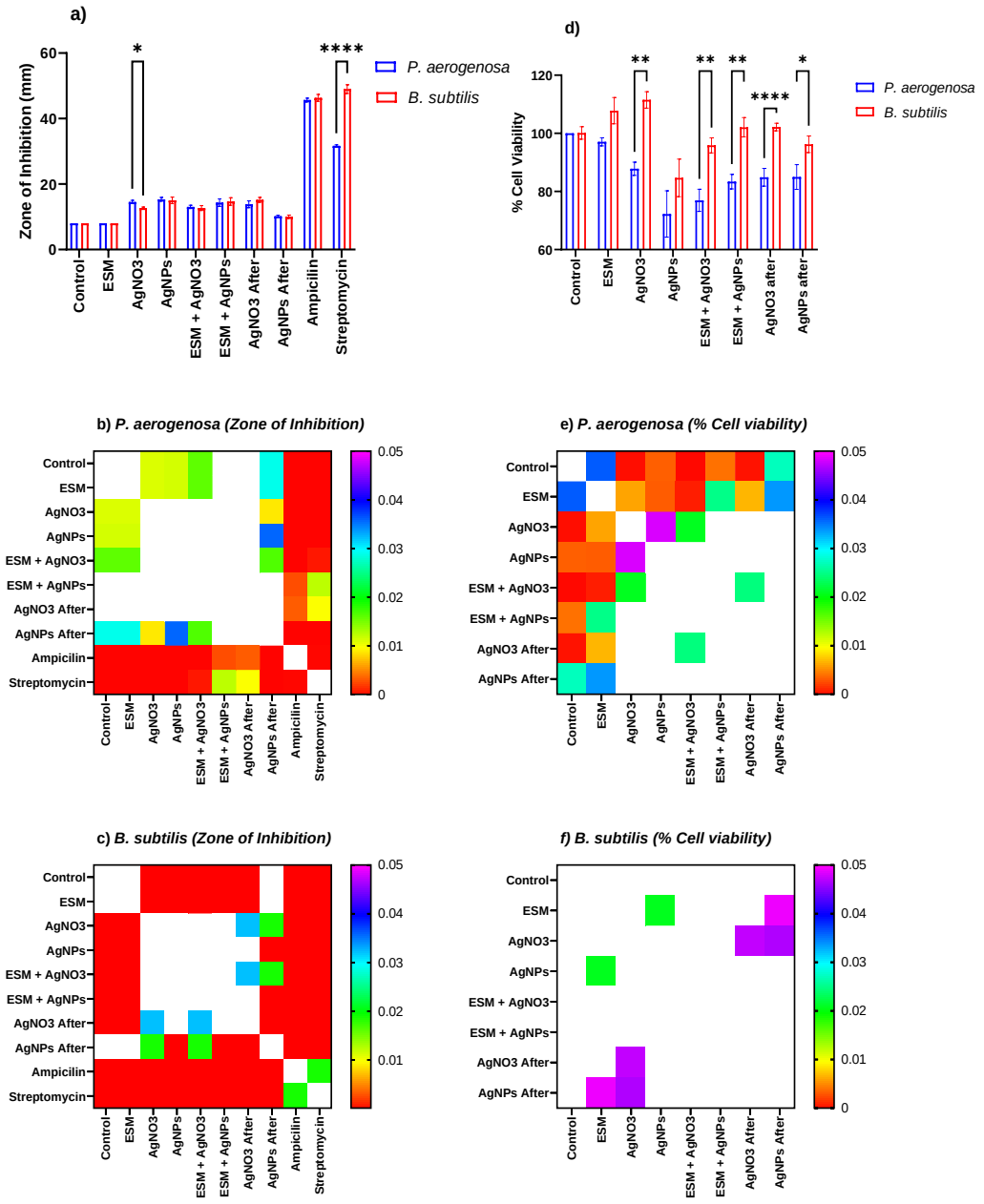

Figure 5-11: *Antimicrobial characterisation of ESM composite.* ***(a,d)*** *Results of Zone of Inhibition* ***(a)*** *and % Cell Viability* ***(d)*** *results for the different microbial species exposed to the different combinations of solid materials. The brackets indicate those comparisons between the species that exhibited significant differences.* ***(b,c,e,f)*** *Show heatmaps of the adjusted p-values when comparing the ZoI and % Cell viability results for the various materials. White indicates adjusted p-values > 0.05 (i.e., no*

*significant difference at the 95% confidence level). (**b**,**e**) for P. aeruginosa and (**c**,**f**) for B. subtilis.*

The positive controls, streptomycin and ampicillin, gave extremely large zones as compared to the AgNPs-ESM, indicating that the bacteria were more susceptible to their antimicrobial activity. ESM showed no effect on the growth of either *B. subtilis* or *P. aeruginosa*, implying that all the antimicrobial activity observed in the Ag-ESM was due to the adsorbed AgNPs on the ESM.

According to Figure 5-11a, the results of the zone of the inhibition tests presented show significant inhibition to the growth of both *P. aeruginosa* and *B. subtilis*. This revealed that ESM alone had the least effect on either bacterium, while AgNPs were the most effective, followed by $AgNO_3$ excluding the antibiotics. This observation could be the result of the reduction of $AgNO_3$ to AgNPs during absorption. $AgNO_3$, after adsorption, had the most antibacterial effect. As expected, the AgNPs medium after adsorption had the least significant because most of its antimicrobial particles have been absorbed into the ESM surface.

When the components were exposed to bacteria in a liquid medium, the MTT assay showed that *P. aeruginosa* is more susceptible to the antimicrobial activity of AgNPs-ESM compared to *B. subtilis* (Figure 5-11d). *P. aeruginosa* showed a percentage cell death of 27.77% and 23.16% for AgNPs and AgNPs-ESM, respectively. In contrast, it is evident that 10 µM $AgNO_3$, ESM, and $AgNO_3$-ESM had no significant cytotoxic effect on *B. subtilis* while AgNPs and AgNPs-ESM showed minimal antimicrobial activity with 15.34% and 4.15% cell death for AgNPs and AgNPs-ESM, respectively, when compared to the control samples.

The results were supported by Tukey multiple comparison tests [217], which assessed the significance of the differences in the observations for ZOI and MTT for *B. subtilis* and *P. aeruginosa.* The results are summarized in Figure 5-11b,c,e,f, and show that when agar-well diffusion was used, there was no observable difference between the antimicrobial activity of AgNPs-ESM against *B. subtilis* and *P. aeruginosa*—except for a small but significant difference in the $AgNO_3$ only well, and a much more significant effect of Streptomycin on *P. aeruginosa* (It has been observed that *P.*

aeruginosa exhibits intrinsic antibiotic resistance to Streptomycin [218]). In contrast, marked differences in the effects on *B. subtilis* and *P. aeruginosa* were observed in the MTT tests, with *B. subtilis* exhibiting significant tolerance to metabolic inhibition while *P. aeruginosa* was significantly inhibited.

Based on the results, $AgNO_3$ and AgNPs produces ESM composites with good antimicrobial properties and can be used for further applications such as wound healing and incorporation into antimicrobial concrete.

5.4 CONCLUSIONS

ESM has proven to be a great absorption agent for both $AgNO_3$ and AgNPs. This is because of its fiber-like structure, as observed through SEM micrographs, the result obtained by [219]. Absorption was optimum at 70% concentration, pH 6, after 48 hours of agitation time and at room temperature. The strong AgNP peaks recorded at 394 nm is a function of surface plasmon resonance (SPR) vis-à-vis the absence of particle aggregation. These observations are inconsonant with the findings. Both AgNPs and $AgNO_3$ were evenly absorbed on ESM as observed by EDX maps, with 15.68% and 4.87% composition for $AgNO_3$ and AgNPs, respectively.

During the adsorption of $AgNO_3$, an increase in several FTIR peaks was observed. This was thought to be an indication of the reduction of $AgNO_3$ to Ag nanoparticles by the ESM. This assumption was later confirmed by the result of XPS analysis and the zone of inhibition test of $AgNO_3$ after on *B. subtilis.* XPS results, in conjunction with other microstructural analyses, revealed that ESM was able to synthesize Ag NPs from $AgNO_3$ during adsorption.

This optimized composite is deemed to find good use in antimicrobial applications in the medical and construction fields. With respect to the availability of ESM and the continuous advocacy for a circular economy, Ag/ES M composites will be a good step toward achieving a waste reduction in the food industry.

CHAPTER 6 CYTOTOXIC AG MODIFIED EGGSHELL MEMBRANE NANOCOMPOSITES AS BACTERICIDES IN CONCRETE MORTAR

Submitted to International Journal of Molecular Sciences: Refer to; Aina, S. T., Kyomuhimbo, H. D., Du Plessis, B., Mjimba, V., Haneklaus, N., & Brink, H. G. (2023). Cytotoxic Ag Modified Eggshell Membrane Nanocomposites as Bactericides in Concrete Mortar. International Journal of Molecular Sciences

Chapter Abstract

Against the backdrop of escalating infrastructure budgets worldwide, a notable portion – up to 45% – is allocated to maintenance endeavors rather than innovative infrastructure development. A substantial fraction of this maintenance commitment involves combatting concrete degradation due to microbial attacks. In response, this study endeavours to propose a remedial strategy employing nano metals and repurposed materials within cement mortar.

The methodology entails the adsorption of silver nitrate ($AgNO_3$) or silver nanoparticles (AgNPs) onto eggshell membranes yielding silver-eggshell membrane composites (Ag-EMs). Subsequently, the resulting Ag-EMs were introduced in different proportions to replace cement, resulting in the formulation of ten distinct mortar compositions. A thorough analysis encompassing a range of techniques, such as spectrophotometry, scanning electron microscopy, thermogravimetric analysis, X-ray fluorescence analysis, X-ray diffraction (XRD), and MTT assay, was performed on these composite blends. Additionally, evaluations of both compressive and tensile strengths were carried out.

The mortar blends 3, 5 and 6, characterized by 2% ESM/$AgNO_3$, 1% ESM/AgNPs, and 2% ESM/AgNPs cement replacement, respectively, exhibited remarkable antimicrobial efficacy, manifesting in substantial reduction in microbial cell viability (up to 50%) of typical waste activated sludge. Concurrently, a marginal reduction of

approximately 10% in compressive strength was noted, juxtaposed with an insignificant change in tensile strength.

This investigation sheds light on a promising avenue for addressing concrete deterioration while navigating the balance between material performance and structural integrity.

6.1 INTRODUCTION

Concrete is undoubtedly the most used construction material having found acceptance in a wide variety of applications. Notable is the fact that this mixture of cement, fine aggregate, coarse aggregate, and water (in the case of concrete) or just cement sand and water (mortar) is nowhere near its end of life [5,223,224]. Statista [225] reported that 4.1 billion tons of cement was produced in 2022 as against 1.39 billion tons in 1995.

As versatile as it is, one principal dilemma of concrete structures is its high cost of maintenance which has been seen to go as high as 45% of the total infrastructure budget in the UK and EU [5]. This expensive maintenance has been necessitated due to environmental factors, human factors, use over time, and microbial attack (especially in wet conditions) [6].

The need to prolong the life of concrete while reducing the cost of maintenance has therefore necessitated various research with some aimed at inhibiting bacterial growth and biofilm formation. Among many other antimicrobial agents, silver and silver nanoparticles (AgNPs) are some of the most promising bacterial inhibitors [6,22].

The size, shape, surface charge, concentration, and colloidal state are the key physio-chemical factors that significantly influence the antimicrobial effectiveness of silver nanoparticles (AgNPs). Some of the shapes documented in literature include oval, spherical, cubic, cylinder, and triangular, which are sometimes attributed to different synthesis techniques [171,226,227]. These synthesis techniques include physical, chemical, or green methods. The chemical method, which involves the use of

reducing agents and stabilizers such as formaldehyde, hydrazine, and sodium borohydride, is one such techniques [168].

Eggs are characterized as being porous, bioceramic, calcareous, and oval. Chicken eggs possess the necessary strength to withstand physical and pathogenic threats while still facilitating the exchange of water and gases necessary for embryo development [28,29,179]. Lining the walls of the eggshell is the shell membrane (ESM). ESM is a fibrous biomaterial that possesses a high surface area and excellent adhesion ability [180]. As indicated in Li et al. (2017) [182], the adsorption of metal ions by ESM is facilitated by electrostatic, hydrogen bonding, and van der Waals forces, which are activated when ESM is exposed to these ions.

Globally, egg production continues to rise with each passing year and with this increase comes the need to manage the shell waste. In 2008, 62 million metric tons was recorded. This grew to 76.7 million metric tons in 2018 and 86.3 million metric tons in 2021 [19,23,24]. Worthy of note is the approximately 10 million metric tons increase recorded between 2018 and 2021 (4 years), an increase that previously took about 13 years. With a shared mix of 452,000 tons of eggs in 2018, the South African poultry industry is not left behind. Despite the 10.2% shell content, these figures calls for a fast and decisive action especially when all other waste are put into context [25].

The concerning upward trajectory of waste production provides the basis for the concept of a circular economy. Circular economy aims to eliminate waste through the perpetual use of resources. This approach involves implementing practices such as reuse, sharing, repair, renovation, remanufacturing, and recycling to establish a closed system that minimizes the utilization of resources and the production of waste, pollution, and emissions [7,11]. Essentially, the idea is that all "waste" should become "food" for another process [12].

Various researchers have repeatedly exemplified the use of composites including eggshells, eggshell membranes, and metal nanoparticles. In construction, ES and ESM are particularly useful in full or partial replacement of aggregates in masonry applications, production of lightweight foamed concrete, aggregate stabilization, and power insulation [42,48,85–90].

In the light of these use cases and many more, concrete structures keeps suffering from microbial attacks leading to their quick deterioration and consequently huge maintenance cost [6,228,229]. Some of the organisms involved in the biodeterioration of concrete structures include *Pseudomonas*, *Arthrobacter*, Algae, *Salmonella*, *E. coli*, and *Acidithiobacillus*. These organisms are usually found to attack concrete structures in waterlogged arears, sewers, splash zones, and reservoirs [230,231].

For this research, *Bacillus subtilis*, *Pseudomonas aeruginosa*, and industrially obtained waste activated sludge (WAS) were selected. *Pseudomonas aeruginosa*, a gram-negative pathogen, is an opportunistic bacterium that is widely distributed and exhibits a high adaptability to different environmental conditions, including aquatic environments [211]. With a resistance rate of 33.9%, it displays significant resistance to antimicrobial agents, posing a considerable challenge in controlling its growth and spread, particularly in aquatic settings [212,213].

On the contrary, *Bacillus subtilis*, despite being gram-positive, demonstrates remarkable resilience against harsh conditions such as high temperatures, UV radiation, and ɣ-radiation. It can be found in various environments and readily adapts to thrive in diverse settings across the biosphere, ranging from soil to marine habitats [214,215]. Among different bacterial groups, *B. subtilis* exhibits the highest occurrence in hospital settings, and a substantial proportion of its strains are resistant to multiple antimicrobials. The ability of *B. subtilis* to withstand adverse conditions presents challenges for cleaning and disinfection efforts [216].

WAS is a microbial biomass resulting from the dissolution of organic contaminants in municipal wastewater treatment facilities. Due to its mode of formation, WAS is a home to a consortium of aerobic and anaerobic microbial organisms. This consortium primarily encompasses eukaryotes, bacteria, archaea, and viruses, with bacteria being the predominant presence within the system. Some of the bacteria include *Proteobacteria, Bacteroidetes, Acidobacteria, Firmicutes, and Nitrospirae* [232-234].

As explained by Qi et al. (2020) [6], antimicrobial agents can either be inorganic or organic. Inorganic antimicrobial agents typically exhibit a prolonged lifespan and

excellent resistance to high temperatures. However, they often come with side effects such as toxicity. On the other hand, organic antimicrobial agents demonstrate a clear bactericidal effect in a short period and offer a broad spectrum of activity against various pathogens. However, they tend to have poor resistance to high temperatures. An ideal option is therefore one that combines both properties.

Examples of inorganic antimicrobial agents that have been used in concrete are heavy metals, copper coating, Zinc oxide, Silver-loaded zeolite, Zeomighty, Sodium tungstate, and silver nanoparticles. Organic antimicrobial agents include ConShield, ConBlock, eggshell, Quats, and eggshell membranes [6,22,171,229,235].

It is on this premise that this paper presents a novel approach using a composite of eggshell membrane and silver nitrate or silver nanoparticles as microbial cell inhibition agents in cement mortar while optimizing the mechanical strength of the mortar.

6.2 MATERIALS AND METHODS

6.2.1 Preparation of Ag Modified Eggshell membranes (Ag-EMs)

The Ag-EMs were created using the method previously outlined [236]. The procedure was as follows:

Eggshells were procured from nearby restaurants around the University of Pretoria. These shells were promptly washed after collection and then dried at 60°C for one hour. Following decontamination, the shells were stored in plastic bags until the separation phase. To aid membrane separation, the shells were soaked in 1 mol/L acetic acid for 17 minutes. The extraction of the ESM was then carried out manually [219]. All extracted membranes underwent a rinsing process with deionized water, subsequent drying, and storage.

To modify the ESM, silver nitrate ($AgNO_3$) and silver nanoparticles (AgNPs) were employed. AgNPs were synthesized through the chemical reduction of $AgNO_3$. The chemical reduction process, as detailed in [180,237], employed $NaBH_4$ as the reducing agent and trisodium citrate dihydrate ($Na_3C_6H_5O_7 \cdot 2H_2O$) as a ligand. In the

initial steps, a solution of $Na_3C_6H_5O_7 \cdot 2H_2O$ (0.01 M, 100 mL), $AgNO_3$ (0.01 M, 50 mL), and $NaBH_4$ (0.01 M, 50 mL) was prepared using deionized water. Subsequently, 1 mL of $AgNO_3$, 1 mL of $Na_3C_6H_5O_7 \cdot 2H_2O$, and 20 mL of deionized water were combined in a 100 mL beaker, which was then positioned in an ice bath. Stirring the solution with a magnetic stirrer for 5 minutes yielded a nano silver solution. $NaBH_4$ was then added dropwise until the suspension turned a bright yellow, and the mixture was continuously stirred for two hours to guarantee a complete reduction reaction.

ESMs of varying particle sizes, ranging from 1 mm to 5 mm, were subjected to adsorption with both synthesized AgNPs and $AgNO_3$. This adsorption process involved introducing the dried ESM into 40 ml glass Polytops containing diluted solutions of AgNPs or $AgNO_3$. These setups were subsequently placed on an oscillator at 25°C and a pH of 6 for 48 hours to facilitate the adsorption process.

6.2.2 Preparation of Cement Mortar

The mortar was formulated in compliance with the specifications of the European Committee for Standardization (CEN), as outlined in EN 196-1:2005 [238], and adhered to the guidelines provided by the South African Bureau of Standards, as stated in SANS 50196-1:2006 [239].

For the control sample (Mix 1), the preparation involved weighing and mechanically mixing one part of 52.5R cement, three parts of CEN standard sand, and half a part of water for a duration of 150 seconds. To create variation, nine additional mixes were produced by substituting a portion of the cement content with 1%, 2%, and 5% of ESM and modified ESM, as detailed in Table 6-1. All the mixtures underwent mechanical mixing for a period of 150 seconds. Subsequently, the mixed mortar was placed into a series of three prism moulds measuring 40mm x 40mm x 160mm (Figure 6-1) and left for 24 hours before being demoulded. Following demoulding, the specimens were immersed in water for curing over a period of 28 days.

Table 6-1: *Mix Design*

Mix No	Membrane	% Replacement	Membrane (g)	Cement (g)	Sand (g)	Water (g)
1	-	0	-	500	1500	250
2	$AgNO_3$/ESM	1	5	495	1500	250
3	$AgNO_3$/ESM	2	10	490	1500	250
4	$AgNO_3$/ESM	5	25	475	1500	250
5	AgNPs/ESM	1	5	495	1500	250
6	AgNPs/ESM	2	10	490	1500	250
7	AgNPs/ESM	5	25	475	1500	250
8	ESM	1	5	495	1500	250
9	ESM	2	10	490	1500	250
10	ESM	5	25	475	1500	250

Figure 6-1: *Mixed Mortar in Prism Mould*

6.2.3 Characterization of ESM Modified mortar.

X-ray diffraction (XRD) was used to understand the mineralogy of the mortar mixes while their oxide composition was determined with the use of Xray fluorescence (XRF) analysis. During the XRD analysis, the samples were prepared utilizing the standardized Panalytical backloading system, which ensures a nearly random distribution of particles. Analysis of the samples was performed using a PANalytical X'Pert Pro powder diffractometer configured in θ–θ mode, equipped with an X'Celerator detector. The instrument employed Fe-filtered Co-Kα radiation (λ=1.789Å) along with variable divergence- and fixed receiving slits. To determine the mineralogy, the measured diffraction pattern was compared to patterns in the

ICSD database, and the best-fitting pattern was selected using X'Pert Highscore plus software. The relative amounts of each phase, expressed as weight percentages of the crystalline portion, were estimated using the Rietveld method with X'Pert Highscore plus software.

To carryout XRF analysis, 10-30 grams of powdered sample were combined with 20 drops of Moviol (PVA) and pressed with a force of 10 tons. The Thermo Fisher ARL Perform'X Sequential XRF instrument, along with the Uniquant software, was utilized for the analyses. The software examined all elements in the periodic table from sodium (Na) to uranium (U), but only reported the elements detected above the specified limits. The reported values were not normalized since no LOI (Loss on Ignition) process was conducted to determine changes in crystal water and oxidation states. A standard sample material was prepared and analysed using the same procedure as the mix samples.

The morphology of all mortar mix was studied in a Zeiss Ultra PLUS FEG scanning electron microscope (SEM). Samples were dried before being sputter-coated with carbon in a Quorum Q150T ES coater for imaging. SEM energy dispersive x-ray analysis (EDX) was also conducted to understand the distribution and elemental composition of each mix.

Thermal analysis (TGA) was conducted to examine the change in mass with an increase in temperature of each mortar mix. This was investigated using a TGA5500 thermogravimetric analyser to observe the impact of elevated temperatures on each mortar mix. The alteration in mass was assessed as the temperature rose from ambient temperature to 900°C, with a heating rate of 10°C/min in the presence of nitrogen.

6.2.4 Antimicrobial activity of ESM Modified mortar.

The antimicrobial activities against *Bacillus subtilis*, *Pseudomonas aeruginosa*, and waste activated sludge (WAS) was determined using MTT assay. MTT assay, which stands for 3-(4,5-dimethylthiazolyl-2)-2,5-diphenyltetrazolium bromide assay, is a reliable and sensitive colorimetric method employed to assess the metabolic activity

of cells. This assay involves the reduction of a tetrazolium dye by specific bacterial enzymes, resulting in the formation of an insoluble purple compound called formazan. The concentration of formazan is determined by measuring its absorbance using a spectrometer in the wavelength range of 500 to 700 nm. As the number of viable bacteria increases, the concentration of formazan also increases, leading to a more pronounced purple coloration and higher absorbance values [220–222].

To grow overnight cultures of both bacteria, nutrient broth was used at a temperature of 37 ˚C while shaking at 150 rpm until an optical density of 0.4 was reached. The cultures were then subjected to centrifugation, and the supernatant was washed twice using distilled water before being resuspended in distilled water. The optical density was then adjusted to approximately 1.

Ground mortar was exposed to both bacteria in aerobic and anaerobic conditions. For the aerobic test, 1ml bacteria was exposed to 2g of mortar in 24ml broth in an incubator at 37 ˚C and 200RPM for 4 hours using 100ml dark vials. Similar procedure was used for the anaerobic test with the addition of sodium nitrate.

At the end of the fourth hour, 2.5ml MTT was added to the medium and further exposed for 3 hours at 160 RPM in the absence of light. The absorbance was measured at 700 nm using a VWR UV-1600PC spectrophotometer. A stock solution of 5 mg/mL of MTT in 0.1 M PBS (pH 7) was used. Mix 8,9, and 10 was not tested due to the lack bacteria inhibition by eggshell membrane [236].

An atomic absorption spectrometer, (Perkin Elmer AAnalyst 400, Waltham, Massachusetts) was used to measure silver concentration in the solution after exposure with an SJ hollow silver lamp.

6.2.5 Mechanical Strength Test

The density of each prism was calculated by weighing each in air and water and using the formular:

$$\frac{\rho_m}{\rho_w} = \frac{\mathrm{W(air)}}{\mathrm{W(air)-W(water)}} \quad (1)$$

Where,

ρ_m density of mortar in g/cm^3.

ρ_w density of water in g/cm^3 = 1 g/cm^3

W(air) is weight in air in g.

W(water) is weight in water in g.

Flexural strength test was carried out in triplicate using a Versa Tester with the 3 points loading system (Figure A6.1). The load was vertically applied with the loading roller at a rate of 50 N/s until fracture. The flexural strength was calculated in MPA using:

$$R_f = \frac{1.5 \times F_f \times l}{b^3} \quad (2)$$

Where,

R_f is the flexural strength, in megapascals.

b is the side of the square section of the prism, in millimetres.

F_f is the load applied to the middle of the prism at fracture, in newtons.

l is the distance between the supports, in millimetres.

Both half of each prism used for flexural test was kept and used for compressive test. An AutoMax UTest material testing machine was used to conduct the compressive test at a loading rate of 2400 N/s until fracture (Figure A6.1). The compressive strength was calculated in MPA using:

$$R_c = \frac{F_c}{1600} \quad (3)$$

Where,

R_c is the compressive strength, in megapascals.

F_c is the maximum load at fracture, in newtons.

6.3 RESULTS

6.3.1 Synthesis of AgNPs and production of ESM composites

As observed in Figure 6-2, X-ray diffraction analysis implies that despite the addition of Ag modified membranes to mixes 2 through 7, the mineralogy of the mortar mixes remains unchanged. This indicates that the produced cytotoxic mortar will have comparable characteristics to standard mortar. Quartz was the most predominant mineral followed by Portlandite, calcite, Mayenite, with traces of Brownmillerite, Larnite, and Ettringite.

The oxide composition shown in Figure 6-3 follows a similar analogy as the XRD result with relatively constant composition across the mix. A two-way ANOVA comparison of the XRF data indicated that no significant difference between the compositions of the different mixes were confirmed (P = 0.9995) and that the variations between the results is most likely a result of random chance [240].

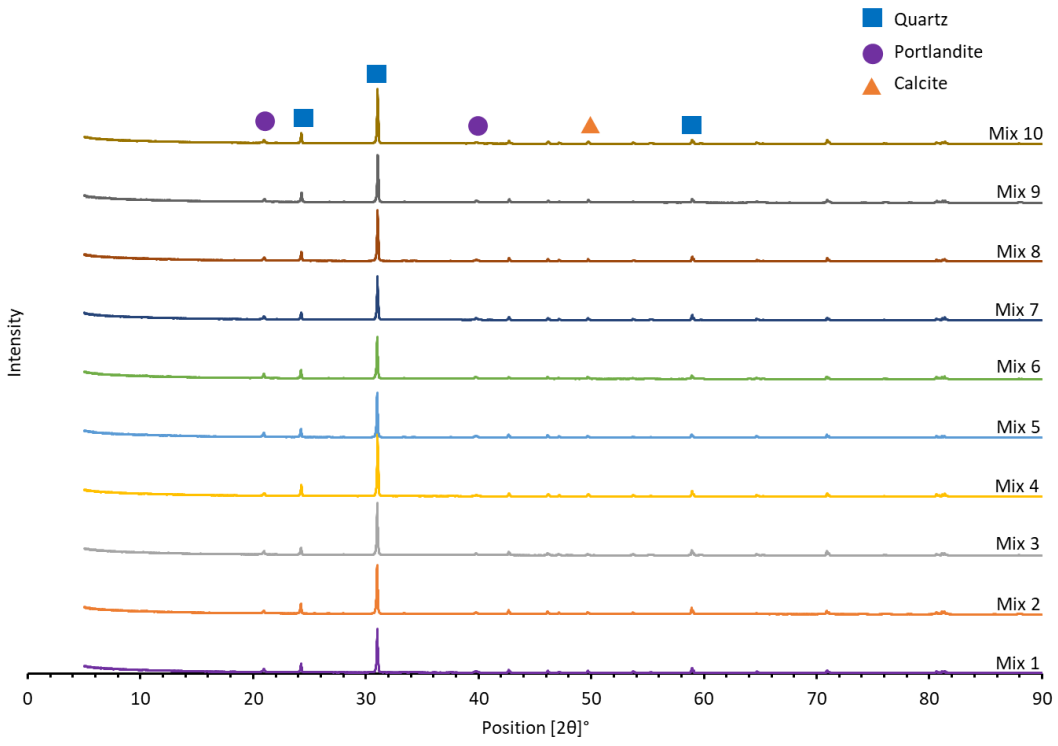

Figure 6-2: *XRD mineralogy pattern of the mortar mixes.*

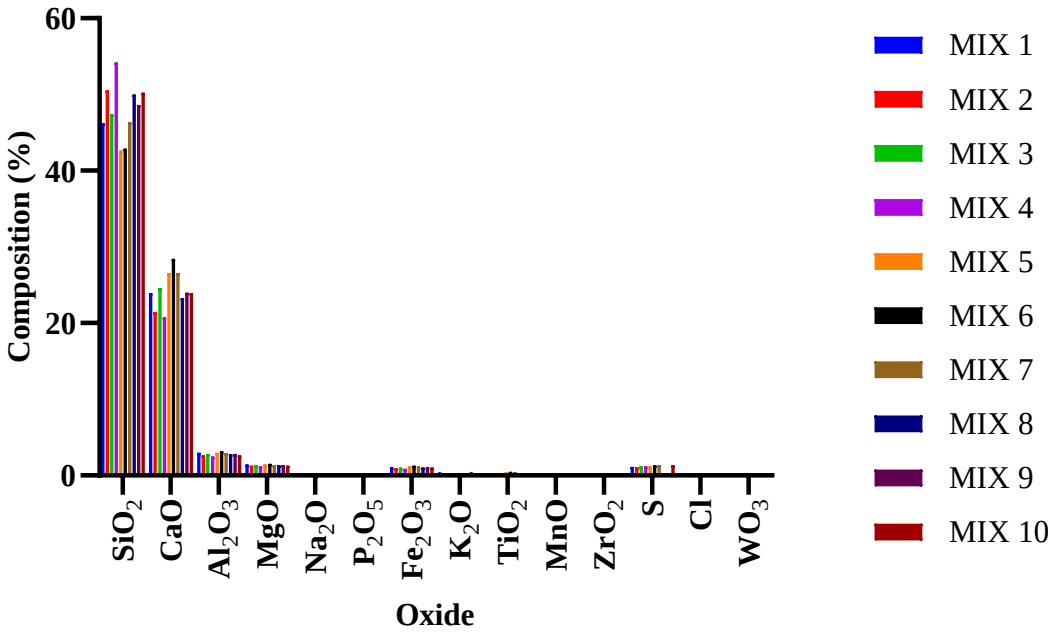

Figure 6-3: *XRF oxide compositions of the different concrete mixes.*

Furthermore, A TGA5500 thermogravimetric analyser was used to observe the temperature stability of the mixes from 30 °C to 900 °C (Figure 6-4). Thermogravimetric (TG), derivative thermogravimetry (DTG), and Differential Scanning Calorimetry (DSC) analysis were employed (Figure A6.1). All mix samples experienced two stages of weight loss. The initial loss which was gentle occurred over a wide temperature range of 30 °C and 150 °C. This loss can be attributed to loss of moisture content. The second significant loss was very abrupt and quick occurred between 390 °C and 420 °C. All mixes were relatively thermally stable compared to the control mix, mix 1 with a maximum difference of 5% weight loss due to the presence of shell membrane. The eggshell membrane was also tested as illustrated in Figure 6-4b and turns completely into ash after 300 °C, leaving approximately 10% weight at >700 °C.

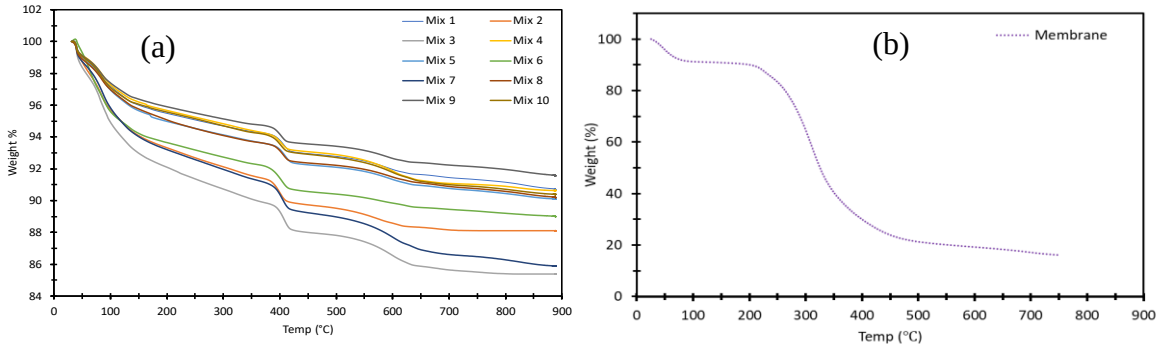

Figure 6-4: *Thermogravimetric analysis of a) mixes 1 to 10 and b) eggshell membrane.*

SEM-EDS analysis was previously conducted and confirmed the adsorption of AgNPs and $AgNO_3$ on the membrane, notably both $AgNO_3$ and AgNPs were uniformly absorbed onto the membrane's surface [236]. The porous fibril structure, known for its ability to enhance ESM's absorption capacity [219], was found to be effective. In the current study the retention of the Ag within the mortar mix was confirmed (Figure 6-5a and b, Figure A6.2, and Table A6.1).

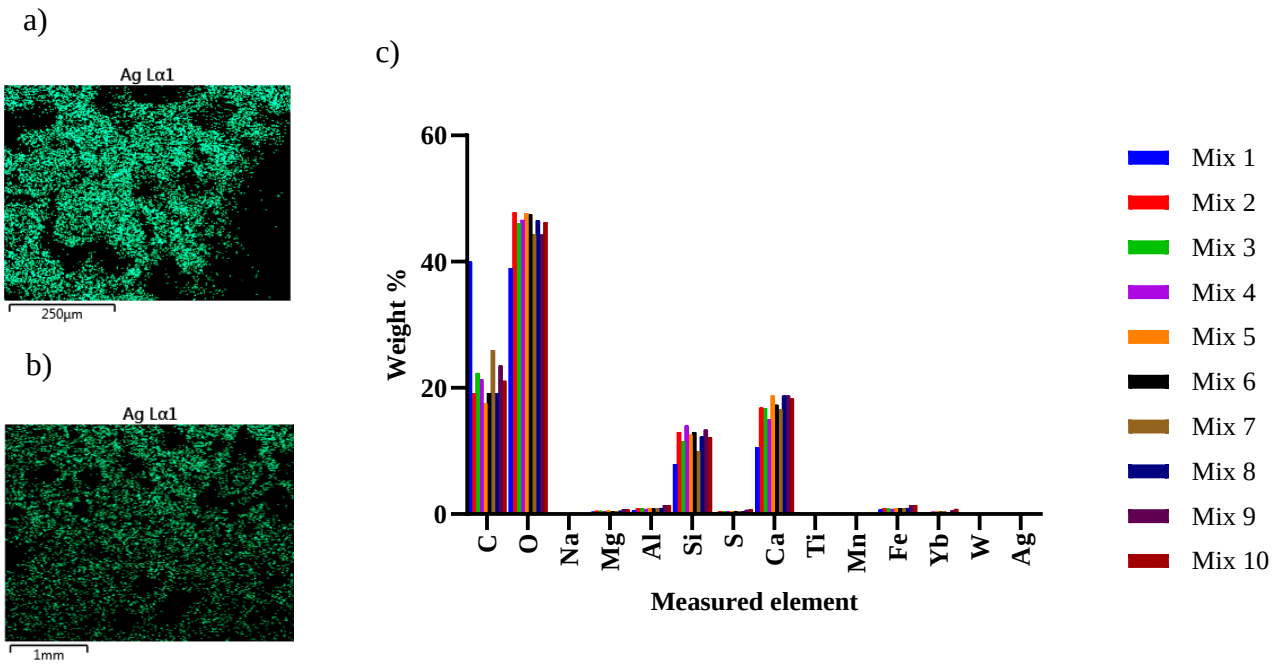

Figure 6-5: *SEM EDS Ag distribution map of (a) $AgNO_3$/ESM Mortar (MIX 4), (b) AgNPs/ESM Mortar (MIX 7), (c) The elemental compositions of the different mortar mixes (as measured by EDS)*

Ag EDS measurements of the mixes supported the presence of Ag in Mixes 3, 4, 7, 8, with increasing Ag content measured. No Ag was measured by EDS in Mixes 2 and 5, likely due to the detection limit of the machine – the Ag content of Mixes 3 and 6 were only 0.06% and 0.05%, respectively.

The material exhibited relatively similar macroscopic features with limited differences observable from the SEM micrograph (Figure A6.3) and the elemental compositions for the different mixes as measured by EDS (Figure 6-5c and Figure A6.4) were found to exhibit no significant differences when applying a two-way ANOVA analysis, the P value was found to be greater than 0.9999.

6.3.2 Antimicrobial Activity of Mortar Composite

The effects of Ag-impregnated mortar composites are illustrated in Figure 6-6a. Figure 6-6b summarizes the P-values obtained from the two-way ANOVA comparisons (Tukey's multi-comparison test) between the control group and mixes 1-7. Notably, the most significant differences were observed when introducing Ag/ESM mortar mixes to the waste activated sludge (WAS). The P-values indicated highly significant differences ($p < 0.0001$) between the control and mixes 3-7 for anaerobic runs, and between the control and mixes 2-7 for aerobic runs. However, the comparison between the control and mix 2 in the anaerobic run did not show significant differences ($p = 0.2307$). The most pronounced cytotoxic effect of the antimicrobial composites on WAS occurred under anaerobic conditions, resulting in a cell viability of 36.8±6.1% for AgNPs composite mix 5. Under aerobic conditions, the cytotoxic effect was observed with mix 4, resulting in a cell viability of 51.0±4.8% for WAS.

Furthermore, in the anaerobic WAS run, significant differences were observed between mixes 1 and mixes 2 to 7, mixes 2 and 5, mixes 5 and 7, and mixes 6 and 7 (Figure 6-6c). In the case of aerobic runs, significant differences were measured between mixes 1 and 3 to 7, and mixes 2 and 4 (Figure 6-6d). However, for the runs involving *B. subtilis* and *P. aeruginosa*, no significant differences were observed

between the control group and any of the mortar mixes in either the anaerobic or aerobic runs.

To explain these inhibitory results, Figure 6-6e displays the silver concentrations measured using Atomic Absorption Spectroscopy (AAS) after exposure to *B. subtilis*, *P. aeruginosa*, and WAS. The measured Ag results were consistent with the initially dosed amounts. Notably, the Ag concentrations in solution were relatively low, ranging from approximately 0.1 mg/L to 0.7 mg/L for $AgNO_3$-impregnated mortar mixes and from around 0.07 mg/L to 0.2 mg/L for AgNPs-impregnated mortars.

It's important to mention that the minimum inhibitory concentration for AgNO3 was reported to be at least 1 mg/L for *B. subtilis* [241] and between 8 and 16 mg/L for *P. aeruginosa* [242], while for AgNPs, it ranged between 2 and 5 mg/L for both *B. subtilis and P. aeruginosa* [241,243]. In the case of WAS, the efficacy of Ag^+ and AgNPs was significantly more pronounced, with Ag^+ concentrations as low as 0.5 mg/L (from $AgNO_3$) and AgNPs at 0.2 mg/L reported to inhibit enriched nitrifying bacteria by up to 50% and 60%, respectively [244,245].

The pH levels of the individual bacterium cultures were initially recorded as 6.82, 7.01, and 6.61 for *B. subtilis*, *P. aeruginosa*, and WAS, respectively, before exposure. After exposure, all culture pH values rose to around 12 (see Figure 6-6f). This shift in pH has been shown to impact WAS systems, leading to increased concentrations of volatile fatty acids (VFA), ammonia, and phosphate, while suppressing methane production, indicating the disruption of normal biological function under these high pH conditions [246]. In contrast, *B. subtilis* and *P. aeruginosa* demonstrated greater resistance to pH changes [247,248].

The limited impact of the different mortar mixes on *B. subtilis* and *P. aeruginosa* cultures can be attributed to the relatively low Ag concentrations in solution (below inhibitory concentrations) and the cultures' resistance to elevated pH levels. In contrast, the significant inhibition of WAS by the mortar mixes, including the concrete-only mortar (mix 1) in aerobic runs, may be attributed to the presence of Ag^+ or AgNPs in the mixture, which has been shown to affect WAS, along with the elevated pH levels recorded in the solutions. These findings suggest potential

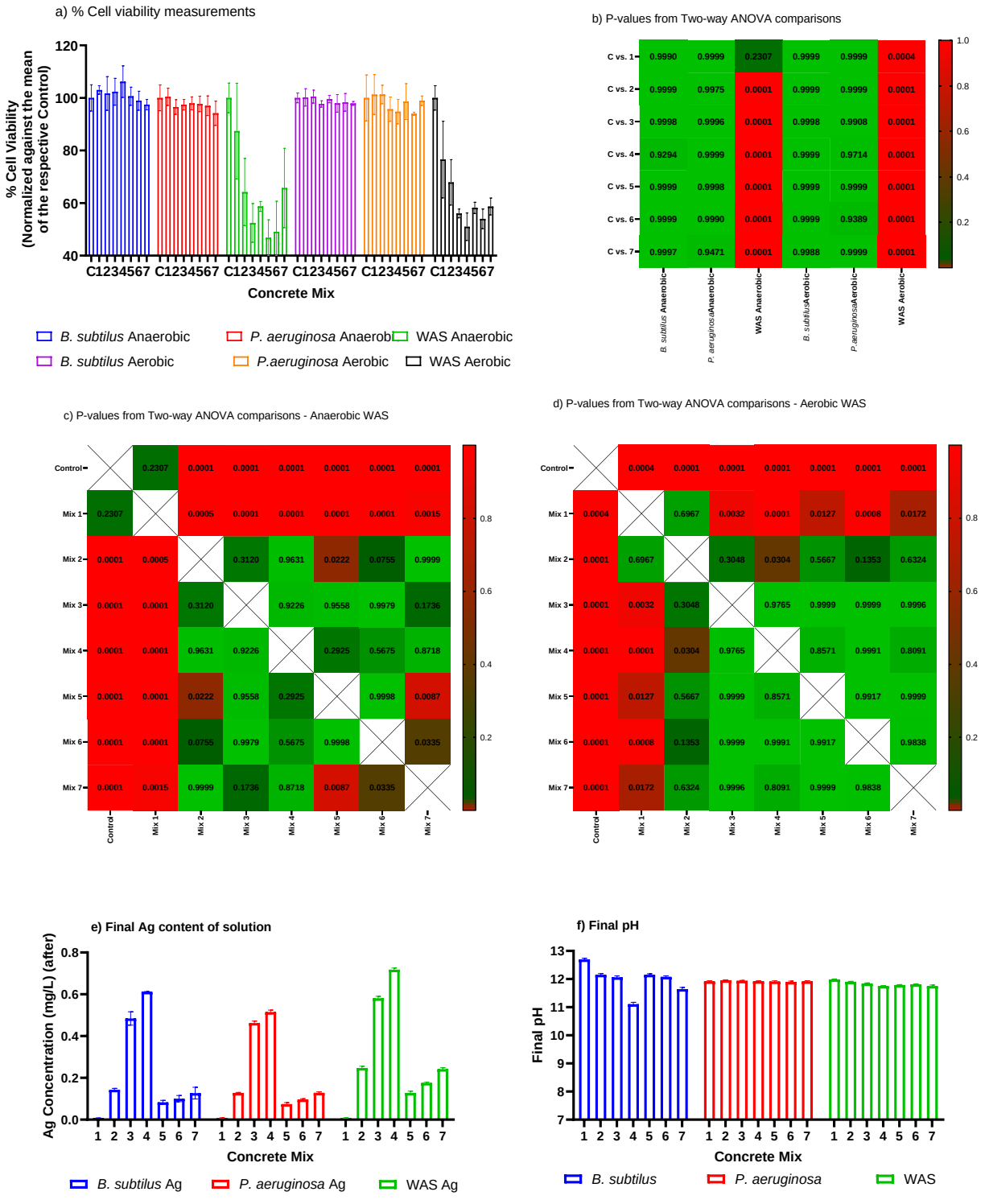

Figure 6-6: *Antimicrobial characterisation and statistical analysis of mortar composite. a) % Cell viability measurements for the concrete mixture experiments normalized against the means of the control experiment for each microbial culture, b), c), and d) P-values from Two-way ANOVA comparisons between the % Cell*

viabilities for the control and different concrete mixes, the Anaerobic WAS and Aerobic WAS runs, respectively, e) The Ag concentrations of the aqueous solutions for each concrete mix exposed to different microbial cultures, f) the final pH of the respective concrete mixes exposed to different microbial cultures.

applications of antimicrobial mortar mixtures, even at low Ag/ESM concentrations, within sewage carriage systems. However, it's important to note that these applications may not effectively control *B. subtilis* or *P. aeruginosa* contamination.

6.3.3 Mechanical Strength Characteristics of Mortar Composite

After a curing period of 28 days, the hardened cubes underwent testing to assess both compressive and tensile strength, as indicated in Figure 6-7a. In terms of compressive strength, the control mix displayed an average value of 68.88±0.88 MPa (mean ± standard deviation). However, the composite mixes exhibited a noteworthy decline in compressive strength, ranging from 64.03±1.55 MPa for mix 2 to 41.35±3.20 MPa for mix 10. Statistical analyses using two-way ANOVA further confirmed the significance of these differences in comparison to the baseline (mix 1). This decline aligns with prior research findings that have reported reduced compressive strength as the proportion of eggshell powder increases [85,86,249]. Additionally, there were no statistically significant differences observed among mixes with similar eggshell fractions (2 vs. 5 vs. 8, 3 vs. 6 vs. 8, and 7 vs. 10), underscoring that the primary factor contributing to the compressive strength decrease is the content of eggshell powder (ESM).

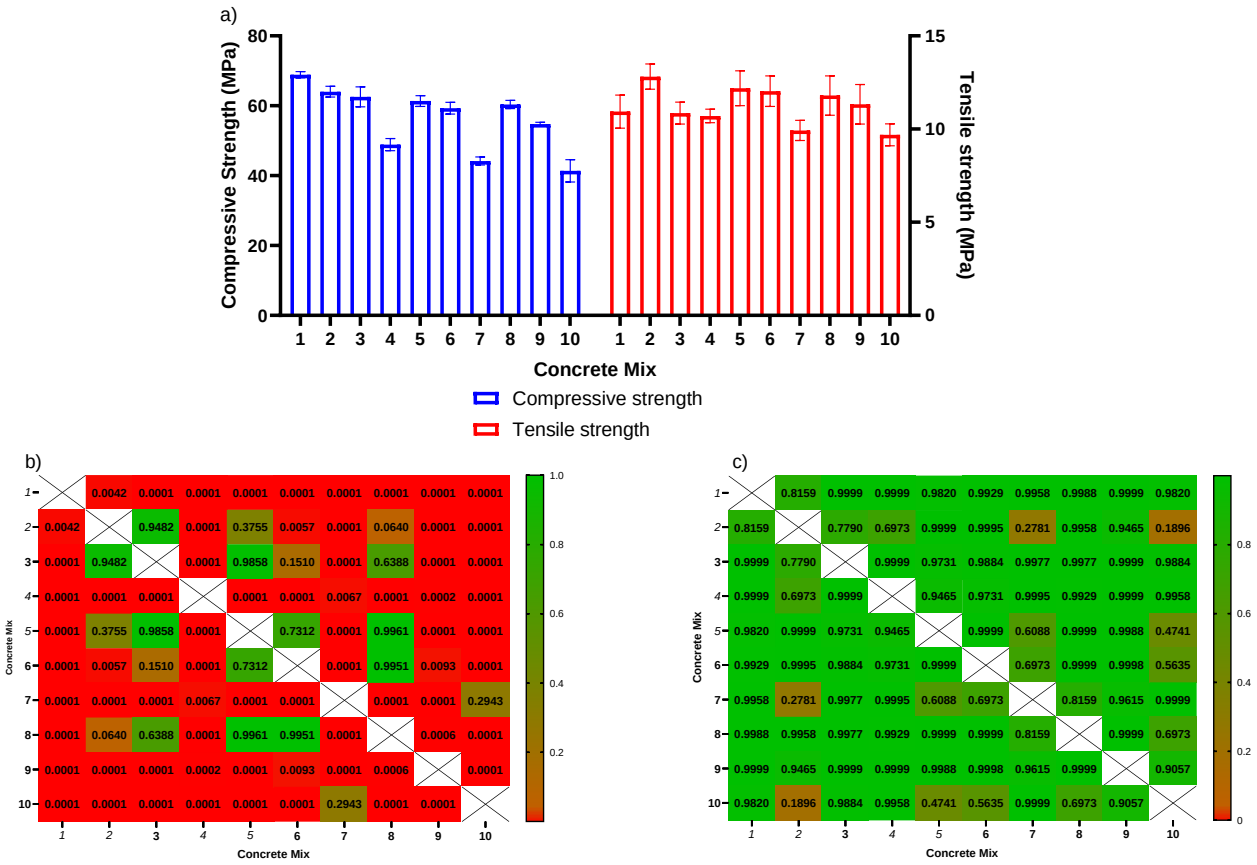

Figure 6-7: *Mechanical results and statistical analysis of mortal composite. a) Comparisons of compressive and tensile strengths for the different concrete mixes, b) and c) The p-values obtained from the two-way ANOVA analyses comparing each concrete mix to each other concrete mix as related to the compressive and tensile strengths, respectively.*

In contrast, the tensile strength of the mixes did not exhibit significant differences when compared to the control mix (Figure 6-7c). The control mix registered an average tensile strength of 10.94±0.89 MPa, while the remaining mixes reported tensile strengths ranging from 12.81±0.68 to 9.69±0.59 MPa. Analysing the tensile strengths across the various mixes through two-way ANOVA revealed no statistically significant distinctions (at α=0.05) between any of the mixtures.

The most favourable combinations in this study were blends 3, 5, and 6. Blend 3 contained 2% ESM/$AgNO_3$, blend 5 contained 1% ESM/AgNPs composite, and

blend 6 contained 2% ESM/AgNPs composite. None of these blends caused a noteworthy alteration in the cell viability of either *B. subtilis* or *P. aeruginosa* when compared to the control. However, when assessing the cell viability of waste activated sludge (WAS) in anaerobic systems, it was found that blends 3, 5, and 6 resulted in viabilities of 52.4% ± 7.4%, 46.8% ± 6.9%, and 49.1% ± 11.6%, respectively, in contrast to the control. Under aerobic conditions, the cell viability for these three blends was 56.0% ± 1.7%, 58.2% ± 2.1%, and 54.0% ± 3.7%, respectively. Statistical analysis using two-way ANOVA revealed no significant differences at the $\alpha = 0.05$ level among these results.

Importantly, the proposed optimal blends exhibited compressive strengths of 62.6 MPa ± 2.8 MPa, 61.4 MPa ± 1.5 MPa, and 69.3 MPa ± 1.54 MPa, respectively, compared to 68.9±0.9 MPa for the control without eggshell, representing an approximate 10% reduction in strength. Additionally, the tensile strengths of these blends were 10.9 MPa ± 0.6 MPa, 12.2 MPa ± 0.9 MPa, and 12.0 MPa ± 0.8 MPa, respectively, which did not exhibit statistically significant changes at the $\alpha = 0.05$ level when compared to the control's tensile strength of 10.9±0.9 MPa.

6.4 CONCLUSION

The findings presented have further underscored the advantages of composite materials and composite nanomaterials. A composite cytotoxic mortar was successfully manufactured, possessing a mineral composition akin to standard mortar. However, it exhibited an exceptional antimicrobial property, resulting in up to a 50% reduction in cell viability in WAS, all while marginally enhancing tensile strength and showing only a slight reduction in compressive strength.

From these results, it can be concluded that mixes 3, 5 and 6 provided the optimal balance between antimicrobial properties (there were no significant differences for mixes 3 to 7 measured in terms of antimicrobial activities), and the loss in compressive/tensile strength of the concrete.

In the context of promoting a circular economy, the utilization of eggshell and its membrane has further demonstrated their practicality. The implementation of this

antimicrobial composite holds the potential to not only mitigate waste management challenges but also to safeguard concrete structures against microbial deterioration.

CHAPTER 7 CONCLUSIONS AND RECOMMENDATIONS

7.1 SIGNIFICANT FINDINGS

The results observed from this study have shown that waste eggshell can be upcycled in the construction industry towards a greener future. The study's findings demonstrated the remarkable efficacy of acetic acid in a relatively short span of seventeen minutes. Specifically, acetic acid proved to be highly effective in weakening the bond between the shell and its semipermeable membrane. Moreover, this process was conducted with a keen focus on minimizing the dissolution of calcium while simultaneously maximizing the leaching of valuable compounds and proteins such as collagen.

The isolated and treated shell, after undergoing calcination and leaching, yielded calcium oxide of comparable quality to that traditionally derived from limestone in the context of cement production. This result underscored the potential for sustainable and resource-efficient alternatives in industrial processes.

Taking the research a step further, the extracted semipermeable membrane found a new application as an adsorbent material for silver nanoparticles. Silver nanoparticles of absorbance peak ranging from 390 nm to 400 nm and average particle size of 29.8 nm was synthesized. According to [180,184] and [189], this peak range and size signifies silver nanoparticles suitable for antimicrobial use. The optimal conditions for the adsorption process were identified at a pH level of 6, a temperature of 25 °C, and a duration of 48 hours of agitation in consonant with [180,190]. The results for the kinetics model fits demonstrate that the AgNPs adsorption was best described by a 2-PA process with a R^2 = 0.982 indicating an heterogenous interactions between the adsorbate and the adsorbent surface sites [191,192]. This behaviour has been reported previously for biosorption of Cu-ions [209].

The resulting nanocomposite exhibited significant antimicrobial properties when tested against *Pseudomonas aeruginosa* and *Bacillus subtilis*. The outcomes were truly remarkable, with a substantial reduction in cell viability noted: a remarkable

27.77% reduction for *Pseudomonas aeruginosa* and a notable 15.34% decrease for *Bacillus subtilis*.

Building upon these promising results, the research delved into practical applications of the nanocomposite. Specifically, its cytotoxic properties were assessed in the context of concrete mortar. This investigation was motivated by the pressing need to address escalating infrastructure costs associated with the maintenance of concrete structures that suffer from microbial attacks in moist environments. To simulate real-world conditions, waste activated sludge (WAS), along with *Pseudomonas aeruginosa* and *Bacillus subtilis*, were introduced in both aerobic and anaerobic conditions.

Notably, WAS exhibited the highest susceptibility to the nanocomposite with the most significant reduction in cell viability. While *Pseudomonas aeruginosa* and *Bacillus subtilis* experienced a maximum of 9% and 5% cell death, respectively, with a 2% cement replacement using the nanocomposite, WAS demonstrated an impressive 50% reduction in cell viability. The lower cell death recoded for PA and BS can be attributed to their resistance to pH [247,248]. Additionally, there was approximately 10% reduction in compressive strength similar to reports from [85,86,249] and a notable 20% increase in tensile strength, further highlighting the potential of this nanocomposite as a versatile solution for enhancing the durability and resilience of concrete structures exposed to challenging microbial environments. The most optimum mixes in this study were mix 3 (2% ESM/$AgNO_3$), mix 5 (1% ESM/AgNPs), and mix 6 (2% ESM/AgNPs) subject to the use case.

These results are of great significance given that the global production of eggshells amounted to approximately 8.7 million metric tons in 2021. Repurposing the shell and its membrane in this manner holds significant environmental significance. This involves minimizing the demand for landfill space, cost savings, and a decrease in the emission of greenhouse gases.

The unique repurposing of eggshells and their membranes holds significant economic value. Initially, the funds typically used for handling over 8 million tons of eggshell waste could be redirected towards more lucrative ventures. The valorisation process

also yields valuable income sources through the recovery of shell membrane and other biochemical compounds, such as collagen, which are in high demand. Additionally, in the context of rising global infrastructure budgets, incorporating eggshell membrane as an antimicrobial additive in concrete could lead to substantial savings, potentially up to 40%, in maintenance costs.

In essence, this study not only highlights the versatile and eco-friendly use of waste eggshells but also provides a foundation for further exploration and application of these innovative materials in the construction industry. As we continue to seek sustainable solutions to address environmental and economic challenges, the insights gained from this research can contribute to a greener and more resilient future for construction practices.

7.2 RECOMMENDATIONS FOR FUTURE STUDIES

Eggshell was successfully upcycled. As a part of the quest for a greener construction industry, calcium oxide from eggshells should be used as a replacement for its limestone counterpart while also employing the shell membrane as an antimicrobial agent. The overall study has provided in-depth insight into the circularity potential of the eggshell in the construction industry; however, some limitations exist. All results were obtained in a controlled environment on a laboratory scale and therefore may not be a perfect representation of what is obtainable on the field and in a large scale. A large scale in-situ study is therefore proposed to further understand the properties demonstrated in the research.

Likewise, more research is needed to evaluate the practicality and economic feasibility of large-scale implementation of the proposed eggshell membrane separation process. The potential environmental impacts of acetic acid use in the membrane separation process should also be considered and mitigated. Furthermore, considerations should be given to the scalability of the biochemical compound removal process, the quality and consistency of the CaO produced, the environmental impact of the extraction process, and the market demand for the recovered compounds.

In addition, eggshells from different breeds of chickens as well as from different parts of the world also need to be properly examined to determine difference in properties that can influence desired results.

Future studies on the use of eggshell membrane as a composite with other antimicrobial agents and sustainably sourced nanometals is also encouraged. This should include adsorption kinetics, process and parameters and antimicrobial properties.

Finally, a life cycle analysis on the use of Ag/membrane composite in concrete is recommended. Also, potential challenges such as the sourcing and processing large quantities of eggshell membranes, the impact on the mechanical properties of concrete, and the environmental implications of silver nanoparticles should be thoroughly investigated.

REFERENCES

1. Nhamo, G.; Mjimba, V. Biting the Hand That Feeds You : Green Growth and Electricity Revenues in South African Metropolitans. *Public Munic. Financ.* **2014**, *3*, 19–31.

2. Embong, R.; Shafiq, N.; Kusbiantoro, A.; Nuruddin, M.F. Effectiveness of Low-Concentration Acid and Solar Drying as Pre-Treatment Features for Producing Pozzolanic Sugarcane Bagasse Ash. *J. Clean. Prod.* **2016**, *112*, 953–962, doi:10.1016/j.jclepro.2015.09.066.

3. Flower, D.J.M.; Sanjayan, J.G. *Greenhouse Gas Emissions Due to Concrete Manufacture*; 2016; Vol. 12;.

4. Part, W.K.; Ramli, M.; Cheah, C.B. An Overview on the Influence of Various Factors on the Properties of Geopolymer Concrete Derived From Industrial Byproducts. *Handb. Low Carbon Concr.* **2016**, *77*, 263–334, doi:10.1016/B978-0-12-804524-4.00011-7.

5. Gardner, D.; Lark, R.; Jefferson, T.; Davies, R. A Survey on Problems Encountered in Current Concrete Construction and the Potential Benefits of Self-Healing Cementitious Materials. *Case Stud. Constr. Mater.* **2018**, *8*, 238–247, doi:10.1016/j.cscm.2018.02.002.

6. Qiu, L.; Dong, S.; Ashour, A.; Han, B. Antimicrobial Concrete for Smart and Durable Infrastructures: A Review. *Constr. Build. Mater.* **2020**, *260*, 120456, doi:10.1016/j.conbuildmat.2020.120456.

7. Ellen MacArthur Foundation Circularity Indicators: An Approach to Measuring Circularity. *Ellen MacArthur Found.* **2015**, *23*, doi:10.1016/j.giq.2006.04.004.

8. Albino, V.; Berardi, U.; Dangelico, R.M. Smart Cities: Definitions, Dimensions, Performance, and Initiatives. *J. Urban Technol.* **2015**, *22*, 3–21,

doi:10.1080/10630732.2014.942092.

9. Kaza, S.; Yao, L.; Bhada-Tata, P.; Van Woerden, F. *What a Waste 2.0: A Global Snapshot of Solid Waste Management to 2050*; The World Bank: Washington, DC, 2018; ISBN 978-1-4648-1329-0.

10. Department of Environmental Affairs *South Africa State of Waste Report. A Report on the State of the Environment. First Draft Report.*; Pretoria, 2018;

11. Geissdoerfer, M.; Savaget, P.; Bocken, N.M.P.; Hultink, E.J. The Circular Economy – A New Sustainability Paradigm? *J. Clean. Prod.* **2017**, *143*, 757–768, doi:10.1016/j.jclepro.2016.12.048.

12. Ellen MacArthur Foundation Towards the Circular Economy - Economic and Business Rationale for an Accelerated Transition. *Greener Manag. Int.* **2012**, *1*, 1–13.

13. Arif, E.; Clark, M.W.; Lake, N. Sugar Cane Bagasse Ash from a High Efficiency Co-Generation Boiler: Applications in Cement and Mortar Production. *Constr. Build. Mater.* **2016**, *128*, 287–297, doi:10.1016/j.conbuildmat.2016.10.091.

14. Shahbaz, M.; Yusup, S.; Inayat, A.; Patrick, D.O.; Pratama, A. Application of Response Surface Methodology to Investigate the Effect of Different Variables on Conversion of Palm Kernel Shell in Steam Gasification Using Coal Bottom Ash. *Appl. Energy* **2016**, *184*, 1306–1315, doi:10.1016/j.apenergy.2016.05.045.

15. Ranjbar, N.; Mehrali, M.; Alengaram, U.J.; Metselaar, H.S.C.; Jumaat, M.Z. Compressive Strength and Microstructural Analysis of Fly Ash/Palm Oil Fuel Ash Based Geopolymer Mortar under Elevated Temperatures. *Constr. Build. Mater.* **2014**, *65*, 114–121, doi:10.1016/j.conbuildmat.2014.04.064.

16. Yusuf, M.O.; Megat Johari, M.A.; Ahmad, Z.A.; Maslehuddin, M. Evolution

of Alkaline Activated Ground Blast Furnace Slag-Ultrafine Palm Oil Fuel Ash Based Concrete. *Mater. Des.* **2014**, *55*, 387–393, doi:10.1016/j.matdes.2013.09.047.

17. Mohammed, B.S.; Foo, W.L.; Abdullahi, M. Flexural Strength of Palm Oil Clinker Concrete Beams. *Mater. Des.* **2014**, *53*, 325–331, doi:10.1016/j.matdes.2013.07.041.

18. Bohlooli, H.; Nazari, A.; Khalaj, G.; Kaykha, M.M.; Riahi, S. Experimental Investigations and Fuzzy Logic Modeling of Compressive Strength of Geopolymers with Seeded Fly Ash and Rice Husk Bark Ash. *Compos. Part B Eng.* **2012**, *43*, 1293–1301, doi:10.1016/j.compositesb.2012.01.012.

19. Shahbandeh, M. Global Egg Production from 1990 to 2018 Available online: https://www.statista.com/statistics/263972/egg-production-worldwide-since-1990/ (accessed on 19 April 2020).

20. Low, N.L.P. Formation and Properties of Glass-Mica Composite Materials. *Ceramurg. Int.* **1980**, *6*, 85–90, doi:10.1016/0390-5519(80)90018-6.

21. Teh, S.H.; Wiedmann, T.; Castel, A.; de Burgh, J. Hybrid Life Cycle Assessment of Greenhouse Gas Emissions from Cement, Concrete and Geopolymer Concrete in Australia. *J. Clean. Prod.* **2017**, *152*, 312–320, doi:10.1016/j.jclepro.2017.03.122.

22. Huang, L.; Chen, R.; Luo, J.; Hasan, M.; Shu, X. Synthesis of Phytonic Silver Nanoparticles as Bacterial and ATP Energy Silencer. *J. Inorg. Biochem.* **2022**, *231*, 111802, doi:10.1016/j.jinorgbio.2022.111802.

23. Oliveira, D.A.; Benelli, P.; Amante, E.R. A Literature Review on Adding Value to Solid Residues: Egg Shells. *J. Clean. Prod.* **2013**, *46*, 42–47, doi:10.1016/j.jclepro.2012.09.045.

24. Shahbandeh, M. Production of Eggs Worldwide 2021 | Statista Available

online: https://www.statista.com/statistics/263972/egg-production-worldwide-since-1990/ (accessed on 5 May 2023).

25. South African Poultry Association *Egg Industry Production Report for November 2019*; 2019;

26. Ferraz, E.; Gamelas, J.A.F.; Coroado, J.; Monteiro, C.; Rocha, F. Eggshell Waste to Produce Building Lime: Calcium Oxide Reactivity, Industrial, Environmental and Economic Implications. *Mater. Struct. Constr.* **2018**, *51*, doi:10.1617/s11527-018-1243-7.

27. Hayajneh, M.T.; Almomani, M.A.; Al-Shrida, M.M. Effects of Waste Eggshells Addition on Microstructures, Mechanical and Tribological Properties of Green Metal Matrix Composite. *Sci. Eng. Compos. Mater.* **2019**, *26*, 423–434, doi:10.1515/secm-2019-0027.

28. Nakano, T.; Ikawa, N.I.; Ozimek, L. Chemical Composition of Chicken Eggshell and Shell Membranes. *Poult. Sci.* **2003**, *82*, 510–514, doi:10.1093/ps/82.3.510.

29. Hussain, A. Delectric Properties and Microwave Assisted Separation of Eggshell and Membrane, McGill University Ste Anne De Bellevue, Quebec, Canada, 2009.

30. Schaafsma, A.; Pakan, I.; Hofstede, G.J.H.; Muskiet, F.A.J.; Van Der Veer, E.; De Vries, P.J.F. Mineral, Amino Acid, and Hormonal Composition of Chicken Eggshell Powder and the Evaluation of Its Use in Human Nutrition. *Poult. Sci.* **2000**, *79*, 1833–1838, doi:10.1093/ps/79.12.1833.

31. Hincke, M.T.; Nys, Y.; Gautron, J.; Mann, K.; Rodriguez-Navarro, A.B.; McKee, M.D. The Eggshell: Structure, Composition and Mineralization. *Front. Biosci.* **2012**, *17*, 1266–1280, doi:10.2741/3985.

32. Statista Production of Eggs Worldwide, 2018 | Statista Available online:

https://www.statista.com/statistics/263972/egg-production-worldwide-since- (accessed on 19 April 2020).

33. Statista Leading Egg Producing Countries Worldwide, 2018 | Statistic Available online: https://www.statista.com/statistics/263971/top-10-countries-worldwide-in-egg-production/ (accessed on 2 July 2020).

34. King'ori, A.M. A Review of the Uses of Poultry Eggshells and Shell Membranes. *Int. J. Poult. Sci.* **2011**, *10*, 908–912, doi:10.3923/ijps.2011.908.912.

35. Rose, M.L.H.; Hincke, M.T. Protein Constituents of the Eggshell: Eggshell-Specific Matrix Proteins. *Cell. Mol. Life Sci.* **2009**, *66*, 2707–2719, doi:10.1007/s00018-009-0046-y.

36. Fernandes, H.R.; Andreola, F.; Barbieri, L.; Lancellotti, I.; Pascual, M.J.; Ferreira, J.M.F. The Use of Egg Shells to Produce Cathode Ray Tube (CRT) Glass Foams. *Ceram. Int.* **2013**, *39*, 9071–9078, doi:10.1016/j.ceramint.2013.05.002.

37. Mugoni, C.; Montorsi, M.; Siligardi, C.; Andreola, F.; Lancellotti, I.; Bernardo, E.; Barbieri, L. Design of Glass Foams with Low Environmental Impact. *Ceram. Int.* **2015**, *41*, 3400–3408, doi:10.1016/j.ceramint.2014.10.127.

38. Souza, M.T.; Maia, B.G.O.; Teixeira, L.B.; de Oliveira, K.G.; Teixeira, A.H.B.; Novaes de Oliveira, A.P. Glass Foams Produced from Glass Bottles and Eggshell Wastes. *Process Saf. Environ. Prot.* **2017**, *111*, 60–64, doi:10.1016/j.psep.2017.06.011.

39. Lammie, D.; Bain, M.M.; Wess, T.J. Microfocus X-Ray Scattering Investigations of Eggshell Nanotexture. *J. Synchrotron Radiat.* **2005**, *12*, 721–726, doi:10.1107/S0909049505003547.

40. Balch, D.-A.; Cooke, R.A. A Study of the Composition of Hen's Egg-Shell

Membranes. *Ann. Biol. Anim. Biochim. Biophys.* **1970**, *10*.

41. Choi, H.J.; Lee, S.M. Heavy Metal Removal from Acid Mine Drainage by Calcined Eggshell and Microalgae Hybrid System. *Environ. Sci. Pollut. Res.* **2015**, *22*, 13404–13411, doi:10.1007/s11356-015-4623-3.

42. Jaques, N.G.; William de Lima Souza, J.; Popp, M.; Kolbe, J.; Lia Fook, M.V.; Ramos Wellen, R.M. Kinetic Investigation of Eggshell Powders as Biobased Epoxy Catalyzer. *Compos. Part B Eng.* **2020**, *183*, doi:10.1016/j.compositesb.2019.107651.

43. Oladele, I.O.; Makinde-Isola, B.A.; Adediran, A.A.; Oladejo, M.O.; Owa, A.F.; Olayanju, T.M.A. Mechanical and Wear Behaviour of Pulverised Poultry Eggshell/Sisal Fiber Hybrid Reinforced Epoxy Composites. *Mater. Res. Express* **2020**, *7*, doi:10.1088/2053-1591/ab8585.

44. Tsai, W.T.; Yang, J.M.; Lai, C.W.; Cheng, Y.H.; Lin, C.C.; Yeh, C.W. Characterization and Adsorption Properties of Eggshells and Eggshell Membrane. *Bioresour. Technol.* **2006**, *97*, 488–493, doi:10.1016/j.biortech.2005.02.050.

45. Carvalho, J.; Araujo, J.; Castro, F. Alternative Low-Cost Adsorbent for Water and Wastewater Decontamination Derived from Eggshell Waste: An Overview. *Waste and Biomass Valorization* **2011**, *2*, 157–167, doi:10.1007/s12649-010-9058-y.

46. Ray, S.; Kumar Barman, A.; Kumar Roy, P.; Kumar Singh, B. Chicken Eggshell Powder as Dietary Calcium Source in Chocolate Cakes. *Pharma Innov. J.* **2017**, *6*, 1–4.

47. Al-Ghouti, M.A.; Salih, N.R. Application of Eggshell Wastes for Boron Remediation from Water. *J. Mol. Liq.* **2018**, *256*, 599–610, doi:10.1016/j.molliq.2018.02.074.

48. Tiong, H.Y.; Lim, S.K.; Lee, Y.L.; Ong, C.F.; Yew, M.K. Environmental Impact and Quality Assessment of Using Eggshell Powder Incorporated in Lightweight Foamed Concrete. *Constr. Build. Mater.* **2020**, *244*, 118341, doi:10.1016/j.conbuildmat.2020.118341.

49. Freire, M.N.; Holanda, J.N.F. Characterization of Avian Eggshell Waste Aiming Its Use in a Ceramic Wall Tile Paste. *Cerâmica* **2006**, *52*, 240–244, doi:10.1590/s0366-69132006000400004.

50. Gautron, J.; Nys, Y. Eggshell Matrix Proteins. In *Bioactive Egg Compounds*; Huopalahti, R., López-Fandiño, R., Anton, M., Schade, R., Eds.; Springer Berlin Heidelberg: Berlin, Heidelberg, 2007; pp. 103–108 ISBN 978-3-540-37885-3.

51. MacNeil, J.H. Method and Apparatus for Separating a Protein Membrane and Shell Material in Waste Egg Shells 2001, *1*.

52. Inoue, M.; Mitani, T.; Miyazaki, N.; Torisaki, A. Method and Device for Separating Membrane from Egg Shell 1995, 5–8.

53. Monferrer, B.A.; Pons, M.M.T. Patents Separation of Inner Membrane of Egg Shells Comprises Breaking in Liquid and Otation , for Centrifugation Drying and Hydrolysis. **2001**, 2181580.

54. Adams, R.G.; Franklin, M.R. Vacuum Treatment of an Input Stream without Ruining Delicate Output Fractions 2006, *1*.

55. Vlad, V.; Ames, I. Eggshell Membrane Separation Method. 2011, *2*.

56. Akikusa, N.; Cao Qiu, X.M. Patents Method for Separating and Recovering Eggshell and Eggshell Membrane, and Apparatus for Separating and Recovering Eggshell and Eggshell Membrane 2012, 1–4.

57. New, L. Eggshell Membrane Separation Process United States Patent No.

8,448,884 B2. **2013**, *2*.

58. Dwivedi, S.P.; Sharma, S.; Mishra, R.K. Characterization of Waste Eggshells and CaCO3 Reinforced AA2014 Green Metal Matrix Composites: A Green Approach in the Synthesis of Composites. *Int. J. Precis. Eng. Manuf.* **2016**, *17*, 1383–1393, doi:10.1007/s12541-016-0164-z.

59. Lee Jie Shin; Barathi Dassan, E.G.; Zainol Abidin, M.S.; Anjang, A. Tensile and Compressive Properties of Glass Fiber-Reinforced Polymer Hybrid Composite with Eggshell Powder. *Arab. J. Sci. Eng.* **2020**, *45*, 5783–5791, doi:10.1007/s13369-020-04561-z.

60. Bhagavatheswaran, E.S.; Das, A.; Rastin, H.; Saeidi, H.; Jafari, S.H.; Vahabi, H.; Najafi, F.; Khonakdar, H.A.; Formela, K.; Jouyandeh, M.; et al. The Taste of Waste: The Edge of Eggshell Over Calcium Carbonate in Acrylonitrile Butadiene Rubber. *J. Polym. Environ.* **2019**, *27*, 2478–2489, doi:10.1007/s10924-019-01530-y.

61. Intharapat, P.; Kongnoo, A.; Kateungngan, K. The Potential of Chicken Eggshell Waste as a Bio-Filler Filled Epoxidized Natural Rubber (ENR) Composite and Its Properties. *J. Polym. Environ.* **2013**, *21*, 245–258, doi:10.1007/s10924-012-0475-9.

62. Holmes, J.; Kassel, P. Can Ground Eggshells Be Used as a Liming Source? **2006**, 235–238, doi:10.31274/icm-180809-866.

63. Planting Science The Effects of Coffee and Eggshells on Fertilizer for Red Clover and Barley Seeds. How to Use Eggshells for Plant Fertilizer. Available online: PlantingScience.org.

64. Phil, G.; Zhihong, M. High Value Products from Hatchery Waste. *Rirdc* **2009**, 09/061.

65. Waheed, M.; Butt, M.S.; Shehzad, A.; Adzahan, N.M.; Shabbir, M.A.; Rasul

Suleria, H.A.; Aadil, R.M. Eggshell Calcium: A Cheap Alternative to Expensive Supplements. *Trends Food Sci. Technol.* **2019**, *91*, 219–230, doi:10.1016/j.tifs.2019.07.021.

66. Schaafsma, A.; van Doormaal, J.J.; Muskiet, F.A.J.; Hofstede, G.J.H.; Pakan, I.; van der Veer, E. Positive Effects of a Chicken Eggshell Powder-Enriched Vitamin–Mineral Supplement on Femoral Neck Bone Mineral Density in Healthy Late Post-Menopausal Dutch Women. *Br. J. Nutr.* **2002**, *87*, 267–275, doi:10.1079/bjn2001515.

67. Liu, Y.; Cai, Z.; Ma, M.; Sheng, L.; Huang, X. Effect of Eggshell Membrane as Porogen on the Physicochemical Structure and Protease Immobilization of Chitosan-Based Macroparticles. *Carbohydr. Polym.* **2020**, *242*, doi:10.1016/j.carbpol.2020.116387.

68. Elizondo-Villarreal, N.; Martínez-De-La-Cruz, A.; Guerra, R.O.; Gómez-Ortega, J.L.; Torres-Martínez, L.M.; Castaño, V.M. Biomaterials from Agricultural Waste: Eggshell-Based Hydroxyapatite. *Water. Air. Soil Pollut.* **2012**, *223*, 3643–3646, doi:10.1007/s11270-012-1137-1.

69. Ummartyotin, S.; Tangnorawich, B. Utilization of Eggshell Waste as Raw Material for Synthesis of Hydroxyapatite. *Colloid Polym. Sci.* **2015**, *293*, 2477–2483, doi:10.1007/s00396-015-3646-0.

70. Ding, Q.; Kang, Z.; He, X.; Wang, M.; Lin, M.; Lin, H.; Yang, D.P. Eggshell Membrane-Templated Gold Nanoparticles as a Flexible SERS Substrate for Detection of Thiabendazole. *Microchim. Acta* **2019**, *186*, 1–9, doi:10.1007/s00604-019-3543-1.

71. Jati, I.R.A.P.; Kisima, A.; Ristiarini, S.; Suseno, T.I.P. Effects of Different Soaking Time Using Calcium Chloride Extracted from Eggshell on Physicochemical and Organoleptic Properties of Sweet Potato Chips. *{IOP} Conf. Ser. Earth Environ. Sci.* **2020**, *443*, 12050, doi:10.1088/1755-

1315/443/1/012050.

72. Orgill, D.P.; Straus Ii, F.H.; Lee, R.C. The Use of Collagen-GAG Membranes in Reconstructive Surgery. *Ann. N. Y. Acad. Sci.* **1999**, *888*, 233–248, doi:10.1111/j.1749-6632.1999.tb07959.x.

73. Elliott, B. Top 6 Benefits of Taking Collagen Supplements Available online: https://www.healthline.com/nutrition/collagen-benefits#2.-Helps-relieve-joint-pain (accessed on 9 July 2020).

74. Ogawa, M.; Portier, R.J.; Moody, M.W.; Bell, J.; Schexnayder, M.A.; Losso, J.N. Biochemical Properties of Bone and Scale Collagens Isolated from the Subtropical Fish Black Drum (Pogonia Cromis) and Sheepshead Seabream (Archosargus Probatocephalus). *Food Chem.* **2004**, *88*, 495–501, doi:10.1016/j.foodchem.2004.02.006.

75. Bogue, R.H. Conditions Affecting the Hydrolysis of Collagen to Gelatin. *Ind. Eng. Chem.* **1923**, *15*, 1154–1159, doi:10.1021/ie50167a018.

76. León-López, A.; Morales-Peñaloza, A.; Martínez-Juárez, V.M.; Vargas-Torres, A.; Zeugolis, D.I.; Aguirre-Álvarez, G. Hydrolyzed Collagen-Sources and Applications. *Molecules* **2019**, *24*, 4031, doi:10.3390/molecules24224031.

77. Ige, J.A.; Anifowose, M.A.; Amototo, I.O.; Adeyemi, A.O.; Olawuyi, M.Y. Influence of Groundnut Shell Ash (GSA) and Calcium Chloride (CaCl2) on Strength of Concrete. *Ann. Fac. Eng. Hunedoara – Int. J. Eng.* **2017**, *15*, 209–214.

78. Ng, C.; Alengaram, U.J.; Wong, L.S.; Mo, K.H.; Jumaat, M.Z.; Ramesh, S. A Review on Microstructural Study and Compressive Strength of Geopolymer Mortar, Paste and Concrete. *Constr. Build. Mater.* **2018**, *186*, 550–576, doi:10.1016/j.conbuildmat.2018.07.075.

79. US Geological Survey *Lime 1*; Reston, Virginia, 2020;

80. Faridi, H.; Arabhosseini, A. Application of Eggshell Wastes as Valuable and Utilizable Products: A Review. *Res. Agric. Eng.* **2018**, *64*, 104–114, doi:10.17221/6/2017-RAE.

81. Occidental Chemical Corporation *Calcium Chloride in Portland Cement Concrete*; 2006;

82. Huang, G.; Ji, Y.; Li, J.; Hou, Z.; Dong, Z. Improving Strength of Calcinated Coal Gangue Geopolymer Mortars via Increasing Calcium Content. *Constr. Build. Mater.* **2018**, *166*, 760–768, doi:10.1016/j.conbuildmat.2018.02.005.

83. Erlin, B.; Hime, W.G. The Role of Calcium Chloride in Concrete. *Concr. Constr. Mag.* **1976**.

84. Jaber, H.A.; Mahdi, R.S.; Hassan, A.K. Influence of Eggshell Powder on the Portland Cement Mortar Properties. *Mater. Today Proc.* **2020**, *20*, 391–396, doi:10.1016/j.matpr.2019.09.153.

85. Ofuyatan, O.M.; Adeniyi, A.G.; Ijie, D.; Ighalo, J.O.; Oluwafemi, J. Development of High-Performance Self Compacting Concrete Using Eggshell Powder and Blast Furnace Slag as Partial Cement Replacement. *Constr. Build. Mater.* **2020**, *256*, 119403, doi:10.1016/j.conbuildmat.2020.119403.

86. Venkata Krishnaiah, R.; Dayakar, P.; Mohan, S.J. Effect of Egg Shell Powder on Strength Behaviour of Concrete. *Int. J. Innov. Technol. Explor. Eng.* **2019**, *8*, 562–564, doi:10.35940/ijitee.I3110.0789S319.

87. Raji, S.A.; Samuel, A.T. Egg Shell As A Fine Aggregate In Concrete For Sustainable Construction. *Int. J. Sci. Technol. Res.* **2015**, *4*, 8–13.

88. Cree, D.; Pliya, P. Effect of Elevated Temperature on Eggshell, Eggshell Powder and Eggshell Powder Mortars for Masonry Applications. *J. Build. Eng.* **2019**, *26*, 100852, doi:10.1016/j.jobe.2019.100852.

89. Bensaifi, E.; Bouteldja, F.; Nouaouria, M.S.; Breul, P. Influence of Crushed Granulated Blast Furnace Slag and Calcined Eggshell Waste on Mechanical Properties of a Compacted Marl. *Transp. Geotech.* **2019**, *20*, doi:10.1016/j.trgeo.2019.100244.

90. Abdelmalik, A.A.; Ogbodo, M.O.; Momoh, G.E. Investigating the Mechanical and Insulation Performance of Waste Eggshell Powder/Epoxy Polymer for Power Insulation Application. *SN Appl. Sci.* **2019**, *1*, 1–12, doi:10.1007/s42452-019-1259-9.

91. Jaques, N.G.; Pereira Barros, J.J.; Dayane dos Santos Silva, I.; Popp, M.; Kolbe, J.; Ramos Wellen, R.M. New Approaches of Curing and Degradation on Epoxy/Eggshell Composites. *Compos. Part B Eng.* **2020**, *196*, doi:10.1016/j.compositesb.2020.108125.

92. Arunya, A.; Thendral, S.; Chitra, R. Properties of Concrete Using Eggshell Powder and Glass Powder as a Cement Replacement. *Int. J. Innov. Technol. Explor. Eng.* **2019**, *8*, 808–810, doi:10.35940/ijitee.I3168.0789S319.

93. Ajala, E.O.; Ajala, M.A.; Odetoye, T.E.; Aderibigbe, F.A.; Osanyinpeju, H.O.; Ayanshola, M.A. Thermal Modification of Chicken Eggshell as Heterogeneous Catalyst for Palm Kernel Biodiesel Production in an Optimization Process. *Biomass Convers. Biorefinery* **2020**, doi:10.1007/s13399-020-00636-x.

94. Gupta, A.R.; Rathod, V.K. Waste Cooking Oil and Waste Chicken Eggshells Derived Solid Base Catalyst for the Biodiesel Production: Optimization and Kinetics. *Waste Manag.* **2018**, *79*, 169–178, doi:10.1016/j.wasman.2018.07.022.

95. Kavitha, V.; Geetha, V.; Jacqueline, P.J. Production of Biodiesel from Dairy Waste Scum Using Eggshell Waste. *Process Saf. Environ. Prot.* **2019**, *125*, 279–287, doi:10.1016/j.psep.2019.03.021.

96. Wong, Y.C.; Ang, R.X. Study of Calcined Eggshell as Potential CaWong, Y. C., & Ang, R. X. (2018). Study of Calcined Eggshell as Potential Catalyst for Biodiesel Formation Using Used Cooking Oil. Open Chemistry, 16(1), 1166–1175. Https://Doi.Org/10.1515/Chem-2018-0127talyst For. *Open Chem.* **2018**, *16*, 1166–1175.

97. Li, Z.; Yang, D.P.; Chen, Y.; Du, Z.; Guo, Y.; Huang, J.; Li, Q. Waste Eggshells to Valuable Co3O4/CaCO3 Materials as Efficient Catalysts for VOCs Oxidation. *Mol. Catal.* **2020**, *483*, doi:10.1016/j.mcat.2020.110766.

98. Brink, H.G.; Mahlangu, Z. Microbial Lead(II) Precipitation: The Influence of Growth Substrate. *Chem. Eng. Trans.* **2018**, *64*, 439–444, doi:10.3303/CET1864074.

99. Kinetic, W.; Murcia-salvador, A.; Pellicer, J.A.; Manuel, V.; Estrella, N.; Gabald, A. Egg By-Products as a Tool to Remove Direct Blue Desorption Properties. **2020**.

100. Al-Ghouti, M.A.; Khan, M. Eggshell Membrane as a Novel Bio Sorbent for Remediation of Boron from Desalinated Water. *J. Environ. Manage.* **2018**, *207*, 405–416, doi:10.1016/J.JENVMAN.2017.11.062.

101. Borhade, A. V.; Kale, A.S. Calcined Eggshell as a Cost Effective Material for Removal of Dyes from Aqueous Solution. *Appl. Water Sci.* **2017**, *7*, 4255–4268, doi:10.1007/s13201-017-0558-9.

102. Sree, G.V.; Nagaraaj, P.; Kalanidhi, K.; Aswathy, C.A.; Rajasekaran, P. Calcium Oxide a Sustainable Photocatalyst Derived from Eggshell for Efficient Photo-Degradation of Organic Pollutants. *J. Clean. Prod.* **2020**, 122294, doi:10.1016/j.jclepro.2020.122294.

103. Ahmad, W.; Sethupathi, S.; Kanadasan, G.; Iberahim, N.; Bashir, M.J.K.; Munusamy, Y. Adsorption of SO2 and H2S by Sonicated Raw Eggshell. *Mater.*

Today Proc. **2020**, 1–7, doi:10.1016/j.matpr.2020.01.084.

104. Doumett, S.; Lamperi, L.; Checchini, L.; Azzarello, E.; Mugnai, S.; Mancuso, S.; Petruzzelli, G.; Del Bubba, M. Heavy Metal Distribution between Contaminated Soil and Paulownia Tomentosa, in a Pilot-Scale Assisted Phytoremediation Study: Influence of Different Complexing Agents. *Chemosphere* **2008**, *72*, 1481–1490, doi:10.1016/j.chemosphere.2008.04.083.

105. Ashrafi, M.; Mohamad, S.; Yusoff, I.; Hamid, F.S. Immobilization of Pb, Cd, and Zn in a Contaminated Soil Using Eggshell and Banana Stem Amendments: Metal Leachability and a Sequential Extraction Study. *Environ. Sci. Pollut. Res.* **2015**, *22*, 223–230, doi:10.1007/s11356-014-3299-4.

106. Mashangwa, T.D.; Tekere, M.; Sibanda, T. Determination of the Efficacy of Eggshell as a Low-Cost Adsorbent for the Treatment of Metal Laden Effluents. *Int. J. Environ. Res.* **2017**, *11*, 175–188, doi:10.1007/s41742-017-0017-3.

107. Rahmani-Sani, A.; Singh, P.; Raizada, P.; Claudio Lima, E.; Anastopoulos, I.; Giannakoudakis, D.A.; Sivamani, S.; Dontsova, T.A.; Hosseini-Bandegharaei, A. Use of Chicken Feather and Eggshell to Synthesize a Novel Magnetized Activated Carbon for Sorption of Heavy Metal Ions. *Bioresour. Technol.* **2020**, *297*, 122452, doi:10.1016/j.biortech.2019.122452.

108. Oke, I.A.; Olarinoye, N.O.; Adewusi, S.R.A. Adsorption Kinetics for Arsenic Removal from Aqueous Solutions by Untreated Powdered Eggshell. *Adsorption* **2008**, *14*, 73–83, doi:10.1007/s10450-007-9047-z.

109. Almeida, P. V.; Santos, A.F.; Lopes, D. V.; Gando-Ferreira, L.M.; Quina, M.J. Novel Adsorbents Based on Eggshell Functionalized with Iron Oxyhydroxide for Phosphorus Removal from Liquid Effluents. *J. Water Process Eng.* **2020**, *36*, 101248, doi:10.1016/j.jwpe.2020.101248.

110. T., R.; Sundararaman, S. Synthesis and Characterization of Chicken Eggshell

Powder Coated Magnetic Nano Adsorbent by an Ultrasonic Bath Assisted Co-Precipitation for Cr(VI) Removal from Its Aqueous Mixture. *J. Environ. Chem. Eng.* **2020**, *8*, 103877, doi:10.1016/j.jece.2020.103877.

111. Karoshi, G.; Kolar, P.; Shah, S.B.; Gilleskie, G. Valorization of Eggshell Waste into Supported Copper Catalysts for Partial Oxidation of Methane. *Int. J. Environ. Res.* **2020**, *14*, 61–70, doi:10.1007/s41742-019-00238-0.

112. Madadi, A.; Wei, J. Characterization of Calcium Silicate Hydrate Gels with Different Calcium to Silica Ratios and Polymer Modifications. *Gels* **2022**, *8*, doi:10.3390/gels8020075.

113. Kang, S.; Lee, J.; Park, S.M.; Alessi, D.S.; Baek, K. Adsorption Characteristics of Cesium onto Calcium-Silicate-Hydrate in Concrete Powder and Block. *Chemosphere* **2020**, *259*, 127494, doi:10.1016/j.chemosphere.2020.127494.

114. Kai, M.F.; Li, G.; Yin, B. Bin; Akbar, A. Aluminum-Induced Structure Evolution and Mechanical Strengthening of Calcium Silicate Hydrates: An Atomistic Insight. *Constr. Build. Mater.* **2023**, *393*, 132120, doi:10.1016/j.conbuildmat.2023.132120.

115. Yu, Q.; Lin, Y.; Guo, T.; Wen, R.; Wang, C.; Tu, Y.; Sas, G.; Elfgren, L. Assessing the Unsaturated Transport and Adsorption Properties of Ions in Nanopores of Realistic Hydrated-Calcium-Silicate Gel Using Molecular Dynamics Simulations. *Comput. Mater. Sci.* **2023**, *222*, 112121, doi:10.1016/j.commatsci.2023.112121.

116. Wang, X.; Ding, S.; Ashour, A.; Ye, H.; Thakur, V.K.; Zhang, L.; Han, B. Back to Basics: Nanomodulating Calcium Silicate Hydrate Gels to Mitigate CO2 Footprint of Concrete Industry. *J. Clean. Prod.* **2023**, 139921, doi:10.1016/j.jclepro.2023.139921.

117. Zhang, G.; Yang, Y.; Li, H. Calcium-Silicate-Hydrate Seeds as an Accelerator

for Saving Energy in Cold Weather Concreting. *Constr. Build. Mater.* **2020**, *264*, 120191, doi:10.1016/j.conbuildmat.2020.120191.

118. Part, W.K.; Ramli, M.; Cheah, C.B. An Overview on the Influence of Various Factors on the Properties of Geopolymer Concrete Derived from Industrial By-Products. *Constr. Build. Mater.* **2015**, *77*, 370–395, doi:10.1016/j.conbuildmat.2014.12.065.

119. Tan, R.R.; Foo, D.C.Y. Process Integration and Climate Change: From Carbon Emissions Pinch Analysis to Carbon Management Networks. *Chem. Eng. Trans.* **2018**, *70*, 1–6, doi:https://doi.org/10.3303/CET1870001.

120. Ikotun, B.D.; Fanourakis, G.C.; Mishra Bhardwaj, S. The Effect of Fly Ash, β-Cyclodextrin and Fly Ash-β-Cyclodextrin Composites on Concrete Workability and Strength. In Proceedings of the Cement and Concrete Composites; 2017; Vol. 78, pp. 1–12.

121. Mohadi, R.; Anggraini, K.; Riyanti, F.; Lesbani, A. Preparation Calcium Oxide From Chicken Eggshells. *Sriwij. J. Environ.* **2016**, *1*, 32–35, doi:10.22135/sje.2016.1.2.32-35.

122. Tangboriboon, N.; Kunanuruksapong, R.; Sirivat, A.; Kunanuruksapong, R.; Sirivat, A. Preparation and Properties of Calcium Oxide from Eggshells via Calcination. *Mater. Sci. Pol.* **2012**, *30*, 313–322, doi:10.2478/s13536-012-0055-7.

123. Fu, L.; Cao, Y.; Kuang, S.-Y.; Guo, H. Index for Climate Change Adaptation in China and Its Application. *Adv. Clim. Chang. Res.* **2021**, doi:10.1016/j.accre.2021.06.006.

124. Simonson, W.D.; Miller, E.; Jones, A.; García-Rangel, S.; Thornton, H.; McOwen, C. Enhancing Climate Change Resilience of Ecological Restoration — A Framework for Action. *Perspect. Ecol. Conserv.* **2021**, *19*, 300–310,

doi:10.1016/j.pecon.2021.05.002.

125. Antwi-Agyei, P.; Wiafe, E.A.; Amanor, K.; Baffour-Ata, F.; Codjoe, S.N.A. Determinants of Choice of Climate Change Adaptation Practices by Smallholder Pineapple Farmers in the Semi-Deciduous Forest Zone of Ghana. *Environ. Sustain. Indic.* **2021**, *12*, 100140, doi:10.1016/j.indic.2021.100140.

126. Deus, R.M.; Mele, F.D.; Bezerra, B.S.; Battistelle, R.A.G. A Municipal Solid Waste Indicator for Environmental Impact: Assessment and Identification of Best Management Practices. *J. Clean. Prod.* **2020**, *242*, 118433, doi:10.1016/j.jclepro.2019.118433.

127. Christensen, T.B. Towards a Circular Economy in Cities: Exploring Local Modes of Governance in the Transition towards a Circular Economy in Construction and Textile Recycling. *J. Clean. Prod.* **2021**, *305*, 127058, doi:10.1016/j.jclepro.2021.127058.

128. Petković, B.; Agdas, A.S.; Zandi, Y.; Nikolić, I.; Denić, N.; Radenkovic, S.D.; Almojil, S.F.; Roco-Videla, A.; Kojić, N.; Zlatković, D.; et al. Neuro Fuzzy Evaluation of Circular Economy Based on Waste Generation, Recycling, Renewable Energy, Biomass and Soil Pollution. *Rhizosphere* **2021**, *19*, 100418, doi:10.1016/j.rhisph.2021.100418.

129. Alao, M.A.; Popoola, O.M.; Ayodele, T.R. Selection of Waste-to-Energy Technology for Distributed Generation Using IDOCRIW-Weighted TOPSIS Method: A Case Study of the City of Johannesburg, South Africa. *Renew. Energy* **2021**, *178*, 162–183, doi:https://doi.org/10.1016/j.renene.2021.06.031.

130. Ayeleru, O.O.; Fajimi, L.I.; Oboirien, B.O.; Olubambi, P.A. Forecasting Municipal Solid Waste Quantity Using Artificial Neural Network and Supported Vector Machine Techniques: A Case Study of Johannesburg, South Africa. *J. Clean. Prod.* **2021**, *289*, 125671, doi:https://doi.org/10.1016/j.jclepro.2020.125671.

131. Department of Environmental Affairs South Africa State of Waste Report South Africa First Draft Report. *Gov. South Africa* **2018**, 68.

132. Saldanha, R.B.; da Rocha, C.G.; Caicedo, A.M.L.; Consoli, N.C. Technical and Environmental Performance of Eggshell Lime for Soil Stabilization. *Constr. Build. Mater.* **2021**, *298*, 123648, doi:https://doi.org/10.1016/j.conbuildmat.2021.123648.

133. Vandeginste, V. Food Waste Eggshell Valorization through Development of New Composites: A Review. *Sustain. Mater. Technol.* **2021**, *29*, e00317, doi:https://doi.org/10.1016/j.susmat.2021.e00317.

134. Md Zain, M.R.; Oh, C.L.; Lee, S.W. Investigations on Rheological and Mechanical Properties of Self-Compacting Concrete (SCC) Containing 0.6 Mm Eggshell as Partial Replacement of Cement. *Constr. Build. Mater.* **2021**, *303*, 124539, doi:https://doi.org/10.1016/j.conbuildmat.2021.124539.

135. Hsieh, S.-L.; Li, F.-Y.; Lin, P.-Y.; Beck, D.E.; Kirankumar, R.; Wang, G.-J.; Hsieh, S. CaO Recovered from Eggshell Waste as a Potential Adsorbent for Greenhouse Gas CO2. *J. Environ. Manage.* **2021**, *297*, 113430, doi:https://doi.org/10.1016/j.jenvman.2021.113430.

136. Bharti, R.; Guldhe, A.; Kumar, D.; Singh, B. Solar Irradiation Assisted Synthesis of Biodiesel from Waste Cooking Oil Using Calcium Oxide Derived from Chicken Eggshell. *Fuel* **2020**, *273*, 117778, doi:https://doi.org/10.1016/j.fuel.2020.117778.

137. Krongkitsiri, P.; Krongkitsiri, W.; Phukird, S.; Tipparach, U. A Comparison of Dielectric Properties of Eggshells from Free-Range System and Control-Range System. *Mater. Today Proc.* **2021**, doi:https://doi.org/10.1016/j.matpr.2021.05.091.

138. Rodriguez, N.; Alonso, M.; Abanades, J.C.; Grasa, G.; Murillo, R. Analysis of

a Process to Capture the CO2 Resulting from the Pre-Calcination of the Limestone Feed to a Cement Plant. *Energy Procedia* **2009**, *1*, 141–148, doi:10.1016/j.egypro.2009.01.021.

139. Sathiparan, N. Utilization Prospects of Eggshell Powder in Sustainable Construction Material – A Review. *Constr. Build. Mater.* **2021**, *293*, 123465, doi:https://doi.org/10.1016/j.conbuildmat.2021.123465.

140. Razali, N.; Azizan, M.A.; Pa'ee, K.F.; Razali, N.; Jumadi, N. Preliminary Studies on Calcinated Chicken Eggshells as Fine Aggregates Replacement in Conventional Concrete. *Mater. Today Proc.* **2020**, *31*, 354–359, doi:https://doi.org/10.1016/j.matpr.2020.06.232.

141. Hamada, H.M.; Tayeh, B.A.; Al-Attar, A.; Yahaya, F.M.; Muthusamy, K.; Humada, A.M. The Present State of the Use of Eggshell Powder in Concrete: A Review. *J. Build. Eng.* **2020**, *32*, 101583, doi:https://doi.org/10.1016/j.jobe.2020.101583.

142. Chong, B.W.; Othman, R.; Ramadhansyah, P.J.; Doh, S.I.; Li, X. Properties of Concrete with Eggshell Powder: A Review. *Phys. Chem. Earth, Parts A/B/C* **2020**, *120*, 102951, doi:https://doi.org/10.1016/j.pce.2020.102951.

143. Aina, S.T.; Du-Plessis, B.J.; Mjimba, V.; Brink, H.G. Effect of Membrane Removal on The Production of Calcium Oxide from Eggshells Via Calcination. *Chem. Eng. Trans.* **2020**, *81*, 1069–1074, doi:10.3303/CET2081179.

144. Murcia-Salvador, A.; Pellicer, J.A.; Rodríguez-López, M.I.; Gómez-López, V.M.; Núñez-Delicado, E.; Gabaldón, J.A. Egg By-Products as a Tool to Remove Direct Blue 78 Dye from Wastewater: Kinetic, Equilibrium Modeling, Thermodynamics and Desorption Properties. *Materials (Basel).* **2020**, *13*, doi:10.3390/ma13061262.

145. Zulfikar, M.A.; Novita, E.; Hertadi, R.; Djajanti, S.D. Removal of Humic Acid

from Peat Water Using Untreated Powdered Eggshell as a Low Cost Adsorbent. *Int. J. Environ. Sci. Technol.* **2013**, *10*, 1357–1366, doi:10.1007/s13762-013-0204-5.

146. Niju, S.; Begum, M.M.M.S.; Anantharaman, N. Modification of Egg Shell and Its Application in Biodiesel Production. *J. Saudi Chem. Soc.* **2014**, *18*, 702–706, doi:10.1016/j.jscs.2014.02.010.

147. Daraei, H.; Mittal, A.; Mittal, J.; Kamali, H. Optimization of Cr(VI) Removal onto Biosorbent Eggshell Membrane: Experimental & Theoretical Approaches. *Desalin. Water Treat.* **2014**, *52*, 1307–1315, doi:10.1080/19443994.2013.787374.

148. (2-Fluorophenoxy)Acetic Acid | C8H7FO3 - PubChem Available online: https://pubchem.ncbi.nlm.nih.gov/compound/223073#section=Synonyms (accessed on 22 February 2021).

149. Bumecaine | C18H28N2O - PubChem Available online: https://pubchem.ncbi.nlm.nih.gov/compound/65770#section=Pharmacology-and-Biochemistry (accessed on 22 February 2021).

150. N-(2-Aminopropyl)Glycyl-L-Prolylalanine | C13H24N4O4 | ChemSpider Available online: http://www.chemspider.com/Chemical-Structure.30855750.html (accessed on 22 February 2021).

151. 9064-67-9 Collagen (Cattle Skin) (9CI) Formula, NMR, Boiling Point, Density, Flash Point Available online: https://www.guidechem.com/dictionary/en/9064-67-9.html (accessed on 22 February 2021).

152. Lysozyme Chloride | C36H61N7O19 - PubChem Available online: https://pubchem.ncbi.nlm.nih.gov/compound/24839946 (accessed on 10 March 2021).

153. 1-Deoxy-5-Aza-D-Allopyran-Uronic Acid | C6H11NO6 - PubChem Available online: https://pubchem.ncbi.nlm.nih.gov/compound/91619589 (accessed on 10 March 2021).

154. Sucralose-6-Uronic Acid | C12H17Cl3O9 - PubChem Available online: https://pubchem.ncbi.nlm.nih.gov/compound/134687352 (accessed on 10 March 2021).

155. O-Sialic Acid | C11H19NO9 - PubChem Available online: https://pubchem.ncbi.nlm.nih.gov/compound/444885 (accessed on 10 March 2021).

156. Sialic Acids | C20H36N2O17 - PubChem Available online: https://pubchem.ncbi.nlm.nih.gov/compound/349960 (accessed on 10 March 2021).

157. Chondroitin Sulphate A | C14H23NO15S - PubChem Available online: https://pubchem.ncbi.nlm.nih.gov/compound/4368136 (accessed on 10 March 2021).

158. Dermatan Sulfate | C14H21NO15S-2 - PubChem Available online: https://pubchem.ncbi.nlm.nih.gov/compound/32756 (accessed on 10 March 2021).

159. Dermatan Hydrogen Sulphate | C18H31NO14S - PubChem Available online: https://pubchem.ncbi.nlm.nih.gov/compound/72682693 (accessed on 10 March 2021).

160. Hyaluronic Acid | C33H54N2O23 - PubChem Available online: https://pubchem.ncbi.nlm.nih.gov/compound/24847767 (accessed on 10 March 2021).

161. Keratan | C28H48N2O32S4 - PubChem Available online: https://pubchem.ncbi.nlm.nih.gov/compound/446715 (accessed on 10 March

2021).

162. Egbo, M.K. A Fundamental Review on Composite Materials and Some of Their Applications in Biomedical Engineering. *J. King Saud Univ. - Eng. Sci.* **2021**, *33*, 557–568, doi:10.1016/J.JKSUES.2020.07.007.

163. Kelly, A.; Mortensen, A. Composite Materials: Overview. *Encycl. Mater. Sci. Technol.* **2001**, 1361–1371, doi:10.1016/B0-08-043152-6/00254-0.

164. Haleem, A.; Pan, J.-M.; Shah, A.; Hussain, H.; He, W. A Systematic Review on New Advancement and Assessment of Emerging Polymeric Cryogels for Environmental Sustainability and Energy Production. *Sep. Purif. Technol.* **2023**, *316*, 123678, doi:10.1016/j.seppur.2023.123678.

165. Chermant, J.-L.; Coster, M. Composites, Microstructure of: Quantitative Description. *Encycl. Mater. Sci. Technol.* **2001**, 1396–1402, doi:10.1016/B0-08-043152-6/00259-X.

166. Haleem, A.; Shafiq, A.; Chen, S.-Q.; Nazar, M. A Comprehensive Review on Adsorption, Photocatalytic and Chemical Degradation of Dyes and Nitro-Compounds over Different Kinds of Porous and Composite Materials. *Molecules* **2023**, *28*, 1081, doi:10.3390/molecules28031081.

167. Haleem, A.; Chen, S.; Pan, J.; Weidong, H. Gamma Radiation Induced Synthesis of Double Network Hydrophilic Cryogels at Low PH Loaded with AuNPs for Fast and Efficient Degradation of Congo Red. *J. Hazard. Mater. Adv.* **2023**, *10*, 100299, doi:10.1016/j.hazadv.2023.100299.

168. Hymavathi, A. Materials Today : Proceedings A Green Synthetic Approach of Silver Nanoparticles Using Premna Tomentosa Leaf Extract and Their Anti-Microbial Study. *Mater. Today Proc.* **2022**, 10–13, doi:10.1016/j.matpr.2022.04.909.

169. Matar, G.H. An Investigation of Green Synthesis of Silver Nanoparticles Using

Turkish Honey Against Pathogenic Bacterial Strains. **2023**, *13*, 1–11.

170. Zhang, J.; Liu, L.; Wang, Y.; Wang, C.; Guo, Y.; Yuan, Z.; Jia, Y.; Li, P.; Sun, S.; Zhao, G. A Highly Selective Red-Emitting Fluorescent Probe and Its Micro-Nano-Assembly for Imaging Endogenous Peroxynitrite (ONOO−) in Living Cells. *Anal. Chim. Acta* **2023**, *1241*, 340778, doi:https://doi.org/10.1016/j.aca.2022.340778.

171. Abass Sofi, M.; Sunitha, S.; Ashaq Sofi, M.; Khadheer Pasha, S.K.; Choi, D. An Overview of Antimicrobial and Anticancer Potential of Silver Nanoparticles. *J. King Saud Univ. - Sci.* **2022**, *34*, 101791, doi:10.1016/j.jksus.2021.101791.

172. Swidan, N.S.; Hashem, Y.A.; Elkhatib, W.F.; Yassien, M.A. Antibiofilm Activity of Green Synthesized Silver Nanoparticles against Biofilm Associated Enterococcal Urinary Pathogens. *Sci. Rep.* **2022**, *12*, 1–13, doi:10.1038/s41598-022-07831-y.

173. Wali, N.; Shabbir, A.; Wajid, N.; Abbas, N.; Naqvi, S.Z.H. Synergistic Efficacy of Colistin and Silver Nanoparticles Impregnated Human Amniotic Membrane in a Burn Wound Infected Rat Model. *Sci. Rep.* **2022**, *12*, 1–12, doi:10.1038/s41598-022-10314-9.

174. Guerrero, D.S.; Bertani, R.P.; Ledesma, A.; Frías, M. de los A.; Romero, C.M.; Dávila Costa, J.S. Silver Nanoparticles Synthesized by the Heavy Metal Resistant Strain Amycolatopsis Tucumanensis and Its Application in Controlling Red Strip Disease in Sugarcane. *Heliyon* **2022**, *8*, e09472, doi:10.1016/j.heliyon.2022.e09472.

175. Li, P.; Guo, Y.; Jia, Y.; Guan, H.; Wang, C.; Wu, Z.; Sun, S.; Qu, Z.; Zhou, P.; Zhao, G. Achieving Metal-Free Phosphorescence in Dilute Solutions for Imaging Hypoxia in Cells and Tumors. *Mater. Chem. Front.* **2021**, *5*, 7170–7175, doi:10.1039/D1QM00733E.

176. Syafiuddin, A.; Fulazzaky, M.A.; Salmiati, S.; Kueh, A.B.H.; Fulazzaky, M.; Salim, M.R. Silver Nanoparticles Adsorption by the Synthetic and Natural Adsorbent Materials: An Exclusive Review. *Nanotechnol. Environ. Eng.* **2020**, *5*, 1, doi:10.1007/s41204-019-0065-3.

177. Hassan, D.M.A.; Farghali, M.R.F. Adsorption of Silver Nanoparticles from Aqueous Solution by Multiwalled Carbon Nanotubes. *Adv. Nanoparticles* **2017**, *06*, 22–32, doi:10.4236/anp.2017.62003.

178. Islam, M.A.; Jacob, M. V; Antunes, E. A Critical Review on Silver Nanoparticles: From Synthesis and Applications to Its Mitigation through Low-Cost Adsorption by Biochar. *J. Environ. Manage.* **2021**, *281*, 111918, doi:10.1016/j.jenvman.2020.111918.

179. Buksh, N.; Yun, C.; Ping, X.; Jhatial, G.H.; Yanhai, S. Chicken Eggshell as a Potential Eco-Friendly , Low-Cost Sorbent : A Mini Review. *J. Environ. Earth Sci.* **2018**, *8*, 28–39.

180. Li, X.; Cai, Z.; Ahn, D.U.; Huang, X. Development of an Antibacterial Nanobiomaterial for Wound-Care Based on the Absorption of AgNPs on the Eggshell Membrane. *Colloids Surfaces B Biointerfaces* **2019**, *183*, 110449, doi:10.1016/j.colsurfb.2019.110449.

181. Cordeiro, C.M.M.; Esmaili, H.; Ansah, G.; Hincke, M.T. Ovocalyxin-36 Is a Pattern Recognition Protein in Chicken Eggshell Membranes. *PLoS One* **2013**, *8*, 1–13, doi:10.1371/journal.pone.0084112.

182. Li, J.; Ng, D.H.L.; Ma, R.; Zuo, M.; Song, P. Eggshell Membrane-Derived MgFe2O4 for Pharmaceutical Antibiotics Removal and Recovery from Water. *Chem. Eng. Res. Des.* **2017**, *126*, 123–133, doi:10.1016/j.cherd.2017.07.005.

183. Odetoye, T.E.; Agu, J.O.; Ajala, E.O. Biodiesel Production from Poultry Wastes: Waste Chicken Fat and Eggshell. *J. Environ. Chem. Eng.* **2021**, *9*,

105654, doi:https://doi.org/10.1016/j.jece.2021.105654.

184. Seo, S.B.; Dananjaya, S.H.S.; Nikapitiya, C.; Park, B.K.; Gooneratne, R.; Kim, T.Y.; Lee, J.; Kim, C.H.; De Zoysa, M. Silver Nanoparticles Enhance Wound Healing in Zebrafish (Danio Rerio). *Fish Shellfish Immunol.* **2017**, *68*, 536–545, doi:10.1016/J.FSI.2017.07.057.

185. Nakamura, T.; Magara, H.; Herbani, Y.; Sato, S. Fabrication of Silver Nanoparticles by Highly Intense Laser Irradiation of Aqueous Solution. *Appl. Phys. A* **2011**, *104*, 1021–1024, doi:10.1007/s00339-011-6499-5.

186. Oves, M.; Khan, M.S.; Zaidi, A.; Ahmed, A.S.; Ahmed, F.; Ahmad, E.; Sherwani, A.; Owais, M.; Azam, A. Antibacterial and Cytotoxic Efficacy of Extracellular Silver Nanoparticles Biofabricated from Chromium Reducing Novel OS4 Strain of Stenotrophomonas Maltophilia. *PLoS One* **2013**, *8*, e59140, doi:10.1371/journal.pone.0059140.

187. Tendenedzai, J.T.; Chirwa, E.M.N.; Brink, H.G. Enterococcus Spp. Cell-Free Extract: An Abiotic Route for Synthesis of Selenium Nanoparticles (SeNPs), Their Characterisation and Inhibition of Escherichia Coli. *Nanomaterials* **2022**, *12*, doi:10.3390/nano12040658.

188. Beckman, C. What Is Z-Average Size Available online: https://www.beckman.com/support/faq/scientific/what-is-z-average-size (accessed on 8 February 2023).

189. Li, J.; Zhai, D.; Lv, F.; Yu, Q.; Ma, H.; Yin, J.; Yi, Z.; Liu, M.; Chang, J.; Wu, C. Preparation of Copper-Containing Bioactive Glass/Eggshell Membrane Nanocomposites for Improving Angiogenesis, Antibacterial Activity and Wound Healing. *Acta Biomater.* **2016**, *36*, 254–266, doi:10.1016/J.ACTBIO.2016.03.011.

190. Velgosova, O.; Čižmárová, E.; Málek, J.; Kavuličova, J. Effect of Storage

Conditions on Long-Term Stability of Ag Nanoparticles Formed via Green Synthesis. *Int. J. Miner. Metall. Mater.* **2017**, *24*, 1177–1182, doi:10.1007/s12613-017-1508-0.

191. Brusseau, M.L.; Rao, P.S.C.; Gillham, R.W. Sorption Nonideality during Organic Contaminant Transport in Porous Media. *Crit. Rev. Environ. Control* **1989**, *19*, 33–99, doi:10.1080/10643388909388358.

192. Brusseau, M.L.; Jessup, R.E.; Suresh, P.; Rao, C. Nonequilibrium Sorption of Organic Chemicals: Elucidation of Rate-Limiting Processes. *Environ. Sci. Technol.* **1991**, *25*, 134–142, doi:10.1021/es00013a015.

193. Azizian, S. Kinetic Models of Sorption: A Theoretical Analysis. *J. Colloid Interface Sci.* **2004**, *276*, 47–52, doi:10.1016/j.jcis.2004.03.048.

194. Largitte, L.; Pasquier, R. New Models for Kinetics and Equilibrium Homogeneous Adsorption. *Chem. Eng. Res. Des.* **2016**, *112*, 289–297, doi:10.1016/j.cherd.2016.06.021.

195. Myslitskaya, N.A.; Khitrin, A. V.; Ivanov, A.M.; Samusev, I.G.; Bryukhanov, V. V. Dynamics of Colloid Silver Nanoparticles in an Evaporating Water Drop. *Russ. Phys. J.* **2012**, *54*, 1280–1285, doi:10.1007/s11182-012-9743-3.

196. Palencia, M.S.; Berrio, M.E.; Palencia, S.L. Effect of Capping Agent and Diffusivity of Different Silver Nanoparticles on Their Antibacterial Properties. *J. Nanosci. Nanotechnol.* **2017**, *17*, 5197–5204, doi:10.1166/jnn.2017.13850.

197. Aliofkhazraei, M. Diffusion of Nanoparticles in Gases and Liquids. In *Handbook of Nanoparticles*; Aliofkhazraei, M., Ed.; Springer International Publishing: Cham, 2016; pp. 1–1426 ISBN 978-3-319-15337-7.

198. Largitte, L.; Pasquier, R. A Review of the Kinetics Adsorption Models and Their Application to the Adsorption of Lead by an Activated Carbon. *Chem. Eng. Res. Des.* **2016**, *109*, 495–504, doi:10.1016/j.cherd.2016.02.006.

199. Cornelissen, G.; Van Noort, P.C.M.; Parsons, J.R.; Govers, H.A.J. Temperature Dependence of Slow Adsorption and Desorption Kinetics of Organic Compounds in Sediments. *Environ. Sci. Technol.* **1997**, *31*, 454–460, doi:10.1021/es960300+.

200. Wang, Z.; Zhao, J.; Song, L.; Mashayekhi, H.; Chefetz, B.; Xing, B. Adsorption and Desorption of Phenanthrene on Carbon Nanotubes in Simulated Gastrointestinal Fluids. *Environ. Sci. Technol.* **2011**, *45*, 6018–6024, doi:10.1021/es200790x.

201. van Veenhuyzen, B.; Tichapondwa, S.; Hörstmann, C.; Chirwa, E.; Brink, H.G. High Capacity Pb(II) Adsorption Characteristics onto Raw- and Chemically Activated Waste Activated Sludge. *J. Hazard. Mater.* **2021**, *416*, 125943, doi:10.1016/j.jhazmat.2021.125943.

202. Weber, W.J.; Morris, J.C. Kinetics of Adsorption on Carbon from Solution. *J. Sanit. Eng. Div.* **1963**, *89*, 31–60.

203. Muedi, K.L.L.; Brink, H.G.G.; Masindi, V.; Maree, J.P.P. Effective Removal of Arsenate from Wastewater Using Aluminium Enriched Ferric Oxide-Hydroxide Recovered from Authentic Acid Mine Drainage. *J. Hazard. Mater.* **2021**, *414*, 125491, doi:10.1016/j.jhazmat.2021.125491.

204. Scott Fogler, H. *Elements of Chemical Reaction Engineering*; Fourth.; Pearson Education Limited: London, 2013; ISBN 0130473944.

205. Harned, H.S.; Hildreth, C.L. The Diffusion Coefficient of Silver Nitrate in Dilute Aqueous Solution at 25°. *J. Am. Chem. Soc.* **1951**, *73*, 3292–3293, doi:10.1021/ja01151a088.

206. Muedi, K.L.; Masindi, V.; Maree, J.P.; Haneklaus, N.; Brink, H.G. Effective Adsorption of Congo Red from Aqueous Solution Using Fe/Al Di-Metal Nanostructured Composite Synthesised from Fe(III) and Al(III) Recovered

from Real Acid Mine Drainage. *Nanomaterials* **2022**, *12*, 776, doi:10.3390/nano12050776.

207. Langmuir, I. The Adsorption of Gases on Plane Surfaces of Glass, Mica and Platinum. *J. Am. Chem. Soc.* **1918**, *40*, 1361–1403, doi:10.1021/ja02242a004.

208. Girods, P.; Dufour, A.; Fierro, V.; Rogaume, Y.; Rogaume, C.; Zoulalian, A.; Celzard, A. Activated Carbons Prepared from Wood Particleboard Wastes: Characterisation and Phenol Adsorption Capacities. *J. Hazard. Mater.* **2009**, *166*, 491–501, doi:10.1016/j.jhazmat.2008.11.047.

209. Hall, C.; Wales, D.S.; Keane, M.A. COPPER REMOVAL FROM AQUEOUS SYSTEMS: BIOSORPTION BY PSEUDOMONAS SYRINGAE. *Sep. Sci. Technol.* **2001**, *36*, 223–240, doi:10.1081/SS-100001076.

210. Xin, Y.; Li, C.; Liu, J.; Liu, J.; Liu, Y.; He, W.; Gao, Y. Adsorption of Heavy Metal with Modified Eggshell Membrane and the in Situ Synthesis of Cu - Ag/ Modified Eggshell Membrane Composites. *R. Soc. Open Sci.* **2018**, *5*, doi:10.1098/rsos.180532.

211. Wu, W.; Jin, Y.; Bai, F.; Jin, S. *Pseudomonas Aeruginosa*; Elsevier Ltd, 2014; ISBN 9780123971692.

212. Poole, K. Pseudomonas Aeruginosa: Resistance to the Max. *Front. Microbiol.* **2011**, *2*, 1–13, doi:10.3389/fmicb.2011.00065.

213. Bassetti, M.; Vena, A.; Croxatto, A.; Righi, E.; Guery, B. How to Manage Pseudomonas Aeruginosa Infections. *Drugs Context* **2018**, *7*, 1–18, doi:10.7573/dic.212527.

214. Kovács, Á.T. Bacillus Subtilis. *Trends Microbiol.* **2019**, *27*, 724–725, doi:10.1016/j.tim.2019.03.008.

215. Earl, A.M.; Losick, R.; Kolter, R. Ecology and Genomics of Bacillus Subtilis.

Trends Microbiol. **2008**, *16*, 269–275, doi:10.1016/j.tim.2008.03.004.

216. Yassin, N.; Ahmad, A. Incidence and Resistotyping Profiles of Bacillus Subtilis Isolated from Azadi Teaching Hospital in Duhok City, Iraq. *Mater. Socio Medica* **2012**, *24*, 194, doi:10.5455/msm.2012.24.194-197.

217. Midway, S.; Robertson, M.; Flinn, S.; Kaller, M. Comparing Multiple Comparisons: Practical Guidance for Choosing the Best Multiple Comparisons Test. *PeerJ* **2020**, *8*, e10387, doi:10.7717/peerj.10387.

218. Pang, Z.; Raudonis, R.; Glick, B.R.; Lin, T.J.; Cheng, Z. Antibiotic Resistance in Pseudomonas Aeruginosa: Mechanisms and Alternative Therapeutic Strategies. *Biotechnol. Adv.* **2019**, *37*, 177–192, doi:10.1016/j.biotechadv.2018.11.013.

219. Aina, S.; du Plessis, B.; Mjimba, V.; Brink, H. Eggshell Valorization: Membrane Removal, Calcium Oxide Synthesis, and Biochemical Compound Recovery towards Cleaner Productions. *Biointerface Res. Appl. Chem.* **2021**, *12*, 5870–5883, doi:10.33263/BRIAC125.58705883.

220. Gavanji, S.; Bakhtari, A.; Famurewa, A.C.; Othman, E.M. Cytotoxic Activity of Herbal Medicines as Assessed in Vitro : A Review. *Chem. Biodivers.* **2023**, *20*, doi:10.1002/cbdv.202201098.

221. Stockert, J.C.; Horobin, R.W.; Colombo, L.L.; Blázquez-Castro, A. Tetrazolium Salts and Formazan Products in Cell Biology: Viability Assessment, Fluorescence Imaging, and Labeling Perspectives. *Acta Histochem.* **2018**, *120*, 159–167, doi:10.1016/j.acthis.2018.02.005.

222. Patravale, V.; Dandekar, P.; Jain, R. Nanotoxicology: Evaluating Toxicity Potential of Drug-Nanoparticles. In *Nanoparticulate Drug Delivery*; Elsevier, 2012; pp. 123–155.

223. Van Damme, H. Concrete Material Science: Past, Present, and Future

Innovations. *Cem. Concr. Res.* **2018**, *112*, 5–24, doi:10.1016/j.cemconres.2018.05.002.

224. Royal Society of Chemistry The Concrete Conundrum. *Chem. World* **2008**.

225. Cement Production Global 2022 | Statista Available online: https://www.statista.com/statistics/1087115/global-cement-production-volume/ (accessed on 24 April 2023).

226. Dakal, T.C.; Kumar, A.; Majumdar, R.S.; Yadav, V. Mechanistic Basis of Antimicrobial Actions of Silver Nanoparticles. *Front. Microbiol.* **2016**, *7*, 1831, doi:10.3389/fmicb.2016.01831.

227. Menichetti, A.; Mavridi-Printezi, A.; Mordini, D.; Montalti, M. Effect of Size, Shape and Surface Functionalization on the Antibacterial Activity of Silver Nanoparticles. *J. Funct. Biomater.* **2023**, *14*, 244, doi:10.3390/jfb14050244.

228. Little, B.J.; Blackwood, D.J.; Hinks, J.; Lauro, F.M.; Marsili, E.; Okamoto, A.; Rice, S.A.; Wade, S.A.; Flemming, H.C. Microbially Influenced Corrosion—Any Progress? *Corros. Sci.* **2020**, *170*, 108641, doi:10.1016/j.corsci.2020.108641.

229. Nath, D.; Jangid, K.; Susaniya, A.; Kumar, R.; Vaish, R. Eggshell Derived CaO-Portland Cement Antibacterial Composites. *Compos. Part C Open Access* **2021**, *5*, 100123, doi:10.1016/j.jcomc.2021.100123.

230. Wei, S.; Jiang, Z.; Liu, H.; Zhou, D.; Sanchez-Silva, M. Microbiologically Induced Deterioration of Concrete - A Review. *Brazilian J. Microbiol.* **2013**, *44*, 1001–1007, doi:10.1590/S1517-83822014005000006.

231. Grengg, C.; Mittermayr, F.; Ukrainczyk, N.; Koraimann, G.; Kienesberger, S.; Dietzel, M. Advances in Concrete Materials for Sewer Systems Affected by Microbial Induced Concrete Corrosion: A Review. *Water Res.* **2018**, *134*, 341–352, doi:10.1016/j.watres.2018.01.043.

232. Zubrowska-Sudol, M.; Sytek-Szmeichel, K.; Krawczyk, P.; Bisak, A. Energy-Positive Disintegration of Waste Activated Sludge—Full Scale Study. *Energies* **2022**, *15*, 555, doi:10.3390/en15020555.

233. Jafari, M.; Botte, G.G. Electrochemical Valorization of Waste Activated Sludge for Short-Chain Fatty Acids Production. *Front. Chem.* **2022**, *10*, doi:10.3389/fchem.2022.974223.

234. Xie, N.; Zhong, L.; Ouyang, L.; Xu, W.; Zeng, Q.; Wang, K.; Zaynab, M.; Chen, H.; Xu, F.; Li, S. Community Composition and Function of Bacteria in Activated Sludge of Municipal Wastewater Treatment Plants. *Water* **2021**, *13*, doi:10.3390/w13060852.

235. Ohshima, Y.; Takada, D.; Namai, S.; Sawai, J.; Kikuchi, M.; Hotta, M. Antimicrobial Characteristics of Heated Eggshell Powder. *Biocontrol Sci.* **2015**, *20*, 239–246, doi:10.4265/bio.20.239.

236. Aina, S.T.; Kyomuhimbo, H.D.; Ramjee, S.; Du Plessis, B.; Mjimba, V.; Maged, A.; Haneklaus, N.; Brink, H.G. Synthesis and Assessment of Antimicrobial Composites of Ag Nanoparticles or AgNO3 and Egg Shell Membranes. *Molecules* **2023**, *28*, 4654, doi:10.3390/molecules28124654.

237. Kumar, R. How Can We Extract Silver from Silver Nitrate? 2018.

238. European Committee for Standardization (CEN). EN 196-1:2005. European Standard. Methods of Testing Cement - Part 1: Determination of Strength. 2005.

239. South African Bureau of Standards (SABS). SANS 50196-1:2006. South African National Standard Methods of Testing Cement - Part 1: Determination Of Strength. 2006.

240. Kiernan, D. Chapter 6: Two-Way Analysis of Variance. In *Natural Resources Biometrics*; Open SUNY Textbooks: New York, NY, 2014 ISBN 978-1-

942341-17-8.

241. Tufail, M.S.; Liaqat, I.; Andleeb, S.; Naseem, S.; Zafar, U.; Sadiqa, A.; Liaqat, I.; Ali, N.M.; Bibi, A.; Arshad, N.; et al. Biogenic Synthesis, Characterization and Antibacterial Properties of Silver Nanoparticles against Human Pathogens. *J. Oleo Sci.* **2022**, *71*, ess21291, doi:10.5650/jos.ess21291.

242. Shahbandeh, M.; Moghadam, M.T.; Mirnejad, R.; Mirkalantari, S.; Mirzaei, M. The Efficacy of AGNO3 Nanoparticles Alone and Conjugated with Imipenem for Combating Extensively Drug-Resistant Pseudomonas Aeruginosa. *Int. J. Nanomedicine* **2020**, *15*, 6905–6916, doi:10.2147/IJN.S260520.

243. Hsueh, Y.H.; Lin, K.S.; Ke, W.J.; Hsieh, C. Te; Chiang, C.L.; Tzou, D.Y.; Liu, S.T. The Antimicrobial Properties of Silver Nanoparticles in Bacillus Subtilis Are Mediated by Released Ag+ Ions. *PLoS One* **2015**, *10*, 1–17, doi:10.1371/journal.pone.0144306.

244. Choi, O.; Hu, Z. Size Dependent and Reactive Oxygen Species Related Nanosilver Toxicity to Nitrifying Bacteria. *Environ. Sci. Technol.* **2008**, *42*, 4583–4588, doi:10.1021/es703238h.

245. Choi, O.; Clevenger, T.E.; Deng, B.; Surampalli, R.Y.; Ross, L.; Hu, Z. Role of Sulfide and Ligand Strength in Controlling Nanosilver Toxicity. *Water Res.* **2009**, *43*, 1879–1886, doi:10.1016/j.watres.2009.01.029.

246. Chen, Y.; Jiang, S.; Yuan, H.; Zhou, Q.; Gu, G. Hydrolysis and Acidification of Waste Activated Sludge at Different PHs. *Water Res.* **2007**, *41*, 683–689, doi:10.1016/j.watres.2006.07.030.

247. Sanjaya, A.P.; Praseptiangga, D.; Zaman, M.Z.; Umiati, V.F.; Baraja, S.I. Effect of PH, Temperature, and Salt Concentration on the Growth of Bacillus Subtilis T9-05 Isolated from Fish Sauce. *IOP Conf. Ser. Earth Environ. Sci.* **2023**, *1200*, 012050, doi:10.1088/1755-1315/1200/1/012050.

248. Ahmed, F.; Mirani, Z.A.; Mirani, P.N.; Imdad, M.J.; Khan, F.Z.; Khan, M.N.; Khan, A.B.; Li, Y.; Zhao, Y. Pseudomonas Aeruginosa Response to Acidic Stress and Imipenem Resistance. *Appl. Sci.* **2022**, *12*, 8357, doi:10.3390/app12168357.

249. Paruthi, S.; Khan, A.H.; Kumar, A.; Kumar, F.; Hasan, M.A.; Magbool, H.M.; Manzar, M.S. Sustainable Cement Replacement Using Waste Eggshells: A Review on Mechanical Properties of Eggshell Concrete and Strength Prediction Using Artificial Neural Network. *Case Stud. Constr. Mater.* **2023**, *18*, e02160, doi:10.1016/j.cscm.2023.e02160.

APPENDIX

In the appendices every number that comes after the letter for figure numbering represents the relevant chapter in that regard.

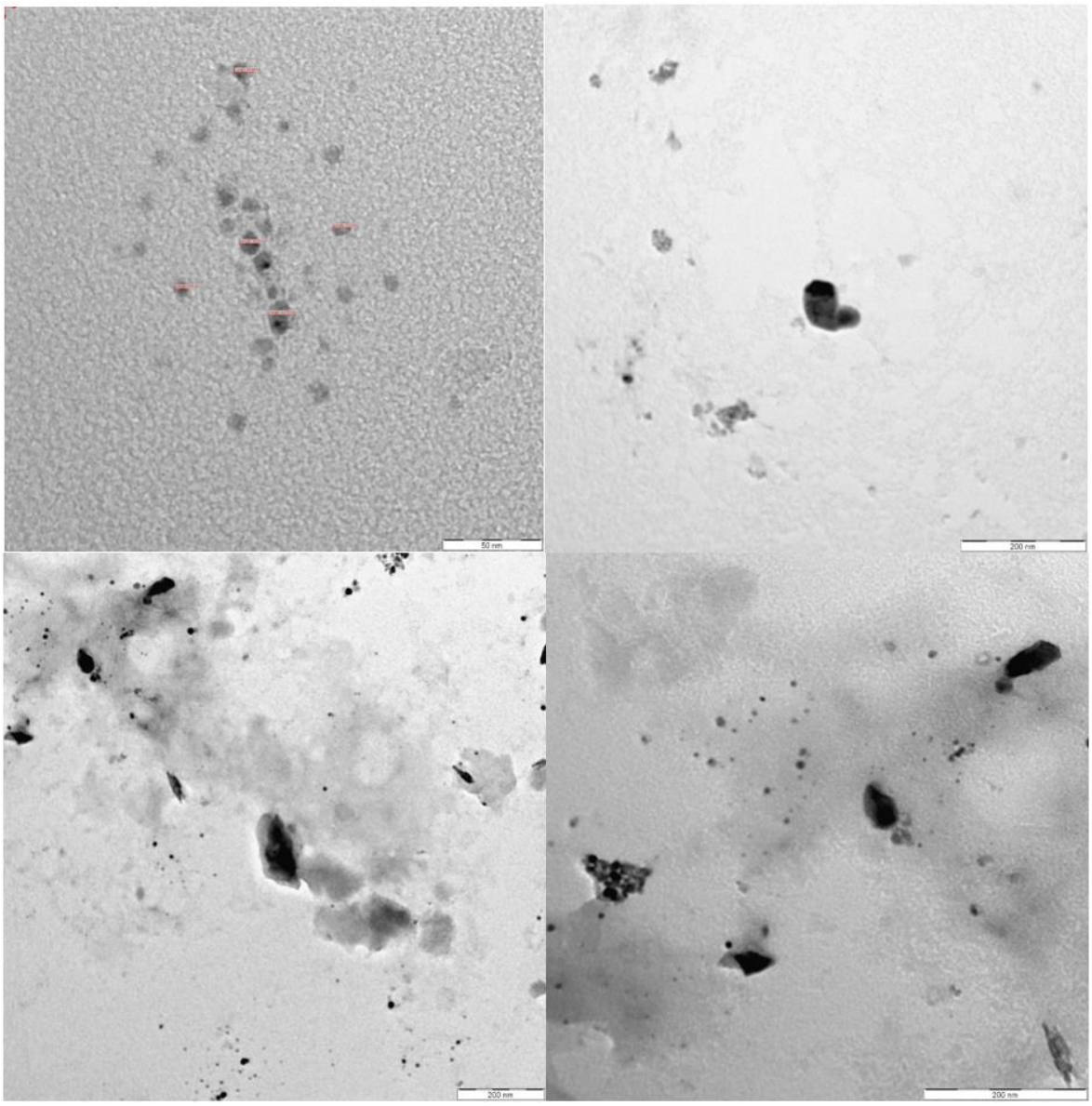

Figure A5.1: *TEM image of particles AgNPs particles at different magnifications (see scale bar)*

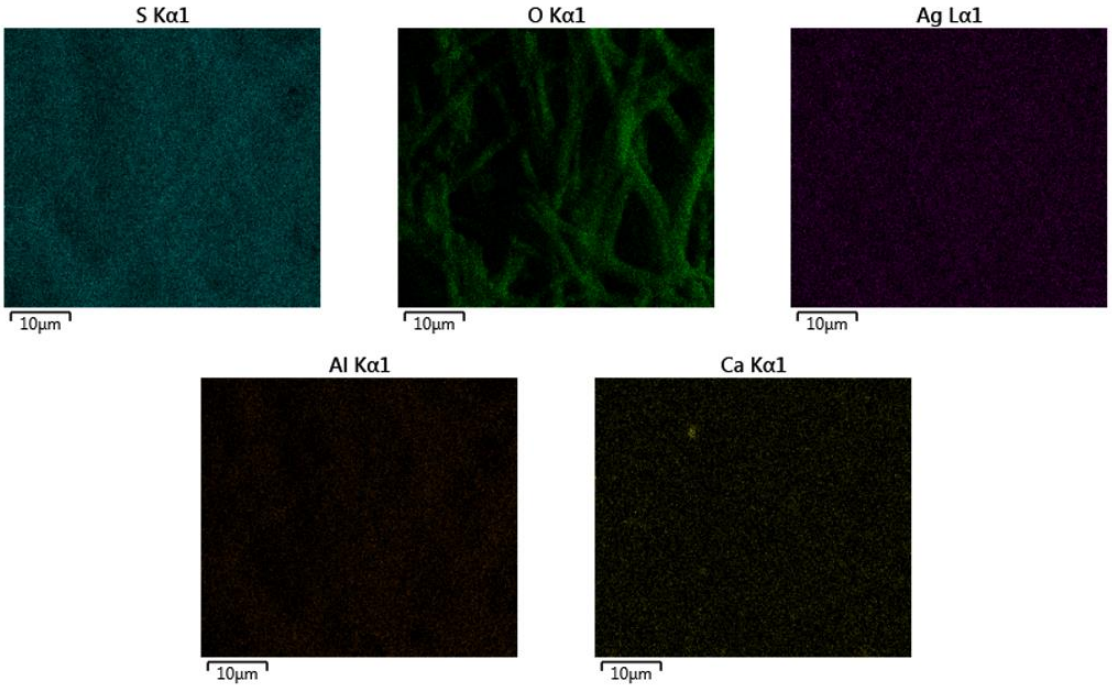

Figure A5.2: *ESM/$AgNO_3$ EDS Map*

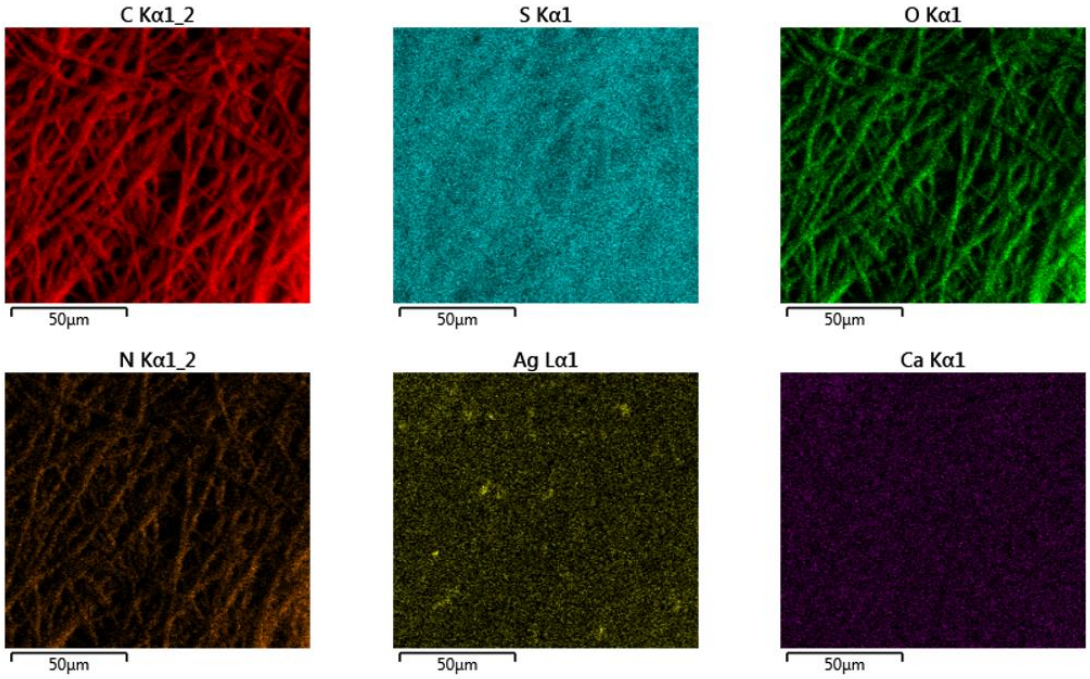

Figure A5.3: *ESM/AgNPs EDS Map*

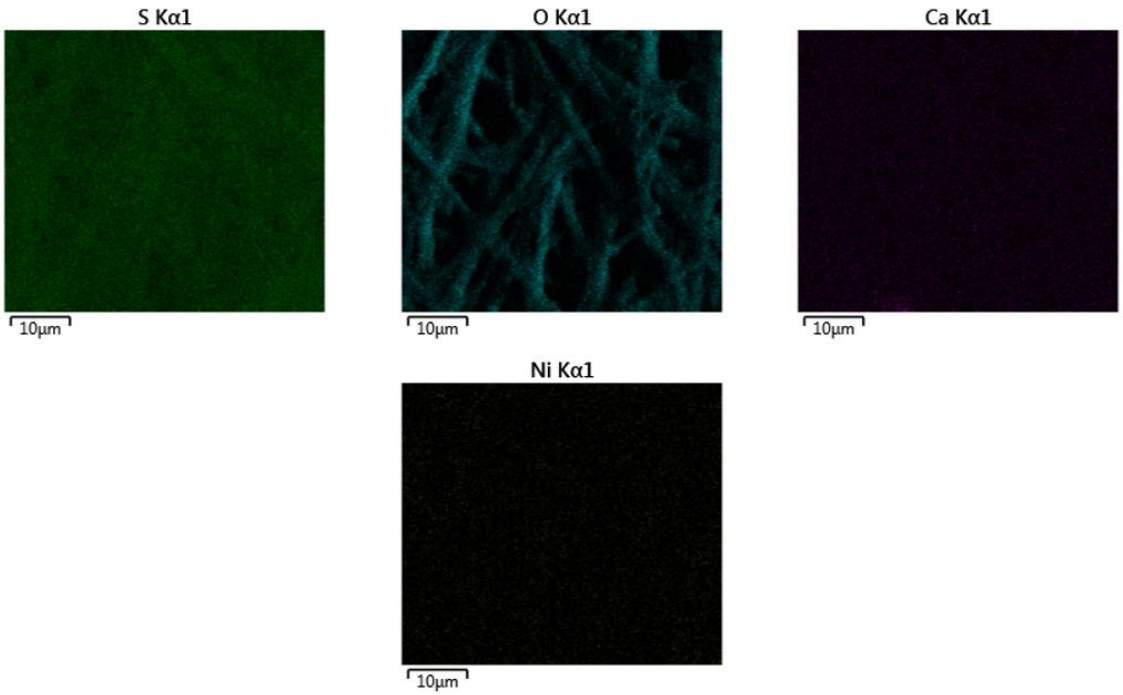

Figure A5.4: *ESM EDS Map*

Figure A6.1: *Tensile (left) and compressive (right) strength test in progress.*

Figure A6.2: *A section of the tested mortar showing imbedded membrane composite.*

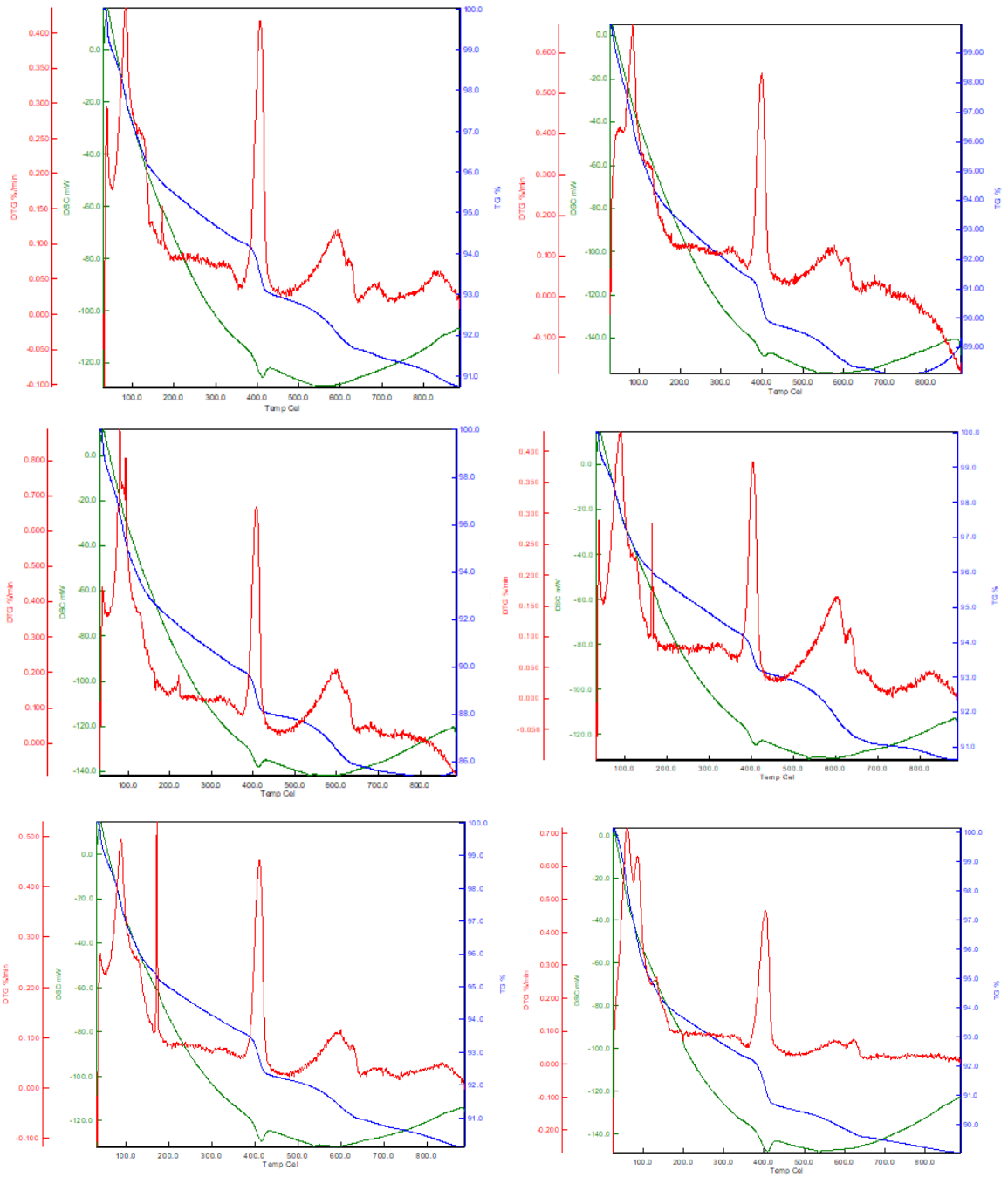

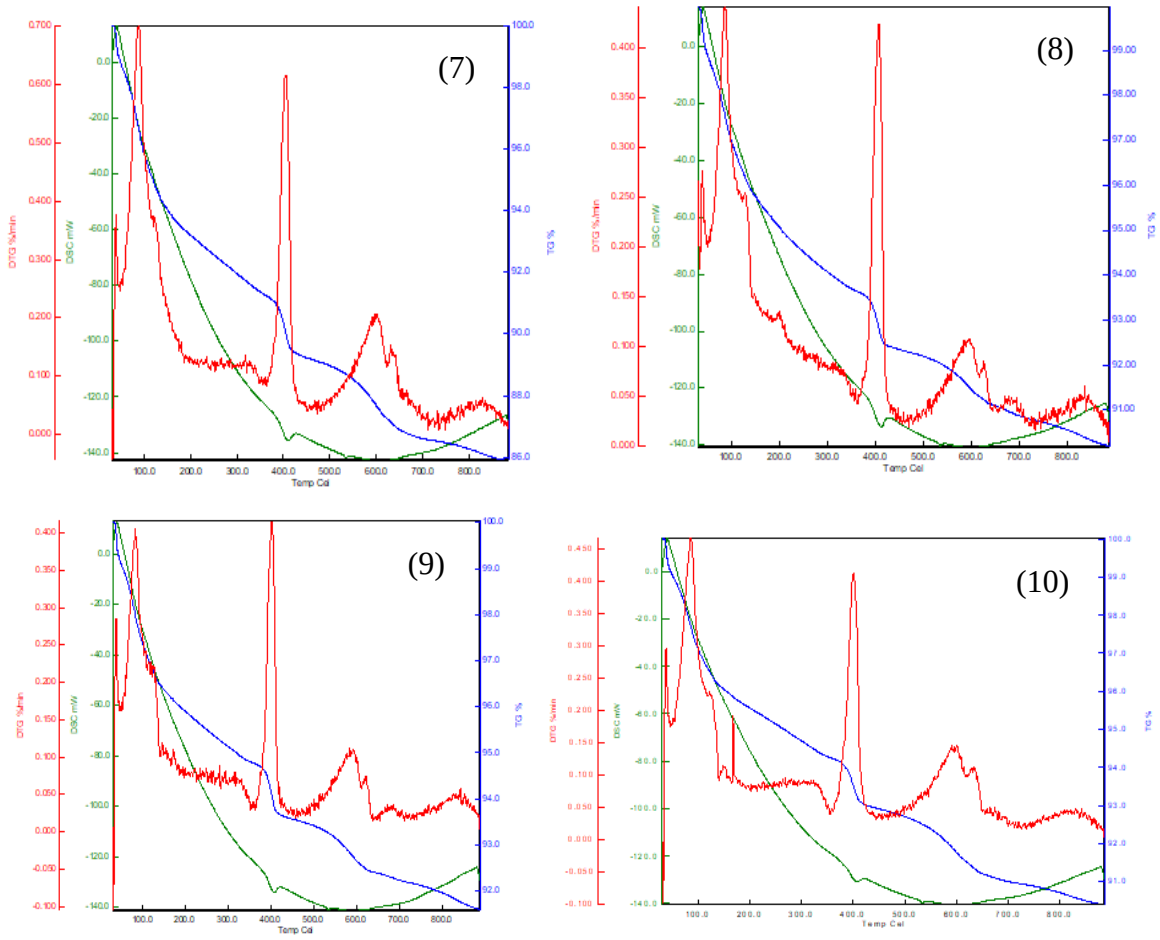

Figure A6.3: *TG, DTG, and DSC analysis of concrete mixes 1 to 10.*

	SEM	EDX
1	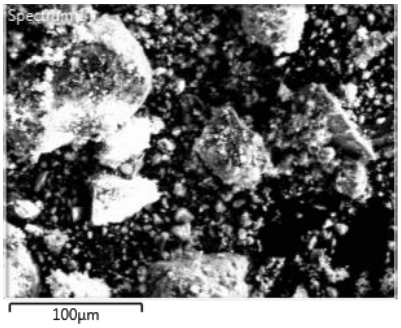	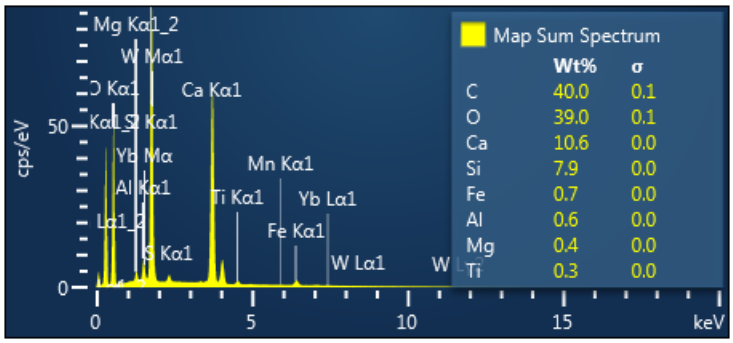
2	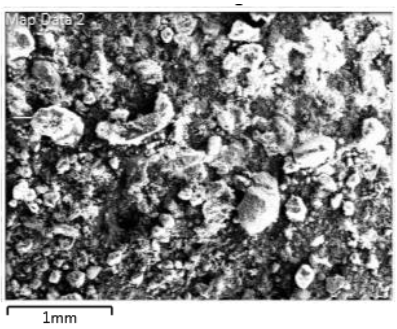	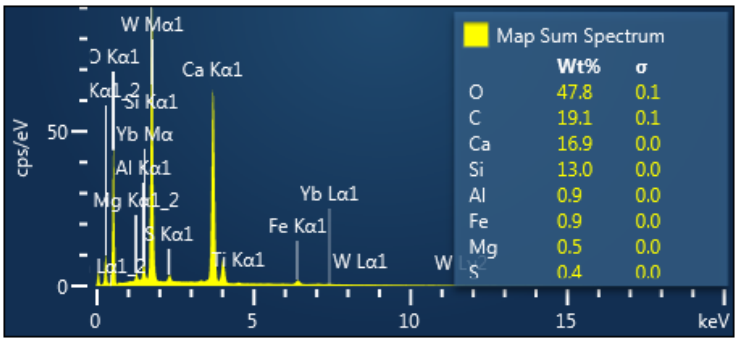
3	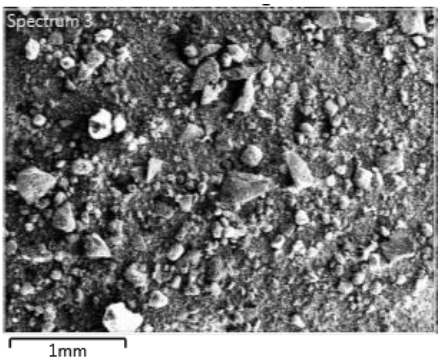	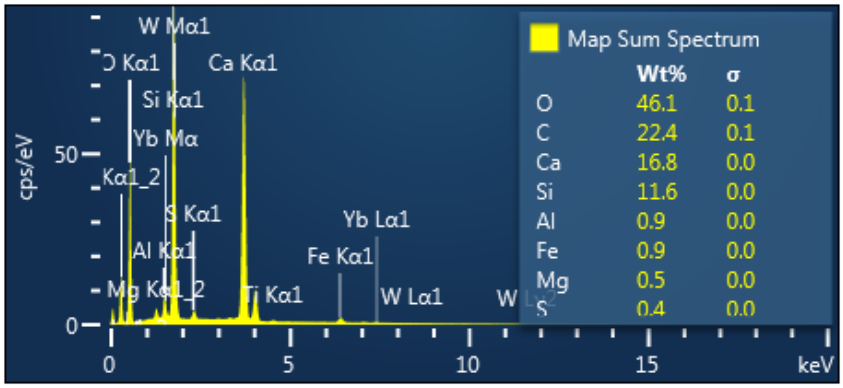
4	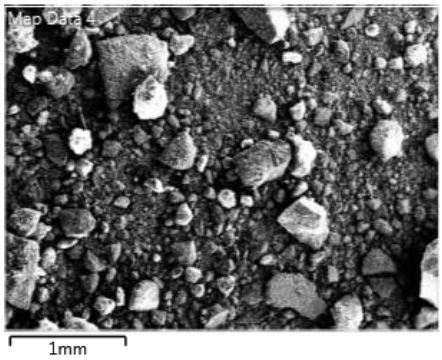	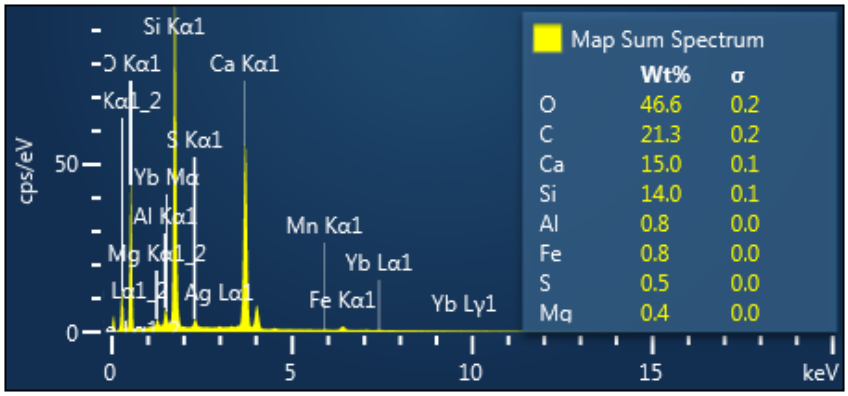

5

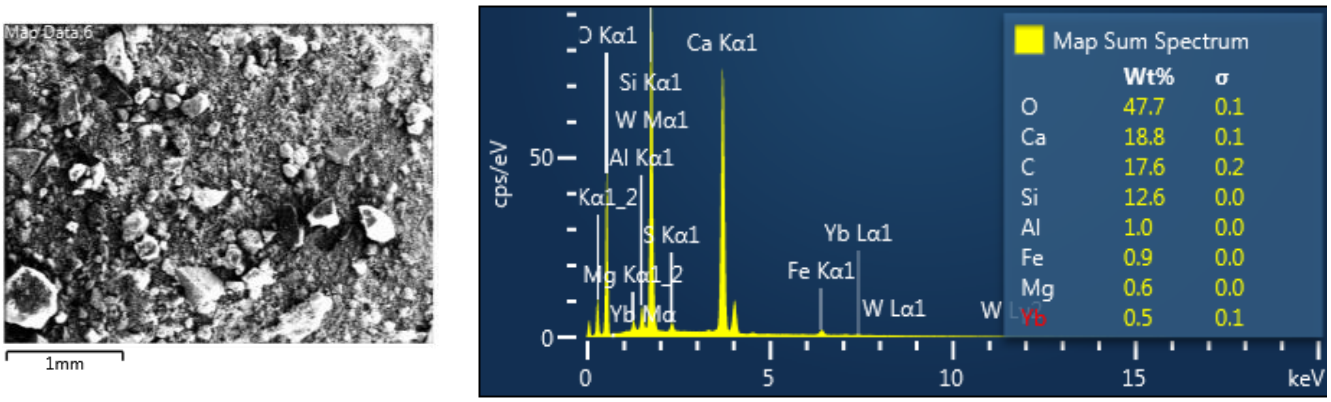

6

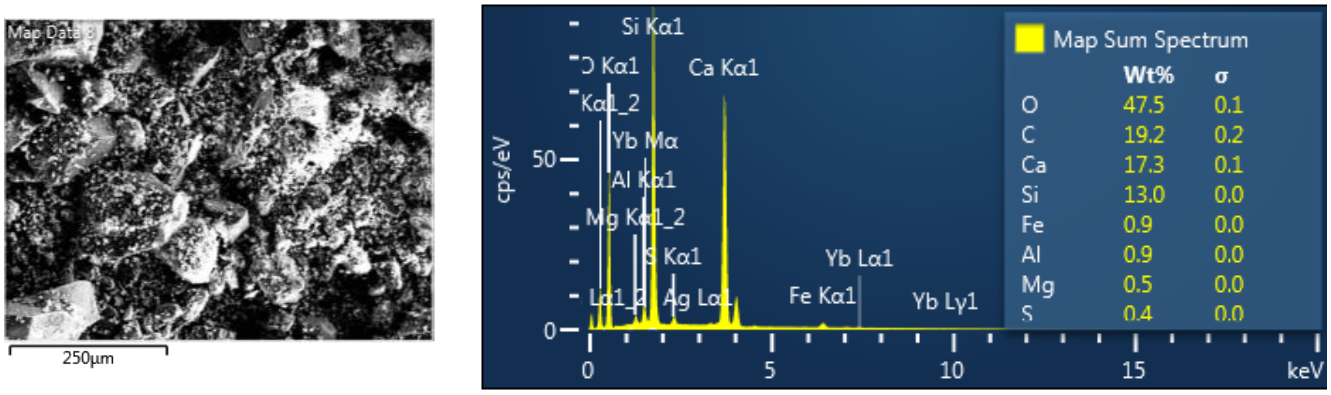

7

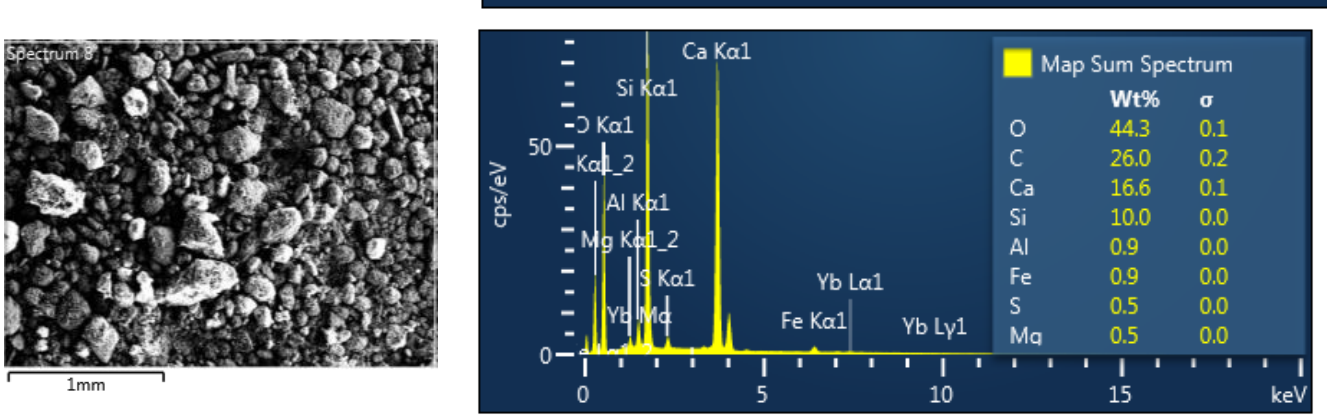

8

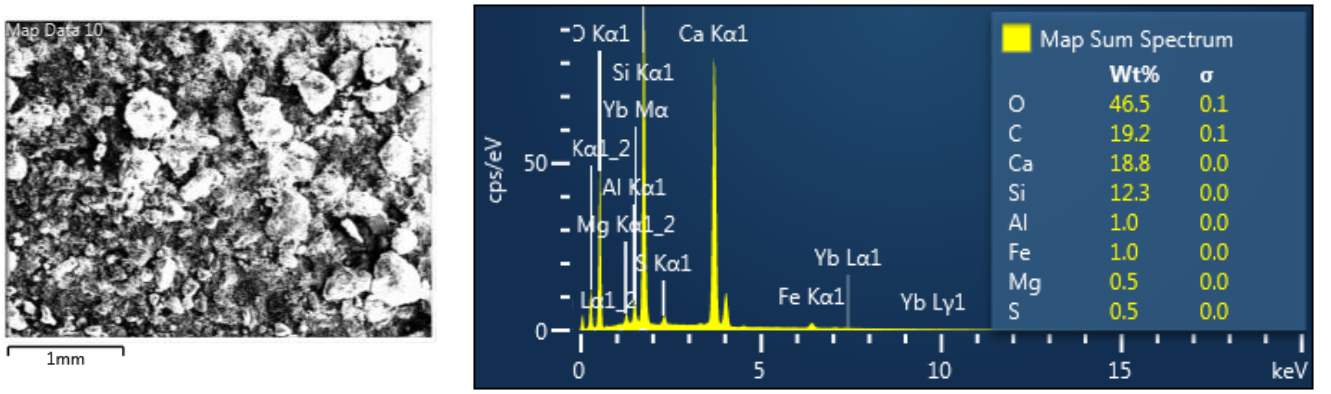

9

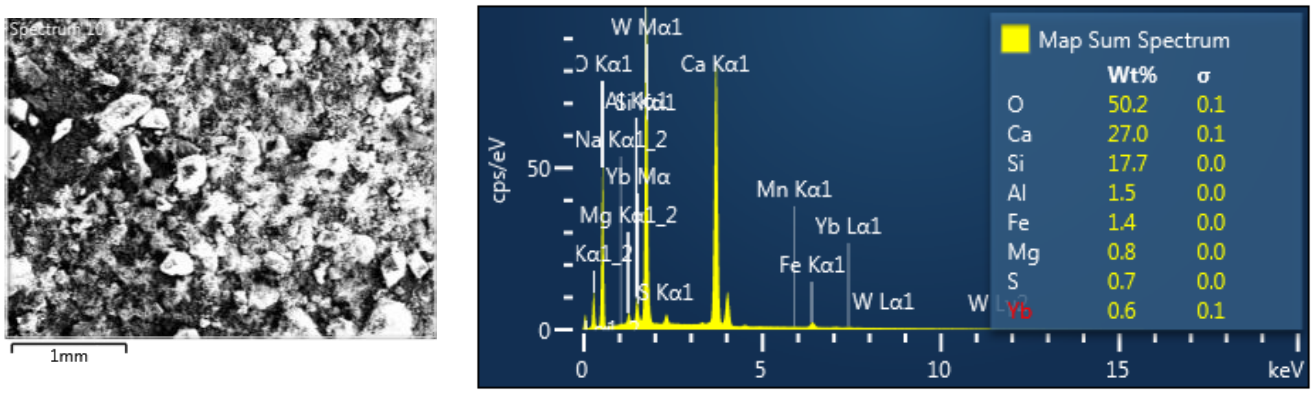

10

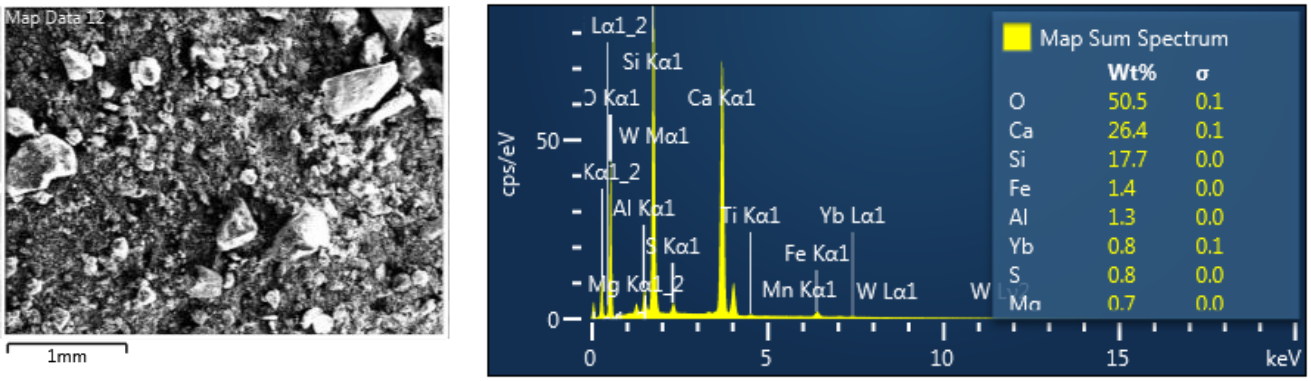

Figure A6.4: *SEM Images and corresponding EDX profiles of mortar mixes.*

Table A6.1: *EDS percentage elemental composition of mortar mix*

Mix/Wt%	1	2	3	4	5	6	7	8	9	10
C	40.02	19.1	22.36	21.3	17.59	19.19	25.96	19.19	23.51	21.14
O	38.96	47.81	46.14	46.64	47.67	47.47	44.31	46.53	44.25	46.28
Na	0	0	0	0	0	0	0	0	0.06	0
Mg	0.36	0.51	0.51	0.43	0.56	0.47	0.46	0.52	0.77	0.71
Al	0.62	0.94	0.91	0.82	0.99	0.85	0.88	0.99	1.45	1.35
Si	7.91	12.99	11.55	14	12.59	12.98	9.96	12.25	13.36	12.16
S	0.25	0.4	0.42	0.45	0.43	0.42	0.48	0.46	0.69	0.76
Ca	10.62	16.86	16.75	14.96	18.76	17.33	16.65	18.76	18.76	18.33
Ti	0.29	0.13	0.15	0	0	0	0	0	0	0.26
Mn	0.04	0	0	0.05	0	0	0	0	0.07	0.09
Fe	0.73	0.92	0.87	0.8	0.94	0.92	0.86	0.97	1.44	1.44
Yb	0.2	0.34	0.35	0.36	0.47	0.37	0.42	0.33	0.6	0.82
W	0	0	0	0	0	0	0	0	0	0
Ag	0	0	**0.06**	**0.2**	0	**0.05**	**0.3**	0	0	0
Total:	100	100	100	100	100	100	100	100	100	100